

Aus der
Medizinischen Klinik und Poliklinik II
Klinik der Universität München
Direktorin: Prof. Dr. med. Julia Mayerle

**Generation of CD44-specific aptamers for
targeted approaches in the treatment of
pancreatic cancer**

Dissertation
zum Erwerb des Doktorgrades der Medizin
an der Medizinischen Fakultät
der Ludwig-Maximilians-Universität zu München



vorgelegt von

Julian Peterhansl

aus Tegernsee

2023

Mit Genehmigung der Medizinischen Fakultät
der Universität München

Berichterstatter: Prof. Dr. Julia Mayerle

Mitberichterstatter: Prof. Dr. Sebastian Kobold
PD Dr. Julian Holch
Prof. Dr. Axel Kleespies, FEBS

Dekan: Prof. Dr. med. Thomas Gudermann

Tag der mündlichen Prüfung: 07.12.2023

Table of Content

1. Overview	1
1.1. Abstract	1
1.2. Zusammenfassung	3
2. Introduction	5
2.1. Clinical significance of PDAC	5
2.2. The role of CD44 in pancreatic cancer	8
2.3. Aptamers as an advantageous targeted drug delivery system	10
3. Research objectives	14
4. Materials and methods	15
4.1. Laboratory materials	15
4.1.1. Equipment.....	15
4.1.2. Consumables.....	16
4.1.3. Software.....	17
4.1.4. Antibodies	18
4.1.5. Cell lines and bacterial cells	18
4.1.6. Plasmids	19
4.1.7. Enzymes and kits	19
4.1.8. Chemicals and reagents.....	19
4.1.9. Buffers and solutions.....	22
4.2. Cell culture conditions	25
4.3. Flow cytometry	25
4.4. SDS-PAGE and Western blot	26
4.5. Bacterial plasmid expansion	27
4.6. Mammalian CD44 protein expression	27
4.7. The SELEX-cycle	28
4.7.1. Overview.....	28
4.7.2. Library pool preparation	30

4.7.3.	<i>In vitro</i> transcription	31
4.7.4.	Basic selection step.....	32
4.7.5.	Advanced selection step	34
4.7.6.	Pool replenishment.....	36
4.7.7.	Aptamer cloning for sequence readout.....	38
4.7.8.	Generation of working aptamer molecules	39
4.8.	Aptamer sequence analysis	41
4.9.	Coupling of Cy3 dye to aptamers.....	41
4.10.	Evaluation of aptamer specificity by flow cytometry.....	42
4.11.	UV-crosslinking of aptamer RNA to cellular CD44.....	42
4.12.	MTT proliferation assay	43
4.13.	Cell cycle analysis	44
4.14.	Modeling of aptamer binding (HADDOCK).....	46
5.	Results.....	47
5.1.	Generation of aptamers in 12 cycles of SELEX.....	47
5.1.1.	Enriched aptamer sequences.....	48
5.1.2.	Analysis of aptamer sequence motifs	49
5.2.	Evaluation the expression of CD44v6 and CD44s in cell line systems.....	51
5.2.1.	Assessment of CD44v6 expression of cell lines.....	52
5.2.2.	Assessment of CD44s expression of cell lines.....	53
5.3.	Evaluation of aptamer-to-target specificity.....	54
5.3.1.	Assessment of aptamer binding to CD44v6 by flow cytometry	54
5.3.2.	Assessment of aptamer binding to CD44 by flow cytometry	57
5.3.3.	Confirmation of aptamer binding to CD44s by UV cross-linking	58
5.4.	<i>In vitro</i> biological effects of CD44-specific aptamers enhanced with 5-Fluorouracil.....	60
5.4.1.	The effect of aptamers on cancer cell proliferation.....	61
5.4.2.	The effects of aptamers on the cancer cell cycle.....	66
5.5.	<i>In silico</i> modeling of aptamer binding to the CD44s protein	69
5.5.1.	Estimation of the most favorable binding patch of CD44.....	70
5.5.2.	Visualization of aptamer binding to CD44.....	72

6. Discussion	75
6.1. Evaluation of the modified SELEX protocol.....	75
6.2. Evaluation of cytostatic effects of CD44-specific aptamers in vitro	76
6.3. Evaluation of the aptamer binding site on CD44 and its biological relevance.....	77
7. References	79
8. Supplement.....	89
8.1. Supplement 1: Sequence information	89
8.1.1. SELEX library primers	89
8.1.2. Aptamer oligonucleotide primers.....	89
8.1.3. Aptamer RNA sequence details	90
8.2. Supplement 2: MTT proliferation assay readout R-script.....	90
9. Appendix	92
9.1. Acknowledgements	92
9.2. Curriculum vitae	93
9.3. Affidavit.....	94

Abbreviations

AUC	Area under the curve
CD44v6	CD44 containing exon variant 6
FC	Flow cytometry
PDAC	Pancreatic ductal adenocarcinoma
PI	Propidium iodide
SELEX	Systematic Evolution of Ligands by EXponential Enrichment
5FU	5-Fluorouracil

Directory of figures

- Figure 1.** Incidence and survival rates depending on cancer type (CJC 2023) [1]
- Figure 2.** Visualization of the CD44 protein from Ponta et al.
- Figure 3.** Aptamers: A Novel Targeted Theranostic Platform by Mahajan, Li et al.
- Figure 4.** Generation and evaluation of CD44-specific aptamers for cancer treatment
- Figure 5.** Schematic representation of the SELEX process
- Figure 6.** Schematic representation of the basic selection step
- Figure 7.** Schematic representation of the advanced selection step
- Figure 8.** Schematic representation of the whole SELEX cycle
- Figure 9.** Analysis of aptamer sequences with the LocARNA Alignment & Folding tool
- Figure 10.** Discovery of motifs in the aptamer sequences with the MEME-suite tool
- Figure 11.** CD44v6 expression of cell lines
- Figure 12.** CD44s expression of cell lines
- Figure 13.** CD44s-expression of cell lines
- Figure 14.** Evaluation of binding of the aptamers to the v6 exon region of CD44
- Figure 15.** Evaluation of aptamer binding to CD44
- Figure 16.** Aptamer cross-linking to CD44s on the cell surface
- Figure 17.** MTT-proliferation assay with 5FU-aptamers on Capan 1 cancer cells
- Figure 18.** MTT-proliferation assay with 5FU-aptamers on Panc 1 cancer cells
- Figure 19.** Isobologram graphs depicting the effects of 5FU-modified aptamers on Capan 1 and Panc 1 cancer cell lines
- Figure 20.** Cell cycle analysis of Capan 1 cells after aptamer treatment
- Figure 21.** Comparison of HADDOCK scores of CD44-aptamer interaction clusters
- Figure 22.** Visualization of aptamer binding to the CD44s protein

Directory of tables

- Table 1.** SELEX-library primers
- Table 2.** Reverse SELEX-primer
- Table 3.** Aptamer oligonucleotides and primers
- Table 4.** Enriched aptamer sequences after 12 rounds of SELEX

1. Overview

1.1. Abstract

Pancreatic ductal adenocarcinoma (PDAC) has become one of the leading causes of cancer related death worldwide due to its aggressive local behavior and early metastatic spread. The heterogenic composition of the tumor itself and its microenvironment decreases the efficacy of common chemotherapeutic drugs. As a result, a combination of high-dose cytostatic agents, the FOLFIRINOX-regimen, has to be employed as a treatment strategy for advanced PDAC. But even this strict therapeutic setup promises a survival benefit of only a couple of months, while posing the risk of severe adverse side effects.

Many studies have shown that overexpression of the cell surface protein CD44 is common in pancreatic ductal adenocarcinoma and is associated with advanced local aggressiveness of tumors, formation of metastases and significant reduction in overall survival. CD44 interacts with hyaluronic acid and other components of the extracellular matrix and is involved in signal transduction on known tumor-promoting subcellular pathways. Furthermore, CD44 and especially its isoform CD44v6, which contains an alternatively spliced exon, convey undesirable cancer stemness traits to PDAC tumors.

To overcome the limitations and difficulties of chemotherapeutic treatment in PDAC, in this study a targeted drug delivery system is implemented. An exceptionally elegant approach to this case is comprised of aptamers, RNA-molecules that are often referred to as 'nucleic acid antibodies'. The binding affinity of aptamer oligonucleotides can be prompted towards any desired molecular target through a process of mutagenesis and evolutionary selection (the SELEX-cycle). The molecules are significantly smaller than antibodies, nontoxic, nonimmunogenic and easily modifiable by incorporation of altered nucleotides into their RNA-backbone.

In this work, aptamers with selective specificity for CD44 were generated, their binding properties were evaluated, and the molecules were modified by incorporation of 5-Fluorouracil in place of every Uracil residue. The respective drug is part of the FOLFIRINOX-regimen in the clinical treatment of PDAC. No specific aptamer selectivity could be achieved for the exon variant 6 of CD44 in an experimental subset. The 5FU-modified CD44-specific aptamers showed a strong cytostatic effect on pancreatic cancer cells in vitro, which scaled with the degree of cellular CD44 expression and was specific for 5FU administration. Interestingly, the generated aptamers exerted supraadditive inhibitory effects on pancreatic cancer cell growth. The observation could be explained by in silico modeling of the molecular interaction, which revealed severe obstruction of the hyaluronan binding pocket of CD44 by the generated aptamers.

More work is needed to obtain a deeper understanding of the mechanistic processes that are caused by treatment with the generated CD44-specific aptamers. However, in general, this novel approach is a step toward overcoming the limitations that are associated with PDAC treatment on multiple molecular levels.

1.2. Zusammenfassung

Das duktale Adenokarzinom des Pankreas (PDAC) ist aufgrund seines aggressiven lokalen Wachstums und der frühen metastatischen Aussaat zu einer der führenden Ursachen für krebisbedingte Todesfälle weltweit geworden. Die heterogene zelluläre Zusammensetzung des Tumors selbst und des Microenvironments limitieren die Wirksamkeit gängiger Chemotherapeutika. Für die Behandlung des fortgeschrittenen PDAC muss daher eine Kombination hochdosierter Zytostatika, das FOLFIRINOX-Regime, eingesetzt werden. Doch selbst dieses aggressive therapeutische Setup verspricht lediglich einen Überlebensvorteil von wenigen Monaten, birgt jedoch das Risiko schwerwiegender unerwünschter Nebenwirkungen.

Mehrere Studien haben gezeigt, dass das Oberflächenprotein CD44 beim duktalem Adenokarzinom des Pankreas häufig überexprimiert ist und mit fortgeschrittener lokaler Tumoraggressivität, Metastasenbildung und einer signifikanten Verschlechterung des Gesamtüberlebens einhergeht. CD44 interagiert mit Hyaluronsäure sowie anderen Komponenten der extrazellulären Matrix und ist an der Signalübertragung über bekannte tumorfördernde subzelluläre Signalwege beteiligt. Darüber hinaus sind CD44 und insbesondere seine Isoform CD44v6, die ein alternativ gespleißtes Exon enthält, Kontributoren von Stammzell-ähnlichen Merkmalen in pankreatischen Tumorzellen.

Als neuer Ansatz zur Überwindung von Limitationen der chemotherapeutischen Behandlung des PDAC wird in dieser Arbeit ein „targeted drug delivery“-System implementiert. Eine besonders elegante Herangehensweise stellen dabei die sogenannten Aptamere dar. Dies sind RNA-Moleküle, die oft als „Nukleinsäure-Antikörper“ bezeichnet werden. Aptamer-Oligonukleotide, die spezifisch an eine beliebige molekulare Zielstruktur binden, können durch einen Prozess von Zufallsmutationen und evolutionärer Selektion (dem SELEX-Zyklus) generiert werden. Die Moleküle sind deutlich kleiner als Antikörper, nicht toxisch, nicht immunogen und einfach modifizierbar durch den Einbau chemisch veränderter Nukleotide in das Rückgrat der RNA.

Im Rahmen dieser Arbeit wurden Aptamere mit selektiver Spezifität für CD44 generiert, im Hinblick auf ihre Bindungskinetik evaluiert und durch Einbau von 5-Fluorouracil anstelle jedes Uracil-Moleküls modifiziert. Dieses Medikament ist Teil des FOLFIRINOX-Regimes zur medizinischen Behandlung des PDAC. In einem experimentellen Nebenversuch konnte keine spezifische Aptamer-Selektivität für die Exon-Variante 6 von CD44 erreicht werden. Die modifizierten, CD44-spezifischen Aptamere zeigten in vitro eine starke zytostatische Wirkung auf Bauchspeicheldrüsen-krebszellen, welche mit zunehmender zellulärer CD44-Expression anstieg und spezifisch auf die Wirkung von 5FU zurückgeführt werden konnte. Interessanterweise konnte ein supraadditiver

Hemmeffekt durch die Aptamere auf das Wachstum der Krebszellen beobachtet werden. Dieser Effekt konnte durch ein in-silico berechnetes Modell der molekularen Interaktionen erklärt werden, das eine starke Obstruktion der Bindungsstelle für Hyaluronsäure auf CD44 durch die generierten Aptamere zeigte.

Weiterführende experimentelle Arbeit ist erforderlich, um ein tiefgreifendes Verständnis über die subzellulären Prozesse zu erlangen, die durch Administration der CD44-spezifischen Aptamere induziert werden. In Zusammenschau der Ergebnisse ist dieser neu entwickelte Ansatz ein wichtiger Schritt für die Weiterentwicklung der PDAC-Therapie, da er das Potential der konventionellen Behandlungsstrategien auf mehreren molekularen Ebenen erweitert.

2. Introduction

2.1. Clinical significance of PDAC

Pancreatic ductal adenocarcinoma comprises one of the leading causes of cancer related death worldwide with a dismal 5-year survival rate of only 11%, while rather moderate improvement of 6% regarding the clinical survival outcome has been observed over the last years [1], [2]. By 2023 PDAC has reached the top 4th rank of cancer caused mortality in women and men [1]. While its incidence is lower compared to other malignant diseases, there is a continuous annual increment of 1%, which poses the risk of PDAC becoming the second leading cause of cancer-related death worldwide by 2030 [1, 3].

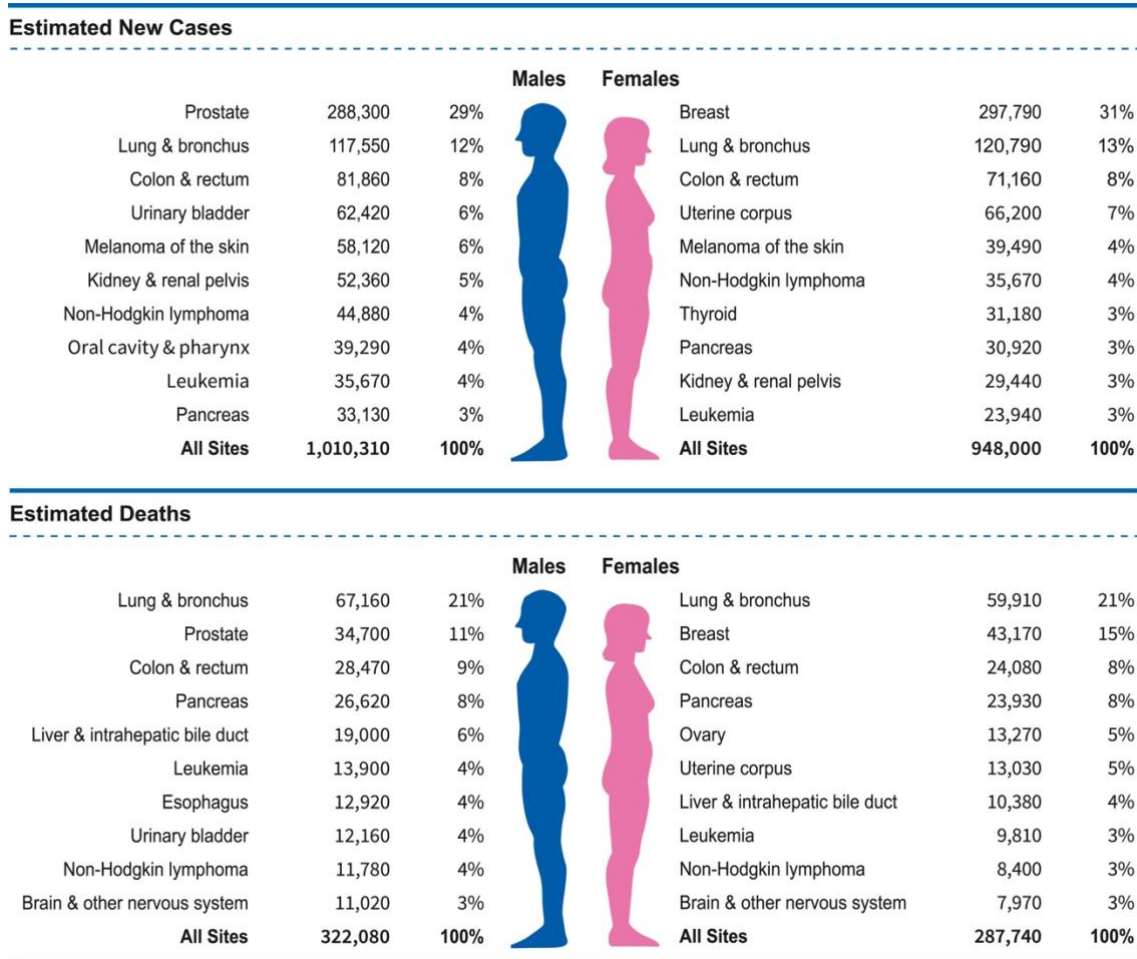


Figure 1. Incidence and survival rates depending on cancer type (CJC 2023) [1]: Pancreatic cancer is comprising 3% of the estimated new cancer cases while reaching the top 4 with 8% of cancer related deaths worldwide.

Among the most prominent reasons for this tumor behavior is the lack of early symptoms and thus diagnosis mainly in late stages of cancer (>80%) with limited treatment options, mostly due to infiltration of adjacent organs and vessels [4]. Surgery remains the only curative approach but is solely applicable in the small fraction of tumors that are locally controlled [5]. Most patients have to rely on aggressive chemotherapy that promises a progression-free survival benefit of a median of 6 to 12 months [5, 6].

The first-line treatment option for “fit” patients is comprised by the FOLFIRINOX regimen (5-Fluorouracil, Oxaliplatin, Irinotecan, and Leucovorin), that poses the risk of severe adverse effects like cytopenia, diarrhea, pain and fatigue [7], [8], [9]. For patients with higher frailty, a limited treatment approach has to be employed, usually by gemcitabine/nab-paclitaxel or even by gemcitabine-monotherapy, which limits the survival rates considerably [10].

One of the main reasons for the relatively low efficacy of antitumor drugs in PDAC is the complex heterogeneity of the tumor itself and of its microenvironment [11], [12], [13]. Strong desmoplastic behavior facilitates the generation of a stromal barrier that impedes the desirable distribution of drugs within the tumor, leading to increased harm to bystander tissue by the chemotherapeutic agents [14]. The extracellular tumor matrix and the cancer-associated fibroblasts contribute significantly to tumor differentiation and progression [15]. Furthermore, a subpopulation of cancer cells with stem-like traits (cancer stem cells) enhances the capacity of self-renewal of the tumors, thus conveying strong chemoresistance [16]. These subpopulations also play a crucial role in cancer differentiation, by orchestrating epithelial-to-mesenchymal transition (EMT) [17], [18] and there is evidence that they facilitate organ specific metastatic tumor spread [19].

PDAC tumors are generally considered to be rather immunologically inactive with lower inflammatory activity and immune cell infiltration [20], [21]. One reason for that is the comparably low level of mutational occurrences, which leads to formation of fewer neoantigen structures, that could serve as immune system activators [22]. This complexity of the PDAC microenvironment is the reason, why the recently implemented immune checkpoint inhibiting drugs (ICIs), that have shown extraordinary treatment efficacy in many solid malignant diseases, show a rather limited therapeutic effect in most pancreatic cancers [23], [24].

The most promising approach to overcome these limitations is the implementation of a targeted drug delivery system that can orchestrate therapeutic agents directly to tumor cells while sparing adjacent tissue and the stromal surrounding, thus reducing cytotoxic side effects [25].

There is one FDA-approved target-specific PDAC therapy in 2023 comprised by the EGFR-inhibitor drug erlotinib in combination with gemcitabine. A randomized phase III-trial showed a statistically significant survival benefit of that treatment in late-stage pancreatic cancer, however the overall improvement of median survival averaged at only 0.33 months compared to the combination of placebo with gemcitabine [26], [27].

Over 85 % of pancreatic tumors show a variation of a KRAS mutation [28], but direct targeting of KRAS and its downstream pathways, such as RAF/MEK/ERK and PI3K/Akt, has faced setbacks as inhibitors often activated feedback pathways, thus diminishing the clinical therapeutic effects [29], [30], [31].

The overexpression of vascular endothelial growth factor (VEGF) has been shown to be associated with tumor progression, metastatic dissemination and worse prognosis in PDAC [32], [33]. Unfortunately, assessed VEGF-inhibitors have largely been ineffective, mostly due to PDAC's dense stroma, which leads to reduced vascularization, thus hindering efficient drug delivery and diminishing the therapeutic potential [34], [35].

The dense fibrous stroma itself, that comprises over 90% of the tumor mass, has also been considered as a therapeutic target because of its crucial role in PDAC pathophysiology [36]. There have been approaches of targeting components of the extracellular matrix environment like hyaluronic acid (HA) by hyaluronidases and matrix-metalloproteases. The effects of those treatment regimens varied considerably and some of the clinical trials had to be halted due to increased drug toxicity and worse survival outcomes [37], [38]. But recent evaluations showed that some combinations like the matrix-metalloprotease 9 plus gemcitabine/gemcitabine and nab-paclitaxel have promising effects while maintaining a low risk profile [39].

Lastly, cancer stem cells (CSCs) and their signaling pathways (Notch, WNT, JAK/STAT) are constantly evaluated as targets for directed treatment approaches. There have been promising results of reduction of CSC frequency, thus enhancing chemotherapy effects in preclinical and early-phase studies [40]. But overall, many studies have shown limited treatment outcomes in their respective settings, suggesting that targeting CSCs alone may not be sufficient [41], [42].

Overall, the field of targeted therapy in pancreatic cancer is continuously expanded in various approaches, due to being one of the most promising frontiers for overcoming the limitations associated with PDAC treatment. There is substantial need for reaching improvement of survival rates and clinical strategies in pancreatic cancer therapy because of its growing epidemiologic relevance.

2.2. The role of CD44 in pancreatic cancer

The CD44 protein, also known as the “Indian blood group” [43], is a cell surface receptor whose main binding targets are hyaluronic acid (HA) [44] and other components of the extracellular matrix [45]. CD44 consists of an aminoterminal domain that binds to extracellular HA, a stem region, a transmembrane segment, and an intracellular part, as visualized by Ponta et al. [46].

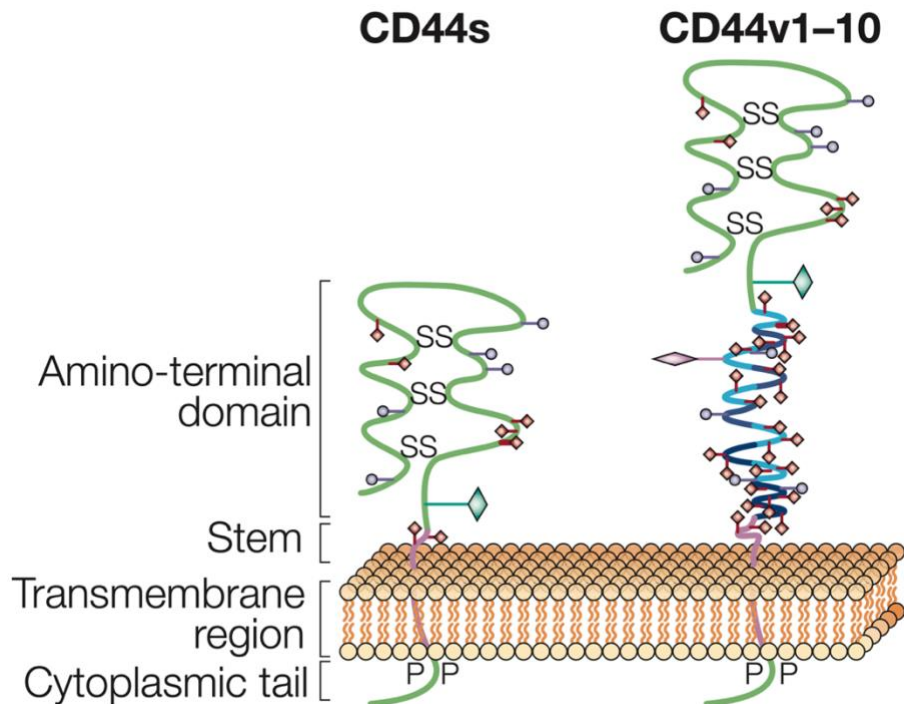


Figure 2. Visualization of the CD44 protein from Ponta et al. [46]: The different regions of the CD44 protein are displayed in relation to the cell membrane. ‘SS’ indicates disulfide bonds, ‘P’ indicates serine phosphorylation, the colored shapes indicate post-translational modification sites. On the right side, the stem region of CD44 is enriched with all possible exon variants that can be obtained by alternative splicing.

The whole protein can vary in size from 82kDa to 200kDa [47] due to two distinct processes that modify the properties of CD44: On the one hand, extensive post-translational modification [48], on the other hand, insertion of variable polypeptides into the stem region by alternative splicing [49]. The transmembrane region of the protein carries the function of receptor regulation by associating CD44 with lipid raft domains, hence bringing different surface receptors into close proximity [50]. The cytoplasmic tail of CD44 interacts with proteins of the ezrin-radixin family, which link the cell surface to

the actin cytoskeleton [51] but it also interacts with crucial kinase signaling pathways, making the CD44 protein a coreceptor [52].

CD44 is known to be overexpressed in pancreatic cancer, reaching a level of CD44-positivity of up to 73% of tumor tissue samples [53], [54]. The protein expression level is associated with advanced local tumor aggression, lymph node invasion and metastasis formation [55]. A study by Li et al. (Int J Clin Exp Pathol. 2015) comparing the median overall survival time of PDAC patients with respect to CD44 showed a significant difference of 28 months in the CD44-negative group, compared to 17 months in the CD44-positive group [54].

Mechanistic analyses indicate that CD44 transduces tumorigenic signaling through the interaction of its cytoplasmic domain with the tyrosine kinase c-Src [56]. This interaction is able to induce downstream activation of multiple known oncogenic pathways such as STAT3, PI3K, and MAPK [54], [56], [57] that induce, hold and promote tumor aggressiveness. Homophilic CD44-receptor interaction has also been reported to activate PAK2/PTK2 or EGFR signal pathways [58]. There is evidence, that CD44 is a major driver of epithelial-mesenchymal transition and the formation of metastases by regulation of membrane-bound matrix metalloproteases [59], [60].

Furthermore, CD44 is one of the stemness markers of cancer cells and seems to strongly contribute to tumorigenesis of clonal populations [61]. Especially in pancreatic cancer, the interaction of CD44 with the extracellular matrix microenvironment promotes stemness characteristics such as self-renewal and drug resistance in tumor cells [62].

A subtype of CD44 has been shown to be directly associated with cancer cell differentiation in PDAC: The splice variant containing exon 6 (CD44v6) [63]. The presence of exon v6 is crucial for HGF / c-Met-signaling [64] which facilitates systemic spread of tumor cells. Higher expression of CD44v6 is associated with significantly lower overall survival [65].

Recent studies have shown that chemotherapeutic treatment of pancreatic cancer cells can induce a phenotypic switch leading to increased invasiveness and drug resistance through facilitation of an isoform change from CD44v to CD44s, leading to increased activity of ABC-transporter expression and capacity for DNA repair, underlining the importance of CD44 in PDAC pathophysiology [66], [67]. Many preclinical studies show that inhibition of the CD44-ligand interactions and CD44-expression lead to significant reduction of cancer cell proliferation, drug resistance, stemness traits and invasiveness [68], [69].

The field of clinical investigation regarding the role of CD44 in PDAC is still sparsely elucidated. Gocke et al. (BMC Cancer, 2021) show in a retrospective tissue analysis,

that the presence of CD44 and CSC markers in postoperative patient samples correlates considerably with the probability of PDAC recurrence [70]. Similar results were obtained by Chih-Po et al. (in vivo, 2018), who showed that CD44-expression was an independent predictor of tumor reoccurrence after 6 months following resection [71].

Taking all of the above into account, CD44 and its splice variant v6 comprise very promising cellular targets for a directed chemotherapeutic approach. The proteins of the CD44 family are enriched in PDAC and associated with unfavorable characteristics, so the depletion of this population seems very beneficial for cancer therapies.

2.3. Aptamers as an advantageous targeted drug delivery system

In the year 1990, Tuerk and Gold identified a nucleic acid oligomer with protein-binding capabilities and used mutagenesis and selectional pressure to increase its target affinity and selectivity by several magnitudes [72]. This method was refined and expanded by Ellington and Szostak to a process of 'Systematic Evolution of Ligands by Exponential enrichment' (short: SELEX), which allowed for the selection of nucleic acid molecules with high affinity to virtually any molecular target [73]. They named the enriched oligonucleotides "aptamers", which basically means "fitting particles".

Modern implementations of the SELEX method employ a library of DNA or RNA molecules with conserved flank regions (for primer-based amplification) and a variable center region composed of random nucleotides (for variable binding properties). This DNA/RNA pool is subjected to multiple rounds of exposure to a target molecule, followed by retrieval and amplification of bound oligonucleotides. If necessary, negative selection steps can be included in order to dispose of unwanted off-target cross-binding. Upon completion of the SELEX-cycle, only sequences with the most favorable desired binding properties are enriched [74].

The aptamer-oligonucleotides comprise a very versatile targeting system with several advantages over traditional selective molecules, such as antibodies. First, the molecular weight of aptamers is significantly lower than the weight of protein-based molecules, enabling better tissue penetration and more desirable biodistribution [75]. Second, the whole selection process can be easily implemented in most laboratories without advanced technical requirements, rendering aptamers very cost-efficient. Furthermore, the aptamer platform offers a wide variety of possible chemical properties through inclusion of altered nucleotides. For example, modification of the 2'-residue of nucleotides by fluoridization makes RNA-aptamers resistant to nuclease degradation [76], incorporation of 5-Fluoro-UTP instead of UTP conveys cytostatic drug effects to the

aptamers [77] while other alterations increase the diversity of possible three-dimensional configurations. Another advantage of aptamers lies in the fact that they can be analyzed and synthesized solely on the basis of their nucleic acid code. This facilitates the generation of antidotes by implementation of complementary antisense oligonucleotides that can specifically neutralize aptamer-mediated effects [78]. And finally, systemic aptamer administration has been shown to induce fewer cytotoxic and immunogenic responses compared to the side effects commonly observed for protein-based drugs [79], [80]. Because of the above-mentioned, favorable properties, aptamers can be utilized in novel approaches of combined, diagnostic and therapeutic targeting of cancer cells, as depicted by Mahajan, Li et al. [77].

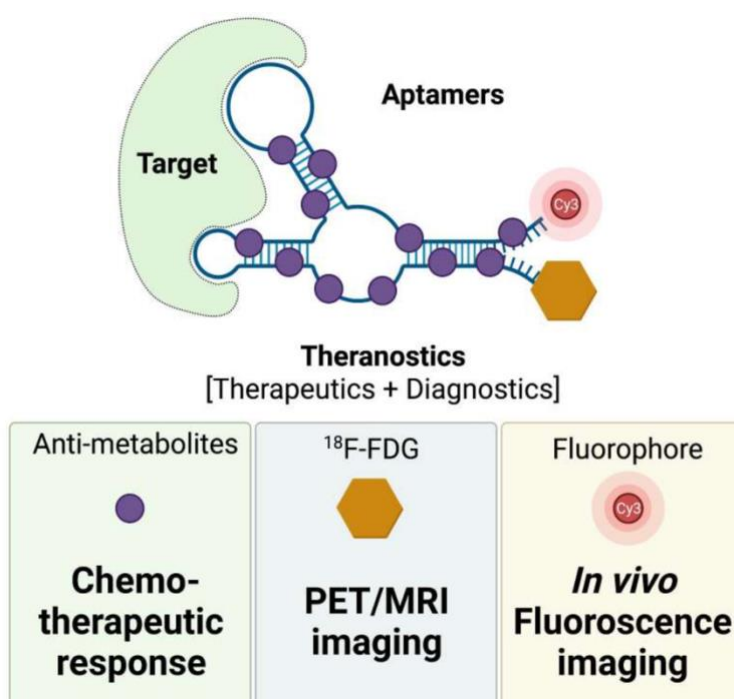


Figure 3. Aptamers: A Novel Targeted Theranostic Platform by Mahajan, Li et al. [77]: Due to their chemical versatility, aptamers can be modified in numerous ways and utilized as a platform for theranostic targeting by combined incorporation of chemotherapeutic agents for cancer treatment, radionuclides for PET/MRI imaging, and fluorescent dyes for in vivo imaging.

Although the concept of aptamers has been known for many years, no loss of interest can be observed, and the system is still modified, expanded, and implemented in a variety of clinical and preclinical applications [81]. The advantages of aptamers add multiple layers of possibilities to the concept of targeted drug delivery. In general, this approach promises to overcome many limitations associated with the utilization of conventional antibody-based strategies.

In the year 2004 the first aptamer therapeutic was approved by FDA. Pegaptanib (“Macugen”) is an RNA oligonucleotide that inhibits VEGF and is clinically in use for intravitreal treatment of oculo-vascular diseases like age related macular degeneration [82]. In August of 2023, a second RNA-aptamer gained FDA approval. Pegol (“Izervay”) showed considerable effects in treatment of geographic macular atrophy by inhibition of the complement protein C5 [83]. By now, no aptamers for the treatment of cancer are approved.

A query of the Clinical Trials Database (www.clinicaltrials.gov) shows, that there are currently 36 clinical studies listed, that involve aptamers (Dec 2023). 3 of these studies focus on cancer diagnosis and treatment, one on distinction of malignant from benign colorectal cancers via labeled ssDNA-aptamers [84], one on molecular biosensors for detection of bladder cancer (NCT02957370) and one on treatment of retinal tumors via a pegylated anti-VEGF aptamer [85].

The majority of research regarding aptamer applications in cancer is still carried out in the preclinical domain. There are multiple creative, promising approaches of aptamer utilization as a theranostic platform [81], [86], [87].

It is possible to select aptamers with inhibitory effects on tumorigenic cellular pathways, which is hard to achieve by implementation of antibodies or peptides [88]. Furthermore, aptamers can be employed as regulatory inhibitors, for example as blockers of Cas9, that lose their inhibitory effect upon binding to a specific target, as shown by Zhao et al. (Nucleic Acids Res. 2021) [89].

Aptamers can be elegantly fused to oligonucleotide agents like si- or sh-RNA via non-covalent binding, thus generating chimeric molecules [90]. This property is assessed in a variety of scientific approaches, like the knock-down of HER2-signaling in breast cancers [91]. An especially promising approach is the implementation of aptamer-carried si-RNA for immune checkpoint modulation, like reduction of PD-L1-expression, which is of rising interest in the field of recent cancer research [92], [93]. Aptamers also hold an advantageous possibility, that cannot easily be matched by antibodies: the generation of so-called “decoy”-aptamer combinations, that mimic polynucleotide targets of cellular proteins, thus disrupting tumor signaling pathways [94].

Of course, the broadest field of application for aptamers is the direct targeting of structures of interest with therapeutic or diagnostic intent. There are various studies in the field of cancer research assessing aptamers for liquid tumor biopsies [95], [96], for potential treatment of hematologic malignancies [97], [98], for potential treatment solid tumors and depletion of cancer stem cell populations [99], [100], [77].

Despite their versatility, the numerous advantages and the vast amount of research being conducted, there are not many aptamers in actual clinical transition compared to antibody-based targeting strategies.

One of the main reasons might be the fact, that most of the research is carried out in individual laboratories, which is a big advantage of the platform. While the production of monoclonal antibodies is usually restricted to specialized institutions, aptamers offer greater accessibility for individual research groups, but this comes at a cost. Generated aptamers have shown to rarely be perfectly applicable for clinical application directly after initial selection [101]. Hence, most of the time there is the necessity to undergo a tedious refinement process.

For example, aptamers have to be assessed for their nuclease resistance in vivo, in order to be applicable to higher-order systems. It is often necessary to modify the aptamers by addition of 2'-F-pyrimidine-residues to improve their stability [102].

Secondly, a known challenge is comprised by the fact, that aptamers tend to be cleared from the bloodstream by renal filtration in vivo, leading to a shortened half-life [103]. A possible solution to this is the PEGylation of the oligonucleotides, thus increasing their size, albeit with the risk of alteration of their binding properties [104].

Oftentimes, the initially selected aptamer pool does not show the full binding potential, making it necessary to alter the nucleotide structures by mutagenesis or chemical modifications [105].

Since the field of aptamer development is relatively new and the implemented concepts differ significantly, there is very limited consistency and standardization in the abovementioned processes [106]. This may lead to the effect, that many of the promising aptamer prototypes are slower in transitioning to clinical applicability, since a lot of re-assessment has to be employed, often without a standardized efficient production pipeline [107].

But on the other hand, this technology gives many researchers the chance to implement creative ideas. Most authors estimate that the vast potential of aptamers will outweigh the challenges once the platform has reached more maturity [81]. As concluded by Zhou and Rossi in 'Nature Reviews Drug Discovery': "The aptamer field has likely touched only the tip of the iceberg" [108].

3. Research objectives

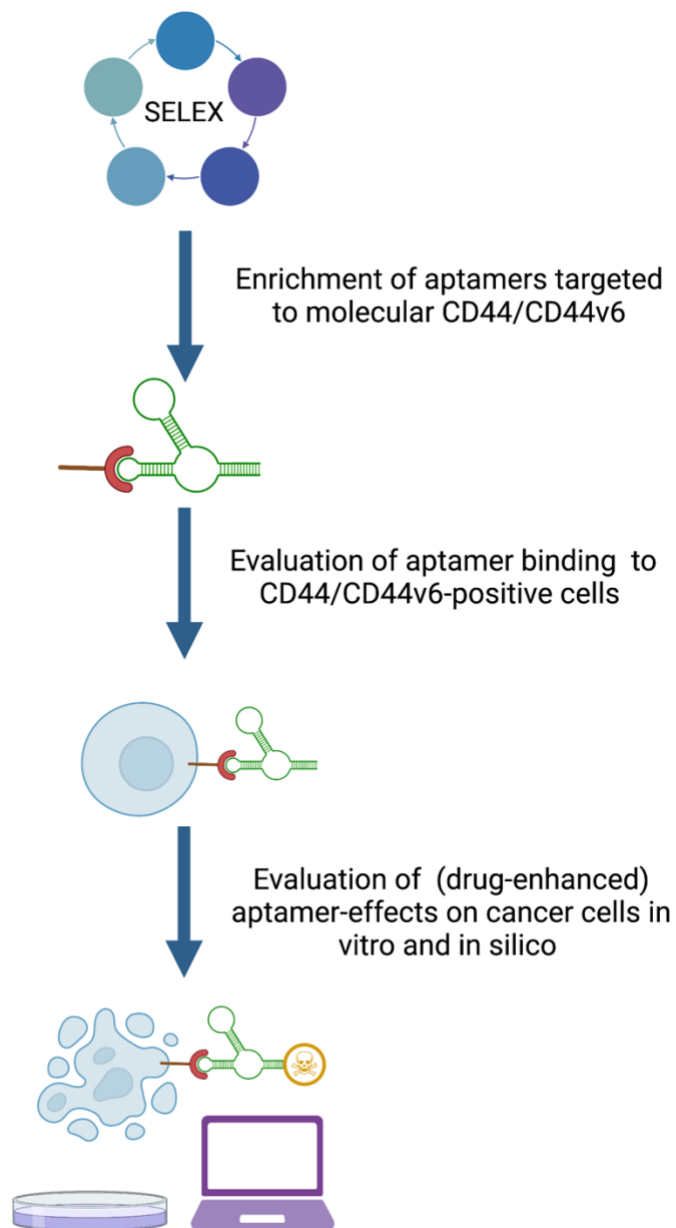


Figure 4. Generation and evaluation of CD44-specific aptamers for cancer treatment: The goal of this work was to generate an alternative approach of targeted drug delivery for the treatment of PDAC. The concept of RNA-based aptamers was implemented to target the cell surface protein CD44 in pancreatic cancer cells. In an experimental subset, the specificity of those aptamers was prompted toward the exon variant 6 of CD44. The CD44-targeted aptamers were modified by incorporation of the cytostatic drug 5-Fluorouracil and their effects on pancreatic cancer cells were assessed in vitro and in silico.

4. Materials and methods

All materials were obtained from publicly accessible sources of laboratory equipment provided by official manufacturers. The software used was licensed through the medical department of LMU Munich, the AG Mayerle working group, or through a personal LMU-student-access. Every quantitative experiment was carried out at 3 biologically distinct time points in sets of technical triplicates.

4.1. Laboratory materials

4.1.1. Equipment

Laboratory equipment	Source
Analytical Balance	Kern, Göggingen, Germany
BD Accuri™ C6 Plus personal flow cytometer	BD Biosciences, Franklin Lakes, USA
Beach scale	Kern, Göggingen, Germany
Binder™ Classic.Line Incubator	Binder, Tuttlingen, Germany
Biological safety cabinet, HeraSafe™	Thermo Fisher Scientific, Waltham, USA
Branson Ultrasonics™ Sonifier 250 D	Emerson, Saint Louis Missouri, USA
CoolNat ice machine	Ziegra, Isernhagen, Germany
DNA/RNA UV-cleaner box	Biosan, Riga, Lettland
Eppendorf™ Research™ Plus Pipettes	Eppendorf, Hamburg, Germany
Fusion Fx Vilber Lourmat UV Transilluminator	Vilber Lourmat GmbH, Eberhardzell, Germany
Heracell 240 CO2 Incubator	BMG Labtech, Ortenberg, Germany
Herafreeze HFU T series freezer -80°C	Thermo Fisher Scientific, Waltham, USA
Incubator Hood TH15	Edmund Bühler GmbH, Bodelshausen, Germany
inoLab pH 720	WTW, Weilheim, Germany
IX50 Phase contrast inverted microscope	Olympus, Shinjuku, Japan
Labogaz 206 bunsen burner	Campingaz, Hattersheim, Germany
Laboratory freezer -150°C	Thermo Fisher Scientific, Waltham, USA
Liebherr™ laboratory refrigerator 4°C	Liebherr-Hausgeräte Ochsenhausen GmbH, Ochsenhausen, Germany
Liebherr™ MediLine freezer -25°C	Liebherr-Hausgeräte Ochsenhausen GmbH, Ochsenhausen, Germany
MastercyclerR pro vapo.protect	Eppendorf, Hamburg, Germany
Milli-Q Integral water purification system	Merck, Darmstadt, Germany

Mini PROTEANR Tetra Cell	Bio-Rad, Herkules, USA
Mini-Sub-Cell GT Electrophoresis Cell	Bio-Rad, Herkules, USA
Mr. Frosty™ Isopropanol freezing chamber	Thermo Fisher Scientific, Waltham, USA
MTS-Shaker	IKA Werke GmbH, Staufen im Breisgau, Germany
Neubauer Improved Bright-Line counting chamber	BLAUBRAND®, Wertheim, Germany
Pipetboy acu 2	Integra, Biebertal, Germany
PIPETMAN® classic	Gilson, Middleton, USA
PowerPac™ Basic Power Supply	Bio-Rad, Herkules, USA
Qbit 4 Fluorometer	Thermo Fisher Scientific, Waltham, USA
SpectraMaxR Plus 384 microplate reader	Molecular Devices, San Jose, USA
Systec™ vertical autoclave, V-Series, VX	Systec, Linden, Germany
Tabletop centrifuge 5418	Eppendorf, Hamburg, Germany
Tabletop centrifuge 5427R	Eppendorf, Hamburg, Germany
Tabletop centrifuge 5702R	Eppendorf, Hamburg, Germany
Tabletop centrifuge Allegra 64R	Beckman Coulter, Indianapolis, USA
Trans-Blot® Turbo™ Transfer System	Bio-Rad, Herkules, USA
Triple Distribution System Microwave M1712N	Samsung, Suwon, South Korea
TS1 ThermoShaker	Biometra GmbH, Göttingen, Germany
UVC 30 Sterilization lamp	Kendro Laboratory Products, North Carolina, USA
W22 waterbath	Medingen, Hohenfels-Liggersdorf, Germany

4.1.2. Consumables

Consumables	Source
Cell culture flasks T75 stand. Vent. Cap	Sarstedt, Nürnberg, Germany
Cell culture plates (6-well, 24-well)	Greiner Bio-One, Kremsmünster, Austria
Cell culture plates (96-well)	Eppendorf, Hamburg, Germany
Cryogenic tube (2ml)	STARLAB, Hamburg, Germany
Falcon round bottom polypropylene tubes with cap	Thermo Fisher Scientific, Waltham, USA
Feather disposable scalpel	Feather, Osaka, Japan
Gel blotting sheets, GB003, Whatman™, 70×100 mm	VWR International GmbH, Ismaning, Germany
Inoculation loops sterile, 1 µl	Carl Roth GmbH + Co. KG, Karlsruhe, Germany
Nitrocellulose blotting membrane	GE Healthcare, Little Chalfont, UK

PCR 8er-SoftStrips & SoftCaps	Biozym Scientific GmbH, Oldendorf, Germany
PCR-clean reaction tubes (1,5ml, SafeLock)	Eppendorf, Hamburg, Germany
Petri dish, PS, 94 x 16 mm, sterile	Greiner Bio-One, Kremsmünster, Austria
pH-indicator strips pH 0 - 14 Universal indicator	Merck, Darmstadt, Germany
Pierce™ Centrifuge Columns, 10 mL	Thermo Fisher Scientific, Waltham, USA
Pipette tips (10µl, 200µl, 1000µl)	Sarstedt, Nürnberg, Germany
Pipette filter tips (10µl, 100µl, 1000µl)	Sarstedt, Nürnberg, Germany
Reaction tubes (0,5ml, 1,5ml, 2ml)	Eppendorf, Hamburg, Germany
Reaction tubes (15ml, 50ml)	Sarstedt, Nürnberg, Germany
Serological pipettes, sterile (5ml, 10ml, 25ml)	Sarstedt, Nürnberg, Germany
Syringe filter ROTILABO® CME, 0,22 µm	Roth AG, Arlesheim, Switzerland
Zeba™ Spin Desalting Columns, 7K MWCO, 0.5 mL	Thermo Fisher Scientific, Waltham, USA

4.1.3. Software

Software	Source
BD Accuri™ C6 Plus Cell Analyzer	BD Biosciences, Franklin Lakes, USA
BindUP	Paz I et al., Nucleic Acids Res, 2016
BioRender	biorender.com, Toronto, Canada
EndNote X9	Thomson Reuters, New York City, USA
FCS Express 6 plus Reader	De Novo, Pasadena, USA
FusionCaptAdvance (7.17.02a)	Vilber Lourmat GmbH, Eberhardzell, Germany
GraphPad Prism 9	GraphPad Software Inc., La Jolla, USA
HADDOCK (version 2.2)	Dominguez et al., J. Am. Chem. Soc (2003); Zundert et al., J. Mol. Biol. (2016)
ImageJ	Wayne Rasband, NIH, Maryland, USA
LocARNA	Freiburg RNA Tools, IIF, Germany
MC-FOLD	Institute For Research In Immunology And Cancer, Montreal, France
MEME	MEME Suite, Timothy L. Bailey et al., Nucleic Acids Res, 2009
Microsoft Office (Word, Excel)	Microsoft, Redmont, USA
Primer-BLAST	National Center for Biotechnology Information, Bethesda, USA
PyMOL (version 2.5)	The PyMOL Molecular Graphics System, Version 2.0 Schrödinger, LLC

R (version 4.0.4)	Open-source
R studio (version 1.4.1106)	Open-source
Softmax Pro 7.0	Molecular Devices, San Jose, USA

4.1.4. Antibodies

Antibodies	Source
6x-His Tag Monoclonal Antibody (4E3D10H2/E3)	Thermo Fisher Scientific, Waltham, USA (Cat # MA1-135)
CD44 (8E2) Mouse-anti-Human antibody	Cell Signaling, Massachusetts, USA (Cat # 5640)
CD44v6 (VFF-18) Mouse-anti-Human antibody, FITC-labeled	Bio-Rad, Herkules, USA (Cat # MCA5950F)
Horse-anti-mouse IgG, HRP-linked secondary antibody	Cell Signaling, Massachusetts, USA (Cat # 7076)
AffiniPure Donkey Anti-Mouse IgG (H+L) secondary antibody, FITC-labeled	Jackson ImmunoResearch Laboratories Inc., Cambridge, UK
Fc Receptor Binding Inhibitor Polyclonal Antibody, eBioscience	Thermo Fisher Scientific, Waltham, USA

4.1.5. Cell lines and bacterial cells

Cell lines	Characteristics
Hek 293T	Human embryonic kidney cell line
UPCI-SCC-040	Human squamous cell carcinoma cell line
UD-SCC-2	Human squamous cell carcinoma cell line
Capan 1	Human pancreatic adenocarcinoma cell line
MiaPaCa 2	Human pancreatic adenocarcinoma cell line
Panc 1	Human pancreatic adenocarcinoma cell line
Bacterial cells	
E. coli; Subcloning Efficiency™ DH5α Competent Cells	Thermo Fisher Scientific, Waltham, USA

4.1.6. Plasmids

Plasmids	Source
Human CD44 ORF mammalian expression plasmid, N-His tag	Sino Biological Inc., Peking, China (Cat # HG12211-NH)
pcDNA™ 3.1 (+) mammalian expression vector	Thermo Fisher Scientific, Waltham, USA (Cat # V79020)

4.1.7. Enzymes and kits

Enzymes and kits	Source
FastDigest BamHI	Thermo Fisher Scientific, Waltham, USA
FastDigest EcoRI	Thermo Fisher Scientific, Waltham, USA
Hi Yield® Plasmid Mini DNA Isolation Kit	Süd-Laborbedarf GmbH, Gauting, Germany
Klenow Fragment (10 U/μL)	Thermo Fisher Scientific, Waltham, USA
Proteinase K, recombinant, PCR grade	Thermo Fisher Scientific, Waltham, USA
QIAGEN Plasmid Midi Kit	Quiagen, Hilden, Germany
QIAquick PCR Purification Kit	Quiagen, Hilden, Germany
Qubit™ Protein Assay Kit	Thermo Fisher Scientific, Waltham, USA
QUIAEX II (Gel Extraction Kit)	Quiagen, Hilden, Germany
REDTaq® ReadyMix™ PCR Reaction Mix	Merck, Darmstadt, Germany
RevertAid RT Reverse Transcription Kit	Thermo Fisher Scientific, Waltham, USA
RiboLock RNase Inhibitor (40 U/μL)	Thermo Fisher Scientific, Waltham, USA
RNase A (10mg/ml)	Quiagen, Hilden, Germany
RNase H (5U/μl)	Thermo Fisher Scientific, Waltham, USA
RNase free DNase I (1U/μl)	Thermo Fisher Scientific, Waltham, USA
T7 DNA Ligase	New England Biolabs, Massachusetts, USA
T7 RNA Polymerase (20U/μl)	Thermo Fisher Scientific, Waltham, USA
ZR small-RNA PAGE Recovery Kit	Zymo Research Europe GmbH, Freiburg, Germany

4.1.8. Chemicals and reagents

Chemicals and reagents	Source
5Fluorouracil (500mg)	Pharmacy KUM, Großhadern, Germany
5Fluoro-UTP (100mM)	Jena bioscience, Jena, Germany
Acid-Phenol:Chloroform, pH 4.5 (with IAA, 125:24:1)	Thermo Fisher Scientific, Waltham, USA

Agarose SERVA (gel electrophoresis)	SERVA, Heidelberg, Germany
Albumine fraction V (Bovine serum albumin, BSA)	Carl Roth GmbH + Co. KG, Karlsruhe, Germany
Ammonium Acetate	Sigma-Aldrich, St. Louis, USA
Ammonium persulfate (APS)	Sigma-Aldrich, St. Louis, USA
Ampicillin sodium salt, CELLPURE® ≥91 %	Carl Roth GmbH + Co. KG, Karlsruhe, Germany
Beta-mercaptoethanol	Sigma-Aldrich, St. Louis, USA
Boric acid	Sigma-Aldrich, St. Louis, USA
Bromophenol blue	Sigma-Aldrich, St. Louis, USA
Cyanin-3-hydrazid	Lumiprobe, Hannover, Germany
Dimethylformamid (DMF)	Carl Roth GmbH + Co. KG, Karlsruhe, Germany
Dimethylformamid (DMSO)	Carl Roth GmbH + Co. KG, Karlsruhe, Germany
Dithiothreitol (DTT)	Thermo Fisher Scientific, Waltham, USA
DNA loading dye (6X)	Thermo Fisher Scientific, Waltham, USA
dNTPs, 10mM	Thermo Fisher Scientific, Waltham, USA
Dulbecco's Modified Eagle's Medium (DMEM), high glucose with L-glutamine	Sigma-Aldrich, St. Louis, USA
EDTA Solution (0,5M), pH 8.0	Thermo Fisher Scientific, Waltham, USA
Ethanol for molecular biology	Merck, Darmstadt, Germany
Fetal Bovine Serum (FBS)	Sigma-Aldrich, St. Louis, USA
Formamide, Deionized	Sigma-Aldrich, St. Louis, USA
GeneRuler 100bp Plus DNA Ladder	Thermo Fisher Scientific, Waltham, USA
GeneRuler Low Range DNA Ladder (10-1000bp)	Thermo Fisher Scientific, Waltham, USA
Gibco™ Opti-MEM™ I Reduced Serum Medium	Thermo Fisher Scientific, Waltham, USA
Glycerol	Carl Roth GmbH + Co. KG, Karlsruhe, Germany
Glycine	Carl Roth GmbH + Co. KG, Karlsruhe, Germany
HisPur™ Ni-NTA Resin	Thermo Fisher Scientific, Waltham, USA
Hydrochloric acid, ROTIPURAN® 37 % fuming, p.a., ACS, ISO	Carl Roth GmbH + Co. KG, Karlsruhe, Germany
IGEPAL® CA-630 (Nonidet P-40)	Sigma-Aldrich, St. Louis, USA
Imidazole	Merck, Darmstadt, Germany
Kanamycin Sulfate - Calbiochem	Merck, Darmstadt, Germany
LB agar (Lennox)	Carl Roth GmbH + Co. KG, Karlsruhe, Germany
LB medium Luria/Müller	Carl Roth GmbH + Co. KG, Karlsruhe, Germany
Lipofectamine™ 2000 Transfection Reagent	Thermo Fisher Scientific, Waltham, USA
Low range ssRNA Ladder (50-1000bp)	New England Biolabs, Massachusetts, USA
Magnesium acetate	Sigma-Aldrich, St. Louis, USA
Magnesium chloride	Carl Roth GmbH + Co. KG, Karlsruhe, Germany
Methanol	Merck, Darmstadt, Germany

MTT, (3-(4,5-dimethylthiazol-2-yl)-2,5-diphenyl tetrazolium bromide)	Sigma-Aldrich, St. Louis, USA
NTP set (ATP, CTP, GTP, UTP, 100mM)	Thermo Fisher Scientific, Waltham, USA
Nuclease free water	Ambion, Naugatuck USA
PageRuler Plus™ prestained Protein Ladder	Thermo Fisher Scientific, Waltham, USA
Penicillin/Streptomycin (100 IU Penicillin, 100µg/ml Streptomycin)	Sigma-Aldrich, St. Louis, USA
Phosphate-buffered-saline (1x, PBS)	Sigma-Aldrich, St. Louis, USA
Pierce™ ECL Western Blotting Substrate	Thermo Fisher Scientific, Waltham, USA
Pierce™ Phosphatase Inhibitor Tablets	Thermo Fisher Scientific, Waltham, USA
Pierce™ Protease Inhibitor Tablets	Thermo Fisher Scientific, Waltham, USA
PMSF Protease Inhibitor	Thermo Fisher Scientific, Waltham, USA
Poly(ethylene glycol), BioUltra, 4,000	Sigma-Aldrich, St. Louis, USA
Potassium chloride	Carl Roth GmbH + Co. KG, Karlsruhe, Germany
Propidium iodide	Sigma-Aldrich, St. Louis, USA
Ribonucleoside Vanadyl Complex	New England Biolabs, Massachusetts, USA
RNase exitus	VWR International GmbH, Ismaning, Germany
ROTIPHORESE®NF-Acrylamid/Bis-Lösung 30	Carl Roth GmbH + Co. KG, Karlsruhe, Germany
Sodium acetate	Carl Roth GmbH + Co. KG, Karlsruhe, Germany
Sodium acetate (3M), pH 5.2	Thermo Fisher Scientific, Waltham, USA
Sodium azide	Carl Roth GmbH + Co. KG, Karlsruhe, Germany
Sodium chloride	Carl Roth GmbH + Co. KG, Karlsruhe, Germany
Sodium deoxycholate	Sigma-Aldrich, St. Louis, USA
Sodium dodecyl sulfate pellets (SDS)	Carl Roth GmbH + Co. KG, Karlsruhe, Germany
Sodium hydroxide pellets	Merck, Darmstadt, Germany
Sodium periodate	Honeywell, Charlotte, USA
SYBR™ Green II RNA Stain	Thermo Fisher Scientific, Waltham, USA
SYBR™ Safe DNA Gel Stain	Thermo Fisher Scientific, Waltham, USA
Tetramethylethylenediamine (TEMED)	Carl Roth GmbH + Co. KG, Karlsruhe, Germany
TRIS base	Carl Roth GmbH + Co. KG, Karlsruhe, Germany
Triton™ X-100	Sigma-Aldrich, St. Louis, USA
Trypan blue solution 0.4%	Sigma-Aldrich, St. Louis, USA
Trypsin-EDTA solution (10x)	Sigma-Aldrich, St. Louis, USA
Tween®20	Carl Roth GmbH + Co. KG, Karlsruhe, Germany
Xylene Cyanol	Carl Roth GmbH + Co. KG, Karlsruhe, Germany

4.1.9. Buffers and solutions

Solution	Composition
Cell culture medium	
Dulbecco's Modified Eagle's Medium (DMEM)	500ml
Fetal Bovine Serum (FBS)	10% (v/v)
Penicillin/Streptomycin (100 IU Penicillin, 100µg/ml Streptomycin)	1% (v/v)
Flow cytometry (FC) buffer	
MgCl ₂	5mM
BSA	1% (w/v)
Sodium azide	0,05% (w/v)
PBS	to 500ml
LB-Medium	
LB-Medium Luria/Müller	12,5g
dd H ₂ O	500ml
LB Agar plates (Ampicillin or Kanamycin)	
LB Agar Lennox	10g
dd H ₂ O	250ml
	autoclave and let cool to 45°C
Ampicillin or	50µg/ml
Kanamycin	25µg/ml
	plate out in dishes
TSS	
Polyethylene.glycol 4000	5g
DMSO	2,5ml
MgCl ₂	300mg
LB-Medium	to 50ml
Lysis buffer	
Tris-HCl, pH 7.4	50mM
NaCl	150mM
Nonidet P-40	1% (v/v)
Sodium deoxycholate	0,25% (w/v)
Protease inhibitor	1X
Phosphatase inhibitor	1X

Protein wash buffer	
Tris-HCl, pH 8	20mM
NaCl	300mM
Imidazole	20mM
Glycerol	10% (v/v)
Protease inhibitor	1X
Phosphatase inhibitor	1X
Protein elution buffer	
Tris-HCl, pH 8	12mM
NaCl	180mM
Imidazole	250mM
Protease inhibitor	1X
Phosphatase inhibitor	1X
Protein storage buffer	
Tris-HCl, pH 8	50mM
KCl	200mM
EDTA	0,1mM
PMSF	0,5mM
DTT	1mM
Laemmli buffer (4X), pH 6.8	
Tris base	125mM
SDS	2% (w/v)
Glycerol	10% (v/v)
Bromophenol blue	0,5% (w/v)
Beta-mercaptoethanol	2% (v/v)
TRIS-Glycine-SDS (10X) running buffer, pH 8.0	
Tris base	250mM
Glycin	1,9M
SDS	35mM
Transfer buffer	
TRIS-Glycine-SDS (1X) running buffer, pH 8.0	80ml
Methanol	20ml
TBS-T (10X), pH 7.3	

Tris base	0,1mM
NaCl	1,5M
Tween®20	0,5% (v/v)
Nucleic acid diffusion buffer	
Ammonium acetate	0,5M
Magnesium acetate	10mM
EDTA	1mM
SDS	0,1% (w/v)
SELEX buffer (1X) [74]	
Tris-HCl, pH 7.4	50mM
NaCl	150mM
MgCl ₂	1mM
Nonidet P-40	0,05% (v/v)
Ribonucleoside Vanadyl Complex	10mM
Proteinase K buffer [74]	
SDS	0,5% (w/v)
EDTA, pH 8	4mM
RIPA lysis buffer	
Tris base, pH 8	50mM
NaCl	150mM
Triton™ X-100	1% (v/v)
Sodium deoxycholate	0,5% (w/v)
SDS	0,1% (w/v)
Propidium iodide (PI) staining solution	
in PBS	
Triton™ X-100	0,1% (v/v)
Propidium iodide	10µg/ml
RNAse A (DNAse free)	100µg/ml
2X RNA loading dye	
Formamide	95% (v/v)
SDS	0,02% (w/v)
Bromophenol blue	0,02% (w/v)
Xylene Cyanol	0,02% (w/v)
EDTA	1mM

4.2. Cell culture conditions

All steps involving handling of the cultured cells were performed under a laminar flow hood maintaining sterile conditions. Buffers and chemicals were used and stored according to the manufacturer's instructions. For routine culture cells were kept in TC flasks with filter caps in 12ml of cell culture medium at 37°C and 5 vol% CO₂. Before harvesting of adherent cultures for splitting or assays, cells were washed with 1x PBS, covered with 2.5ml of 1x Trypsin and incubated at 37°C for different timespans (depending on cell line). Trypsin activity was blocked by adding 7.5ml of culture medium and detached cells were collected and transferred to 15ml-Falcon tubes. The cell suspension was pelleted by centrifugation for 5min at 200g at room temperature, the supernatant was discarded, and the cells were resuspended in suitable amounts of medium or buffer. For counting, an aliquot of cell suspension was mixed with Trypan blue reagent in a 1:1 ratio and 10µl were transferred to a Neubauer counting chamber. Cells in grid quadrants were counted under an optical microscope. For the generation of frozen stocks, cells were grown until 90% of confluency, harvested, spun down, resuspended in FBS + 10% DMSO, aliquoted into cryovials and frozen to -80°C in an isopropanol chamber. For long-term storage cells were transferred to a freezer at -150°C. When reculturing frozen cell stocks, cells were quickly thawed in a 37°C water bath, transferred to 10ml pre-warmed culture medium, spun down and resuspended in a suitable amount of fresh culture medium.

4.3. Flow cytometry

For flow cytometry assays, cells were harvested, counted, and transferred to standard Eppendorf vials (500 000 cells per tube). All further steps were performed at 4°C, centrifugation conditions were set at 200g for 5min, and the incubation was carried out on a shake plate (1000rpm) in the dark. Cells were washed with 300µl of FC buffer and treated with Fc receptor inhibitor for 20min. Cells were spun down and resuspended in 100µl of FC buffer-diluted antibody.

- For the CD44v6 evaluation, a murine monoclonal antibody (VFF-18) labeled with FITC was used in 1:50 dilution. Cells were incubated for 45min, followed by 3-5 washing steps with 300µl FC buffer. The final pellet was resuspended in 300µl of FC buffer and immediately analyzed by flow cytometry. Cells that were treated with 100µl of FC buffer instead of antibody served as control.
- For CD44s evaluation, an unlabeled murine monoclonal primary antibody (8E2) was used in 1:400 dilution. Cells were incubated for 45min, followed by 3-5

washing steps with 300µl FC buffer. The final pellet was resuspended in 100µl of a 1:200 dilution of a monoclonal donkey anti-mouse secondary antibody with FITC-label. The final pellet was resuspended in 150µl FC-buffer and immediately analyzed by flow cytometry. Cells that were treated with 100µl of only secondary antibody served as control.

For readout, the flow cytometer machine (Accuri C6 Plus, BD Biosciences) was used. Cell samples were read until 150µl fluid had passed in medium fluidics (35µl/min) and the FITC-signal was evaluated through the FL-1 filter.

FCS express by DeNovo software was used for the gating of FSC/SSC and FSC-a/FSC-h to filter for dead cells and doublets. The fluorescence intensity of the gated samples and controls was evaluated, and the adapted resolution metric [109] (GeoRD) was calculated using geometric mean and geometric standard deviation:

$$\text{GeoRD} = \frac{\text{geometr.mean (sample)} - \text{geometr.mean (control)}}{\text{geometr.SD (sample)} * \text{geometr.SD (control)}}$$

GeoRD values were compared between the correspondingly treated cell lines using the unpaired t test (two groups) or one-way ANOVA with Turkey post hoc correction for multiple comparisons (>2 groups). Statistical calculation was performed using the GraphPad Prism 9 software and plotting was performed using open-source R Studio.

4.4. SDS-PAGE and Western blot

For the separation of proteins, an SDS-PAGE minisystem was used. The gels were prepared with a 10% separating phase and a 4% stacking phase, 1,5mm thickness and 10 pockets. Protein samples were mixed with Laemmli buffer and heated to 95°C for 5min prior to loading. The gels were run in 1X TRIS-Glycine-SDS at 70V (constant) for 30min, followed by 125V (constant) for 1h.

The blotting was performed semi-dry in TRIS-Glycine-SDS-Methanol at 25V for 30min. The membranes were blocked with 5% BSA in 1X TBS-T for 1h at room temperature. Primary antibodies were diluted to working concentrations in 1% BSA in 1X TBS-T and applied to the membrane for 1h at room temperature or 12h at 4°C. Subsequently, the membranes were washed 3 times with 1X TBS-T. Secondary antibodies were diluted to working concentrations in 1% BSA in 1X TBS-T and applied to the membrane for 1h at room temperature. The membranes were washed for another 3x with 1X TBS-T and developed with ECL substrate. The HRP signal was evaluated by Fusion Fx Vilber Lourmat with exposure times optimized by the machine software.

4.5. Bacterial plasmid expansion

All steps including bacteria were conducted in a clean environment in proximity to a Bunsen burner providing constant upward airflow. DH5- α - E. coli bacteria were expanded in LB medium, collected by centrifugation at 3000g for 5min at 4°C and resuspended in 200 μ l TSS solution to ensure chemical competence (cc). The stocks of cc E. coli were stored at -80°C. For amplification of a plasmid vector, an aliquot of cc DH5- α - E. coli bacteria were thawed slowly (on ice). Up to 500ng of plasmid was added and the bacteria were heated for 2min at 42°C, then kept on ice for 30min. After expansion in 1ml of fresh LB medium at 37°C for 2h shaking at 1200rpm, the bacterial culture was plated on agar plates with suitable selection conditions (Ampicillin or Kanamycin). Bacteria plates were cultured overnight in an incubator at 37°C. Single clone colonies were picked and transferred to 10ml of LB medium in Falcon round bottom polypropylene tubes with a cap. Depending on desired amount of plasmid,

the clones were cultured at 37°C shaking at 200rpm for either

- 12h, followed by plasmid cleanup according to the HiYield Plasmid Mini DNA Kit (SLG) or
- 4h, followed by scale-up culture in 100ml LB-medium in a 250ml conical flask overnight and consecutively by purification of plasmids according to the Plasmid MIDI Kit (QUIAGEN)

The plasmids were eluted in water and their concentration and purity were assessed using the SpectraDrop microplate reader. The aliquots were stored at -20°C.

4.6. Mammalian CD44 protein expression

A human CD44 ORF mammalian expression plasmid with a N-His tag was purchased from Sino Biological Inc. and amplified following the bacterial plasmid expansion protocol (4.5.). The plasmid contained the genetic code for the whole CD44 protein including all exon variants (v2-v10), which was verified by sequencing (Eurofins Genomics sequencing service). The mammalian expression system was used to maintain possible posttranslational modifications to the CD44 protein. A fresh aliquot of frozen human embryonic kidney cells (Hek 293T, P5) was seeded, passaged 3 times, and grown to 80% confluency under general cell culture conditions (4.2.). 30 μ g of CD44-plasmid and 75 μ l of Lipofectamine 2000 were mixed dropwise in 4ml of OptiMEM medium and carefully added per flask of Hek 293T cells. Cells were kept in this medium mix for 24h, then washed with OptiMEM and kept in 10ml OptiMEM. The medium was collected after

2 and 4 days. On the 4th day the cells were treated with lysis buffer, collected in a tube, and sonicated. Cell debris was separated by centrifugation at 20 000g for 20min at 4°C. In the next step, 2ml of Ni-NTA agarose beads were transferred to a 10ml Pierce Spin column with filter and equilibrated with 6 bed volumes of Protein wash buffer. Hek 293T cell lysate was added and incubated with beads for 1h at 4°C with agitation. Then, the fractions of the collected media were passed through the resin. The beads were washed with 9 volumes of Protein wash buffer. After that, 2ml of Protein elution buffer were added and elution flowthrough was collected in 10 fractions. To identify the elution fractions with the highest protein enrichment, Western blot analysis of the fractions was performed with 1:1000 anti His-tag primary antibody for 1h at room temperature and 1:10 000 HRP-linked secondary antibody for 1h at room temperature. The ones with the highest protein content were pooled, and buffer exchange to Protein storage buffer was performed using Zeba Spin Desalting Columns. The final protein concentration was quantified by Qbit fluorometry. The protein aliquots were stored at -80°C.

4.7. The SELEX-cycle

The protocol for the SELEX cycle was based on the setting proposed in 'SELEX to identify protein binding sites on RNA' by James L. Manley [74]. The CD44 protein that was generated by mammalian expression was used for aptamer selection. It was supposed to carry all CD44 exon variants (v2-v10) and post-translational modifications typical for eukaryotic systems. SELEX was performed for **12 cycles** in total, the first 6 rounds following the basic protocol, and then 6 rounds following the advanced protocol. The whole process was carried out in two identical replicate set of conditions (H1 and H2). Sequence details for all SELEX-primers and oligonucleotides can be found in 8.1. (**Supplement 1**).

All steps involving handling of RNA were conducted under conditions that minimize the risk of RNase-contamination. Only RNase-free chemicals and filtered pipet tips were used, and instruments and working surfaces were cleaned with RNase-Exitus Plus.

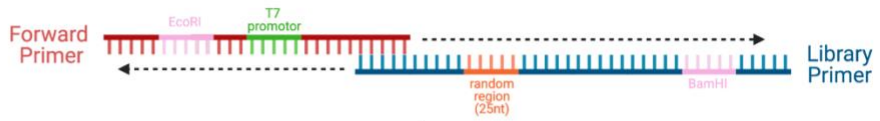
4.7.1. Overview

The following scheme gives insight into the sequence composition of primers and sums up all individual steps of one SELEX cycle. Detailed information about each step, especially the selection process, will be provided in the corresponding chapters.

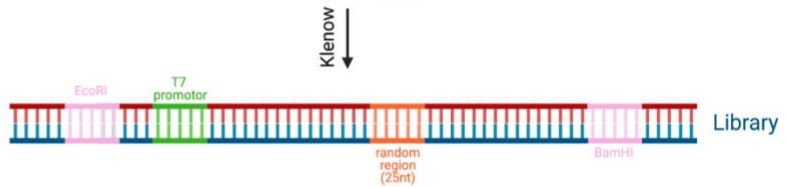
1. ssDNA-library containing region of 25 random nucleotides



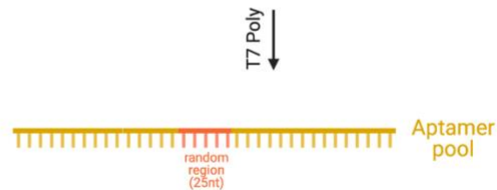
2. Elongation of library



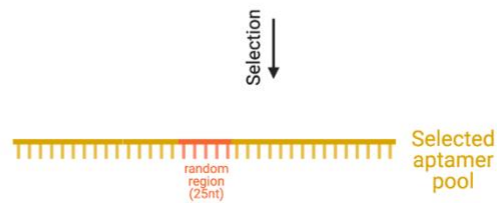
3. dsDNA-SELEX library



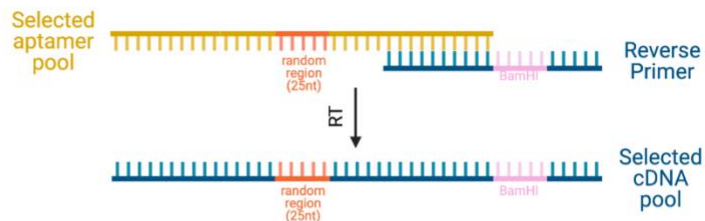
4. Transcription of library to RNA-aptamer pool



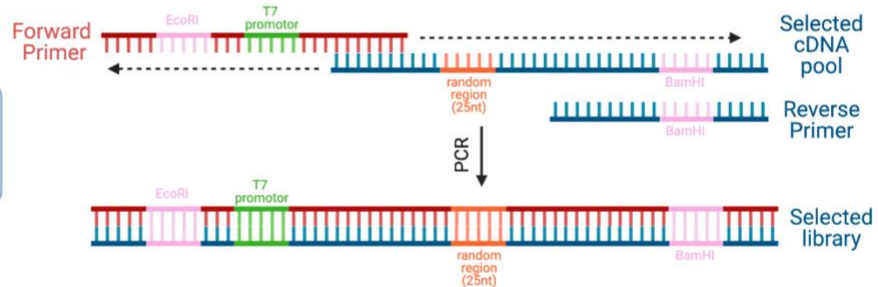
5. Selection for sequences with desired binding properties



6. Reverse transcription to cDNA pool



7. PCR of selected cDNA pool



8. Transcription of selected library for next selection cycle

...

Figure 5. Schematic representation of the SELEX process: A DNA library containing a region of 25 random nucleotides served as the template for generation of a pool of random RNA aptamers. Those aptamers were subjected to a selection process, and sequences showing desired properties were retrieved and used to regenerate a (1x selected) library. This library served as a template for the next SELEX cycle [110].

4.7.2. Library pool preparation

Library Primer 18_25	5'	CGGGGATCCATGGGCACTATTTATATCAACN ₂₅ AATGTCGTTGGTGGCCC	3'
Forward Primer 17_24	5'	CGCGAATTCTAATACGACTCACTATAGGGGCCACCAACGACATT	3'

Table 1. SELEX-library primers

The SELEX library (18_25) and a partially complementary forward primer (17_24) were purchased from Invitrogen in lyophilized form and dissolved in water up to a working concentration of 10µM. The forward primer carried an *EcoRI* restriction enzyme cutting side (blue) and a T7-promotor region (green), which is recognized by the T7-RNA polymerase. The Library primer carried a cutting side of the *BamHI* restriction enzyme (orange) and a region of 25 randomly assembled nucleotides (red). That variable region allows $4^{25} \approx 10^{15}$ possible nucleotide combinations. The primers were annealed and then elongated using the Klenow fragment for 3h at 37°C.

Klenow library elongation	100µl
Klenow buffer (10X, supplied with enzyme)	10µl
Library Primer (10µM) 18_25	8,5µl
Forward Primer (10µM) 17_24	8,5µl
Nuclease free water	63µl
Heat to 75°C	15min
Cool to room temperature, add	
dNTP Mix (2,5mM)	8µl
Klenow Enzyme (10U/µl)	2µl
Incubate at 37°C	3h

This method was chosen over conventional PCR due to the assumption that it would show a lower tendency to favor certain sequences, therefore providing a more uniform distribution of different oligonucleotides in the library pool and a higher efficiency in the generation of double-stranded DNA from single-stranded oligonucleotide templates [111]. The Klenow reaction product was precipitated by adding 1/10 volume of 3M sodium acetate (pH 5.2) and 3 volumes of ethanol. After cooling to -80°C for 30min, the DNA was spun into a pellet by centrifugation at 20 000g for 30min at 4°C. The pellet was dried and resuspended in water. The library DNA was further purified by separation on a 15%-PAGE in 1X TBE buffer and visualized under UV after treatment with 1X SybrSafe DNA Gel Stain in 1X TBE. The correctly sized bands were excised. The DNA was retrieved using the Quiaex II gel extraction kit and concentration and purity were assessed on a SpectraDrop microplate reader. Purified DNA library was stored in water at -20°C.

4.7.3. *In vitro* transcription

To generate a pool of RNA aptamer oligonucleotides, *in vitro* transcription of the DNA library was performed using the T7-RNA polymerase enzyme. To prevent RNA degradation by possible RNase contamination, RiboLock RNase inhibitor was added to the reaction.

In vitro transcription	100µl
Transcription buffer (5X, supplied with enzyme)	20µl
DNA template (1,7pmol/µl)	10µl
NTP-Mix (A-, C-, G-, UTPs, 20mM each)	10µl
Nuclease free water	56µl
RiboLock RNase inhibitor (40U/µl)	1µl
T7 RNA polymerase (20U/µl)	3µl
Incubate at 37°C	5h

Subsequently, a DNA digestion step was included by adding of 10µl of RNase free DNase I (2U/µl) and incubation for 30min at 37°C. To terminate the reaction, 5µl of 0,5M EDTA (pH 8.0) was added, and the mixture was heated to 72°C for 5min. The aptamer RNA was precipitated (as described above for DNA) and the pellet was resuspended in

water. For further purification, RNA was mixed 1:1 with 2x denaturation loading dye and linearized by heating to 95°C for 5min and snap-cooling on ice. The reaction product was loaded onto a prewarmed 15% polyacrylamide gel in 1x TBE containing urea at a concentration of 8mol/l and run at a constant voltage of 150V for 1h.

8M Urea gel for RNA separation	10ml
Bis- polyacrylamide (30%)	4,7ml
Urea	4,8g
TBE (10X)	1ml
Water	to 10ml
TEMED	15µl
APS (10%)	50µl
Pre-run at 150V constant	30min

The gel was soaked in 1X SybrGreen II RNA Gel Stain in 1X TBE for 20min at room temperature and visualized under UV light. Correctly sized bands were excised, and RNA was recovered using a RNA-PAGE-Recovery Kit (by Zymo Research). The product was eluted in water and the concentration and purity of the mixture were assessed using a SpectraDrop microplate reader. RNA was stored at -80°C.

For the first SELEX cycle, SELEX buffer was prepared in 1X and 2X composition. 2X SELEX buffer was added 1:1 to the cleaned RNA to obtain a final concentration of 15µM in 100µl. The mixture was heated to 65°C for 5min and slowly cooled to room temperature to ensure proper folding of the aptamers. The possibility of nonenzymatic degradation of RNA by heating above 50°C in presence of Mg²⁺ ions [112] was ruled out by a visual control of RNA integrity on a urea-PAGE, as described above.

4.7.4. Basic selection step

In the first 6 rounds of SELEX, the 'basic' selection was applied. The aptamer library was selected with regard to binding affinity to the whole CD44-protein (bearing variants v2-v10) without forcing specificity for the v6-exon region.

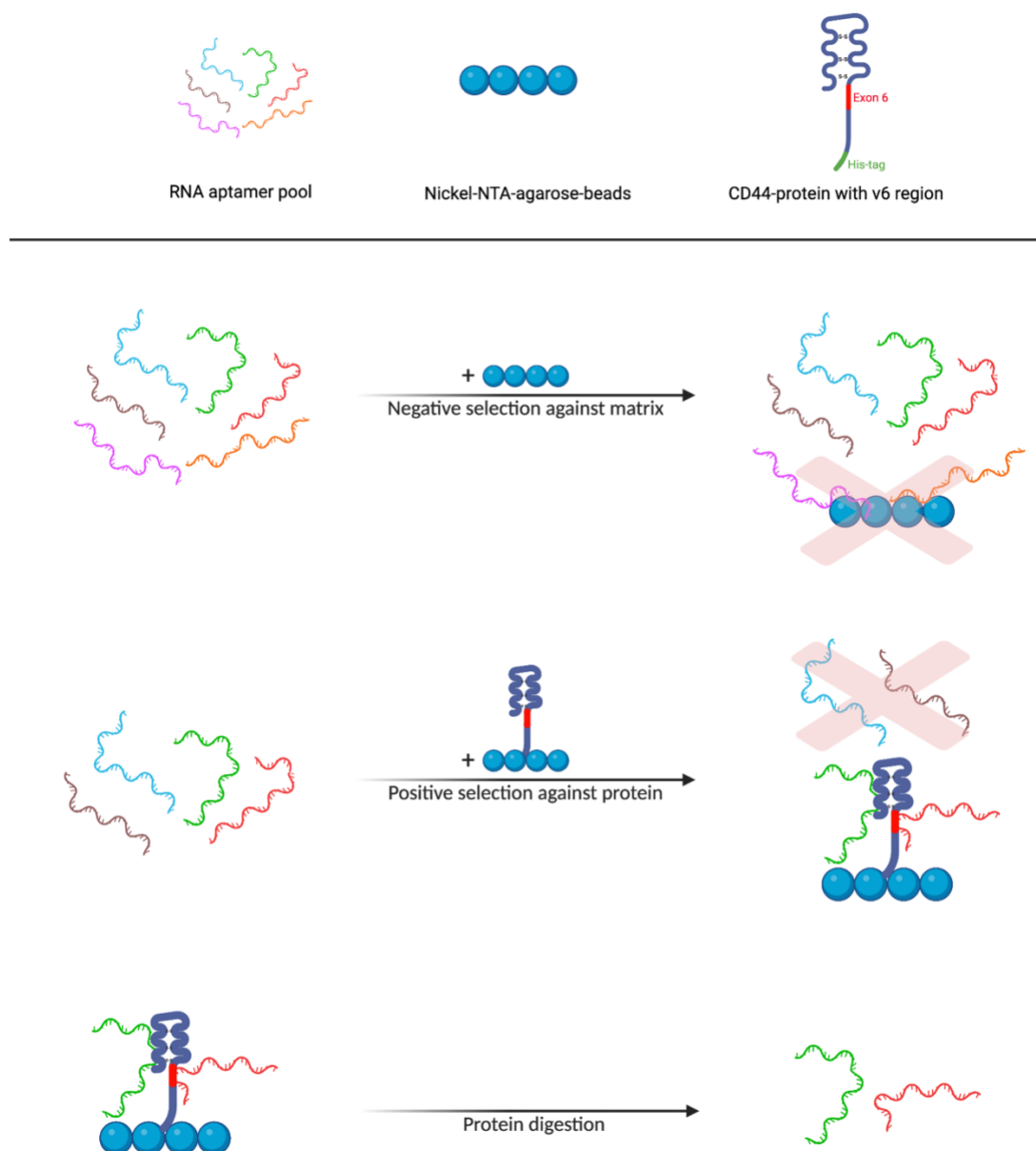


Figure 6. Schematic representation of the basic selection step: The RNA-aptamer pool was precleared against empty Ni-NTA-agarose beads to filter out sequences with matrix avidity. The remaining aptamers were subjected to the actual selection process for binding properties to the CD44 protein. After washing, the protein was digested and bound sequences were retrieved [110].

For the basic selection step of the aptamer pool, 50µl of HisPur Ni-NTA agarose resin beads were transferred to a 1,5ml tube, washed by addition of 250µl of SELEX buffer, and spun for 2min at 2000g at room temperature. The folded RNA library pool (see 4.7.3) was added to the Ni-NTA agarose matrix and incubated at room temperature for 30min on a 1000rpm shaker to keep the beads in suspension. Consecutively, the beads were spun down, and the precleared aptamer pool was collected with the supernatant.

A fresh portion of 50µl of Ni-NTA agarose beads was prepared, washed, and resuspended in 200µl of 1x SELEX buffer. 5µg of purified CD44 protein (with His-tag) from mammalian expression (see 4.6) was added and the mixture was kept at room temperature for 1h at 1000rpm to allow complex formation between His tag and Ni-NTA. The beads were washed 3 times by spinning in 250µl SELEX buffer for 2min at 2000g at room temperature.

The final protein-bead pellet was suspended in the precleared aptamer pool and kept at room temperature for 45min at 1000rpm. Consecutively, the beads were washed 5 times by spinning in 250µl SELEX buffer. The final pellet was suspended in 200µl water. Then, 200µl of 2x Proteinase K buffer and 2,5µl of Proteinase K (600U/µl) were added and the reaction was incubated at 37°C for 20min shaking at 1000rpm. To retrieve the aptamer molecules, 400µl of acidic phenol chloroform in a ratio of 5:1 (pH 4.5) was added to the reaction and the mixture was vortexed for 30s. Centrifugation at 20 000g for 90s separated the reaction into an upper aqueous phase and a lower organic phase. The aqueous phase was collected carefully without disturbing the organic phase and its volume was estimated. RNA was precipitated by adding of 1/10 volume of 3M sodium acetate (pH 5.2) and 3 volumes of 100% ethanol, cooling to -80°C for 30min and centrifuging for 30min at 20 000g and 4°C. The RNA pellet was air-dried, dissolved in 10µl of water, and the concentration and purity were evaluated using a SpectraDrop microplate reader. RNA was stored at -80°C.

Following each selection step, the retrieved aptamer RNA was amplified by RT-PCR (see 4.7.6.) and T7-in vitro transcription (see 4.7.3.) to replenish the aptamer pool for the next selection cycle.

4.7.5. Advanced selection step

In the second 6 rounds of SELEX, an 'advanced' selection method was applied with the aim of forcing the binding specificity of the aptamer pool to the v6 exon region of the CD44 protein. The overall setup was identical to the previously described protocol, with the addition of one antibody in a subset of selection rounds.

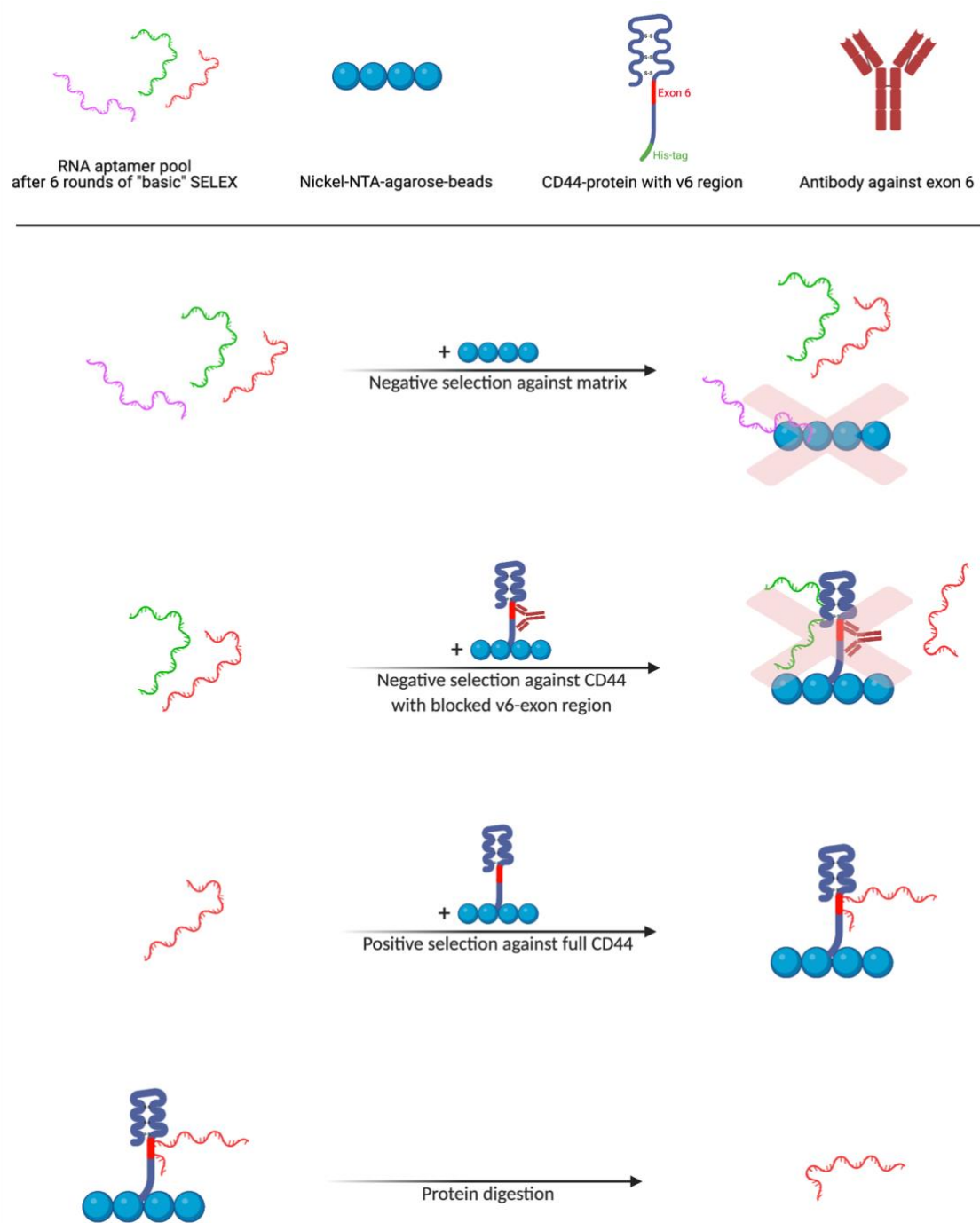


Figure 7. Schematic representation of the advanced selection step: The RNA-aptamer pool was precleared against empty Ni-NTA agarose beads, followed by a second negative selection step against full CD44 with the v6 exon region blocked by a specific antibody. Subsequently, a positive selection step was performed against unblocked CD44, the protein was digested and the bound sequences were recovered [110].

For the advanced selection protocol, the RNA aptamer pool was prepared as described in 4.7.3. and precleared against the empty matrix (see 4.7.4.). In a separate tube, Ni-NTA beads loaded with CD44 protein were prepared as previously described, but after washing they were resuspended in 200µl of SELEX buffer and 5µg of CD44v6-specific antibody (VFF-18 clone) were added. The mixture was kept at room temperature for

45min at 1000rpm to allow proper antibody binding, and then washed 3 times by being spun in 250µl of SELEX buffer. Subsequently, the aptamer pool was added, and the mixture was incubated at room temperature for 30min at 1000rpm. The beads were spun down, the supernatant with negatively selected aptamers was collected and immediately applied to a positive selection step against the full, unblocked CD44 protein as described in the basic selection protocol. Bound RNA was retrieved, amplified, and prepared for the next selection cycle (see 4.7.4.).

4.7.6. Pool replenishment

Reverse Primer (17_25)	5'	CCCGACACCGCGGGATCCATGGGCACTATTTATATCAA	3'
------------------------	----	--	----

Table 2. Reverse SELEX-primer

After each selection step, enriched RNA aptamers were amplified before being subjected to the next round of SELEX. In order to achieve this, reverse transcription was performed using the RevertAid First Strand cDNA Synthesis Kit (by Thermo Fisher). A reverse primer (17_25) was purchased from Invitrogen in lyophilized form and adjusted to 10µM working concentration in water. The reverse primer carried a cutting side of the *BamHI* restriction enzyme (orange). The RT reaction was prepared as described in the kit protocol.

Reverse transcription	20µl
RNA after selection (approx. 25µM)	1µl
Reverse Primer (10µM) 17_25	1,5µl
Nuclease free water	10µl
Heat to 65°C	5min
Snap cool on ice, add	
5X RT-buffer	4µl
dNTP Mix (10mM)	2µl
Ribolock (20U/µl)	0,5µl
Reverse transcriptase (200U/µl)	1µl
Incubate at room temperature	10min
Incubate at 42°C	1h

The reaction was heat inactivated for 15min at 70°C, followed by digestion of RNA by addition of 0,5µl of RNase H (5U/µl) and incubation at 37°C for 20min. The generated cDNA was diluted from the reaction mixture (1:20 in water) and immediately amplified in a PCR reaction.

SELEX PCR reaction	150µl
Nuclease free water	60µl
REDTaq® ReadyMix™ (Sigma Aldrich)	75µl
Forward Primer (10µM) 17_24	4,5µl
Reverse Primer (10µM) 17_25	4,5µl
Aptamer-cDNA (1:20)	6µl

The PCR reaction mixture was separated in PCR-strips and run on a cycler. The optimal annealing temperature settings were evaluated empirically by gradient PCR.

SELEX PCR settings		
95°C	5min	
95°C	30s	x 35
50°C	30s	
72°C	30s	
72°C	10min	
4°C	hold	

The PCR product was loaded onto a 3% agarose gel in 1X TBE containing 1X SybrSafe DNA Gel Stain and ran at constant 70V for 1h. The DNA was visualized under UV light and the bands were excised and recovered using the Quiaex II gel extraction kit. The DNA was eluted in water and concentration and purity were assessed using a SpectraDrop microplate reader. It was stored at -20°C. From this DNA product, in vitro transcription could be performed (as described in 4.7.3.) to prepare the RNA aptamer pool for the following selection step.

4.7.7. Aptamer cloning for sequence readout

After 12 rounds of SELEX (6 rounds following the basic selection protocol, then 6 rounds following the advanced selection protocol), a population of aptamers was enriched. To separate individual aptamer sequences and read the genetic code, a cloning approach was implemented. The plasmid vector pcDNA3 with a resistance gene to ampicillin was purchased from Invitrogen.

After 12 rounds of SELEX, the RNA-aptamer pool was transformed into DNA by RT-PCR (see 4.7.6.). After that, every oligonucleotide was carrying an *EcoRI* and a *BamHI* restriction enzyme cutting side. The same cutting sides can be found on the plasmid in close proximity to each other. 2µg of aptamer DNA and 2µg of pcDNA3 plasmid were individually subjected to a double digestion using FD-*EcoRI* and FD-*BamHI* restriction enzymes (by Thermo Fisher Scientific).

Restriction enzyme digestion	50µl
Aptamer DNA/Plasmid DNA	2µg
10X FD-buffer (supplied with enzyme)	5µl
FD- <i>EcoRI</i>	2,5µl
FD- <i>BamHI</i>	2,5µl
Nuclease free water	to 50µl
Incubate at 37°C	20min

After heat inactivation at 75°C for 5min, a portion of digested aptamer DNA was loaded onto a 3% agarose gel in 1XTBE containing 1X SybrSafe DNA Gel Stain and digested plasmid-DNA was loaded onto a 1% agarose gel, correspondingly. Undigested controls were included for each step to see a small band-shift, indicating successful DNA-aptamer digestion and plasmid linearization, indicating successful plasmid digestion. The DNA was visualized under UV light. The digested aptamer and plasmid DNA were purified using the QIAquick PCR Purification Kit (by Quiagen). The DNA was eluted in water and concentration and purity were assessed using a SpectraDrop microplate reader.

For the ligation reaction, digested aptamer DNA and digested plasmid DNA were mixed in a molar ratio of 2:1.

Ligation	50µl
Digested aptamer/plasmid DNA (2:1)	24µl
2X Ligation buffer (supplied with enzyme)	24µl

T7 DNA Ligase	2µl
Incubate at room temperature	40min

Chemically competent DH5- α - E. coli bacteria were prepared as described in 4.5. The ligation reaction mixture was added, and the bacteria were heat shocked and plated on ampicillin-agar plates. The plates were incubated at 37°C overnight. In this setting, each ligated plasmid would carry the information for one single aptamer sequence, and each bacterium would take up only one plasmid, so each single-clone colony would represent one individual aptamer sequence. Following this logic, 40 bacterial colonies were picked, each one was transferred to 10ml of LB medium in round bottom polypropylene tubes with cap, and expanded overnight in a shaking incubator at 37°C and 200rpm. The plasmids of each colony were purified using the HiYield Plasmid Mini DNA kit (by SLG). The purified plasmids were eluted in water and sent to Eurofins Genomics for sequencing (starting from the SP6 promoter of the pcDNA3-plasmid). The conserved T7-promotor region was used as a landmark to locate the aptamer sequences and read the nucleotide code of the variable regions.

4.7.8. Generation of working aptamer molecules

Aptamer Forward Primer	5'	CGCGAATTCTAATACGACTCACT	3'
Aptamer Reverse Primer	5'	GACACCGCGGGATCCAT	3'
Aptamer H1_1 Oligo	5'	CGCGAATTCTAATACGACTCACTATAGGGGCCACCAACGACATTATGGAAGG TAGGAGGAGATTGTCA	3'
Aptamer H2_1 Oligo	5'	CGCGAATTCTAATACGACTCACTATAGGGGCCACCAACGACATTTAAATCAAC ATAGGTGGATGGTGGT	3'
Aptamer H2_2# Oligo	5'	CGCGAATTCTAATACGACTCACTATAGGGGCCACCAACGACATTGACATCAG CCAGGGTGTAGGGGGAG	3'

Table 3. Aptamer oligonucleotides and primers

To regenerate individual aptamer molecules, aptamer-template oligonucleotides and corresponding forward/reverse primer pairs were generated using the NCBI Primer

BLAST tool. Oligonucleotides were obtained from Eurofins Genomics in lyophilized form and dissolved in water to a working concentration of 10 μ M. The oligonucleotides were amplified by PCR.

Aptamer PCR reaction	150 μ l
Nuclease free water	60 μ l
REDTaq® ReadyMix™ (Sigma Aldrich)	75 μ l
Aptamer Forward Primer (10 μ M)	6,5 μ l
Aptamer Reverse Primer (10 μ M)	6,5 μ l
Aptamer-template oligos (10 μ M)	3 μ l

The PCR reaction mixture was separated into PCR strips and run on a cycler. The optimal annealing temperature settings were evaluated by gradient PCR.

Aptamer PCR settings		
95°C		5min
95°C	30s	x 35
52°C	30s	
72°C	30s	
72°C		10min
4°C		hold

Individual working RNA aptamers were generated by in vitro transcription (as described in 4.7.3).

4.8. Aptamer sequence analysis

For comparison of the enriched aptamer sequence codes, two open source online tools were used. The LocARNA-Alignment & Folding tool by Freiburg RNA Tools [113] (<http://rna.informatik.uni-freiburg.de>) allowed multiple alignment of sequences and the generation of a consensus structure. It was run with the default settings except for the RNA folding temperature (25°C instead of 37°C). The second tool used was the MEME suite (version 5.3.3, <https://meme-suite.org/meme/tools/meme>) [114] for discovery of motifs. It was run in classical mode for RNA, any number of motif repetition, the number of motifs to find was set to 16, the 0-order model served as background and motif length span was set from 3 to 25 nucleotides. The calculated E-value was “an estimate of the expected number of motifs with the given log likelihood ratio (or higher), and with the same width and site count, that one would find in a [...] set of random sequences” [115].

4.9. Coupling of Cy3 dye to aptamers

To label aptamer molecules, Cy3 hydrazide fluorescent dye from Lumiprobe was used. The labeling method was based on a nonenzymatic reaction of hydrazide with the oxidized cis-diol of the 3' terminal ribose, similar to the method proposed by Kodzius et al. [116]. The gel-purified working aptamer RNA (prepared as described in 4.7.8.) was adjusted in 100mM sodium acetate (pH 4.5) to a final volume of 90µl and a maximum RNA concentration of 0,25mM. Then, 10µl of freshly prepared 100mM NaIO₄ solution were added, and the mixture was incubated at 4°C in the dark for 2h. RNA was precipitated by adding of 1/10 volume of 3M sodium acetate (pH 5.2) and 3 volumes of 100% ethanol, cooling to -80°C for 30min and centrifuging for 30min at 20 000g and 4°C. The pellet was dried and resuspended in 100mM sodium acetate (pH 6.0). Cy3-hydrazide (dissolved in DMF) was added to a final concentration of 3mM, and the reaction mixture was incubated at 4°C in the dark for 6h. RNA was precipitated, the pellet was washed with 70% ethanol and resuspended in PBS + MgCl₂. Concentration and purity were evaluated using a SpectraDrop microplate reader.

4.10. Evaluation of aptamer specificity by flow cytometry

For flow cytometry assays, aptamers were generated according to 4.7.8. and labeled with Cy3 as described in 4.9. The Cy3 coupled aptamers were suspended in PBS + MgCl₂, linearized by heating to 65°C for 5 min and slowly cooled to room temperature, allowing proper folding. Following that step, log dilution rows in FC buffer were prepared.

Cells cultured from different cell lines were harvested and washed as described in section 4.3. After washing, the cell suspension was subjected to 20min of blocking at 4°C by 100µl of highly concentrated SELEX library RNA (transcript of SELEX template from round 0 consisting of unselected, random aptamer sequences). The cells were washed 1x with FC buffer and suspended in 100µl of log dilution rows of Cy3 labeled aptamers and incubated for 45min at room temperature on a shaker in the dark. Following incubation, cells were washed 7x with 300µl FC buffer and the finally suspended in 300µl of buffer. As a control, cells were treated with pure Cy3 dye in FC buffer at equimolar concentrations under the same conditions.

For readout, the flow cytometer machine (Accuri C6 Plus, BD Biosciences) was used. Cell samples were read until 150µl fluid had passed in medium fluidics (35µl/min) and the Cy3 signal was evaluated through the FL-1 filter.

FCS express by DeNovo software was used for the gating by FSC/SSC and FSC-a/FSC-h to filter for dead cells and doublets. The median fluorescent intensity was evaluated and corrected for the intensity signal of the control treatment with equimolar, pure Cy3. The data were normalized to the percentage of change over control considering the highest control signal as 100%. Data were plotted and the area under the curve (AUC) was evaluated for each biological replicate. The AUC values were compared using an unpaired t-test. Statistical calculations and plots were made using the GraphPad Prism 9 software.

4.11. UV-crosslinking of aptamer RNA to cellular CD44

To ensure a sufficient amount of cells, MiaPaCa2 cells were harvested at high confluency and 300 000 cells were seeded per well of a 6-well tissue culture plate. Cells were incubated for 24h to achieve optimal adherence.

A very high amount of aptamer RNA was prepared as described in to 4.7.8. and diluted in PBS + 5mM MgCl₂ to 500µl and a concentration of 20µM. The aptamers were heated to 65°C for 5 min and slowly cooled to room temperature to ensure proper folding. The

same amount of SELEX library RNA (transcript of SELEX-template from round 0 consisting of random unselected aptamer sequences) was generated as control.

Cells were washed 1x with PBS and covered with 500µl of aptamer suspension, library RNA suspension or PBS + 5mM MgCl₂ as controls. The plate was incubated for 45min at room temperature on a shaker. After that, it was directly placed on ice and transferred under a sterilization UV-lamp (UVC30, 230V, 50Hz, 0,14A, 2x15W, 254nm) with a distance of 10cm from the UV-bulbs. The plate was irradiated for 10min on ice (without cover).

Following that step, the supernatant was discarded, and cells were lysed using 200µl RIPA lysis buffer per well. The lysate was kept on ice for 10min, then subjected to vigorous sonication to break up the cell membranes. The lysate was kept on ice for an additional 10min, thoroughly vortexed and centrifuged at 20 000g for 15min at 4°C. The supernatant was collected, and the protein concentration was measured by Qbit fluorometry. Cell lysates from aptamer treatment, control SELEX library RNA treatment and control PBS + 5mM MgCl₂ treatment were loaded and run on an SDS-PAGE gel as described in 4.4. After the run, the gel was soaked in 50ml of running buffer with addition of 5µl of 10 000X SybrGreen II RNA stain for 30min at room temperature on a shaker in darkness. The RNA signal was visualized in a UV transilluminator (>5s of exposure time was required). The gel was then blotted and stained for CD44s as described in 4.4. The signals of RNA and CD44s from the gel and the blot were optimized with ImageJ and compared by overlapping the images using the ladder signal as reference.

4.12. MTT proliferation assay

For MTT proliferation assays, Capan 1 and Panc 1 cells were harvested, counted, and plated in a 96-well plate in 50µl of medium at a density of 5000 cells per well. Cells were incubated for 24h to achieve optimal adherence.

Working 5FU-RNA aptamers were prepared as described in 4.7.8. for aptamers H1_1, H2_1, and H2_2# by replacing UTP in the NTP mix with 5FUTP (20mM).

Working RNA aptamers were prepared as described in 4.7.8. for aptamers H1_1, H2_1 and H2_2#, without addition of 5FU.

Pure 5FU was diluted in PBS+MgCl₂ at a stock concentration of 400mM.

Aptamers were linearized by heating to 65°C for 5 min and slowly cooled to room temperature, allowing proper folding.

Dilution rows from every working stock were prepared in cell medium in 2X concentration and 50µl of each concentration aliquot was added per well. Cells were treated with different concentrations of 5FU-aptamers, aptamers, or 5FU for 72h. After that, 20µl of MTT reagent (2,5mg/ml) were added per well and the cells were incubated at 37°C and 5 vol% CO₂ for 4h. The medium was discarded and 200µl of DMSO per well were added, followed by a 30min incubation in darkness. OD values at 570nm were assessed using a SpectraDrop microplate reader and the percentage of viable cells per well was calculated relative to untreated control. ED₅₀ values were objectively calculated for each treatment and each biological replicate using an R script (see 8.2. Supplement 2). The ED₅₀ values for 5FU-aptamers were corrected according to the Uracil content of each aptamer by multiplication (H1_1: x17U, H2_1: x19U, H2_2#: x15U). The corrected ED₅₀ values for 5FU-aptamers were compared with the ED₅₀ values for 5FU alone by unpaired t-test. An efficiency factor was calculated by division of ED₅₀ values for 5FU by the (corrected) ED₅₀ values for 5FU-aptamers. Statistical calculations were performed using the GraphPad Prism 9 software.

To visualize the potentiation of the effect of treatment with 5FU-aptamers, isobolograms were prepared for Capan 1 and Panc 1 using Microsoft Excel. The mean ED₅₀ for the 5FU treatment was marked on the x-axis and the mean ED₅₀ for the aptamer treatment was marked on the y-axis. The points were connected by a line of additivity. Every point below that line would indicate an effect that is more than just additive (synergism), and every point above the line would indicate an effect that is opposite to additivity (antagonism). Each 5FU-aptamer was represented as a point in the graph by setting its corrected ED₅₀ as the x value (representing 5FU content at ED₅₀) and its uncorrected ED₅₀ as the y value (representing aptamer content at ED₅₀). The accumulation of data points below the line of additivity indicated that 5FU-aptamers showed a stronger treatment effect than the sum of the effects of 5FU content and aptamer content alone.

4.13. Cell cycle analysis

For cell cycle analysis, Capan 1 cells were harvested, counted, and plated on a 24-well plate in 250µl of medium at a density of 100 000 cells per well. Cells were incubated for 24h to achieve optimal adherence.

Working 5FU-RNA aptamers were prepared as described in 4.7.8. for aptamers H1_1, H2_1, and H2_2# by replacing UTP in the NTP-mix with 5FUTP (20mM).

Working RNA aptamers were prepared as described under 4.7.8. for aptamers H1_1, H2_1, and H2_2#, without addition of 5FU.

Pure 5FU was diluted in PBS+MgCl₂ at a stock concentration of 400mM.

Aptamers were linearized by heating to 65°C for 5 min and slowly cooled to room temperature, allowing proper folding.

5FU-aptamers were diluted in cell medium to a concentration of 2X of their individual ED₅₀ values (derived from MTT assays):

- H1_1 5FU-Apt: 2X 19nM = 38nM
- H2_1 5FU-Apt: 2X 19nM = 38nM
- H2_2# 5FU-Apt: 2X 41nM = 81nM

Aptamers without 5FU were diluted in cell medium at the same concentration as their respective 5FU-coupled version (derived from MTT assays), since no ED₅₀ values could be calculated for pure aptamers:

- H1_1 Apt: 2X 19nM = 38nM
- H2_1 Apt: 2X 19nM = 38nM
- H2_2# Apt: 2X 41nM = 81nM

5FU was diluted in medium to a concentration of 2X of its ED₅₀ value (derived from MTT assays). Additionally, 5FU was diluted in medium to a concentration of 2X of the corrected ED₅₀ values of each 5FU-aptamer, representing treatment with an amount of 5FU equimolar to the 5FU content of each aptamer variant:

- 5FU: 2X 3124nM = 6248nM
- FU at ED₅₀ of H1_1: 2X 323nM = 646nM
- FU at ED₅₀ of H2_1: 2X 361nM = 722nM
- FU at ED₅₀ of H2_2#: 2X 615nM = 1230nM

250µl of 2X drug concentrations per well were added and cells were treated for 24h. After incubation, cells were harvested and transferred to standard Eppendorf vials. The cell pellet was washed with PBS and resuspended in 300µl of PBS by up and down pipetting. Immediately, 700µl of ethanol (pre-chilled to -20°C) were added per tube and the suspension was vortexed. Cells were fixed in that 70% ethanol solution for 12h at 4°C. After fixation, cells were washed 2 times with 500µl PBS, and every pellet was suspended in 1ml of propidium iodide (PI) staining solution. Cells were incubated at room temperature for 30 min on a shaker in darkness. Following this step, cells were washed 2 additional times with 500µl PBS, and each pellet was suspended in 300µl of flow cytometry buffer.

For readout, a flow cytometer machine (Accuri C6 Plus, BD Biosciences) was used. Cell samples were read until 150µl fluid had passed in medium fluidics (35µl/min) and the PI signal was evaluated through the FL-2-filter.

FCS express by DeNovo software was used for the gating by FSC/SSC and FSC-a/FSC-h to filter for dead cells and doublets. The FL2-A signal was plotted against the count and markers were assigned for each cell cycle phase, depicting the percentage of cells per marked area (marker positions were calibrated on the controls and the settings were then preserved for all samples). The percentages of cells in each cell cycle phase were compared to the untreated control by one-way ANOVA with Turkey post hoc correction for multiple comparisons. Statistical calculations and plots were made using the GraphPad Prism 9 software.

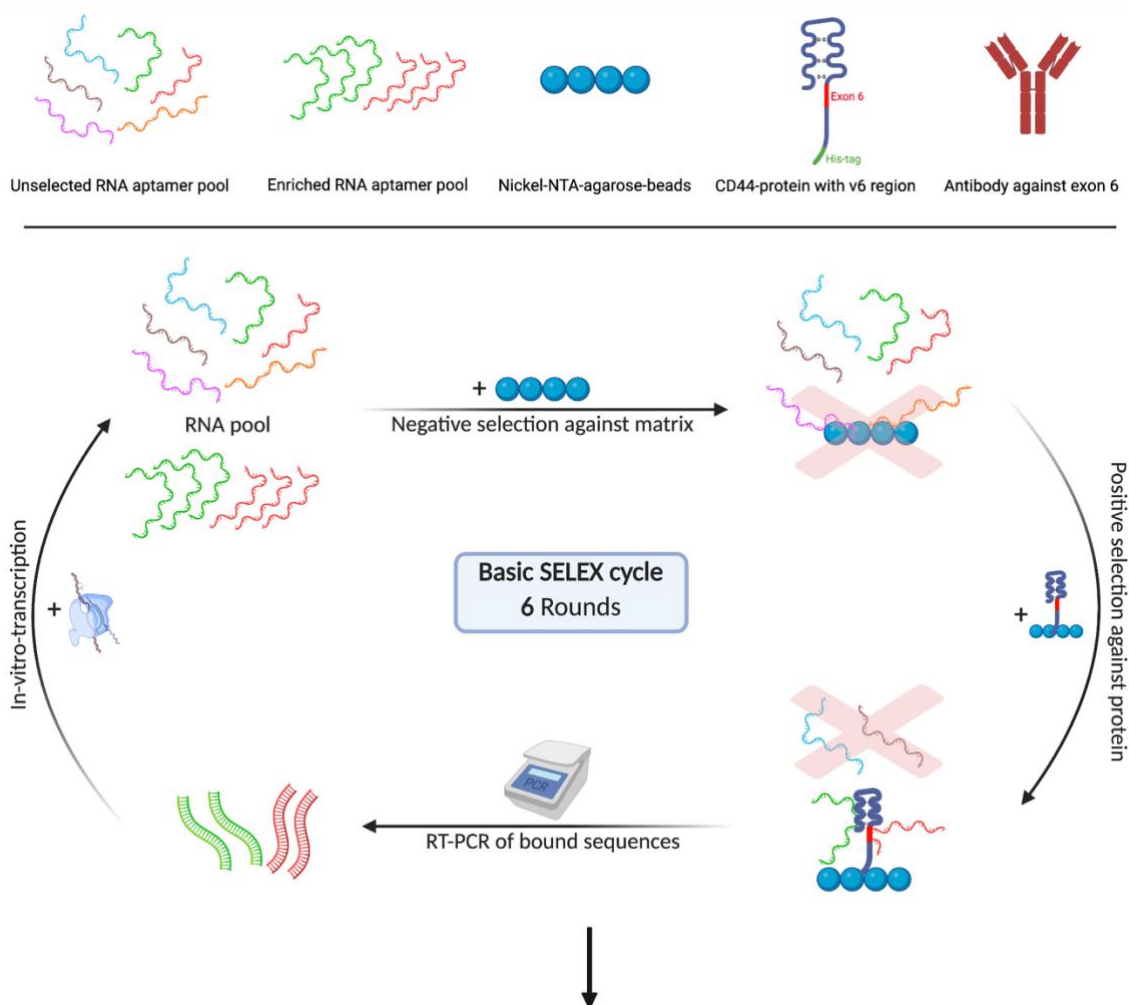
4.14. Modeling of aptamer binding (HADDOCK)

To calculate an in-silico model of binding between the aptamer and CD44, a high resolution crystal structure of the human CD44 hyaluronan binding domain complex (4PZ3) was obtained from RCSB PDB as a .pdb file [117] (<https://www.rcsb.org/structure/4PZ3>). The file was uploaded to the BindUP server (<http://bindup.technion.ac.il>) [118] and 3 positively charged patches of each protein chain were calculated. The aptamer-RNA sequences were pasted into the mask of the MC-Fold-MC-Sym pipeline (<http://www.major.irc.ca/MC-Fold/>) [119], refined, relieved, and analyzed by p-score. The highest ranked .pdb files were downloaded for each aptamer. The binding of aptamers to CD44 was modeled using the HADDOCK2.2 server (<https://milou.science.uu.nl/services/HADDOCK2.2/haddockserver-easy.html>) [120]. RNA and protein molecules were uploaded as .pdb files and all chains were considered. Active residues were chosen as follows: For aptamers, the residues of the variable region, for CD44, the residues of each positively charged patch. Passive residues were defined automatically around active ones. All defined binding clusters were classified according to the HADDOCK score calculated from the weighted sum of “van der Waals intermolecular energy, electrostatic intermolecular energy, distance restraint energy (only unambiguous and AIR (ambig) restraints), radius of gyration restraint energy, direct RDC restraint energy, intervector projection angle restraint energy, pseudo contact shift restraint energy, diffusion anisotropy energy, dihedral angle restraints energy, symmetry restraints energy (NCS and C2/C3/C5 terms), buried surface area, binding energy (Etotal complex - Sum[Etotal components]), desolvation energy” [121]. The HADDOCK scores of the binding clusters were compared by median for each positively charged protein patch. Calculation of statistical significance was not indicated since only the lowest HADDOCK score was of interest. The binding of the top ranked clusters was visualized using the PyMOL2.5 software (<https://pymol.org/2/#page-top>) [122].

5. Results

5.1. Generation of aptamers in 12 cycles of SELEX

A library of RNA molecules bearing the potential to form 10^{15} different structural variants was subjected to the SELEX cycle. A CD44 protein that contains all constantly expressed exons, as well as all common exon variants (v2-v10), served as a target for selection. In the first 6 rounds of SELEX, a basic enrichment approach was applied to filter for general specificity toward CD44(v). The following 6 rounds were conducted under advanced settings with the attempt to force binding specificity of the aptamers toward the variant 6-exon region. The whole process was carried out in 2 identical setups. After 12 rounds of SELEX, the enriched aptamers were cloned and read individually by sequencing.



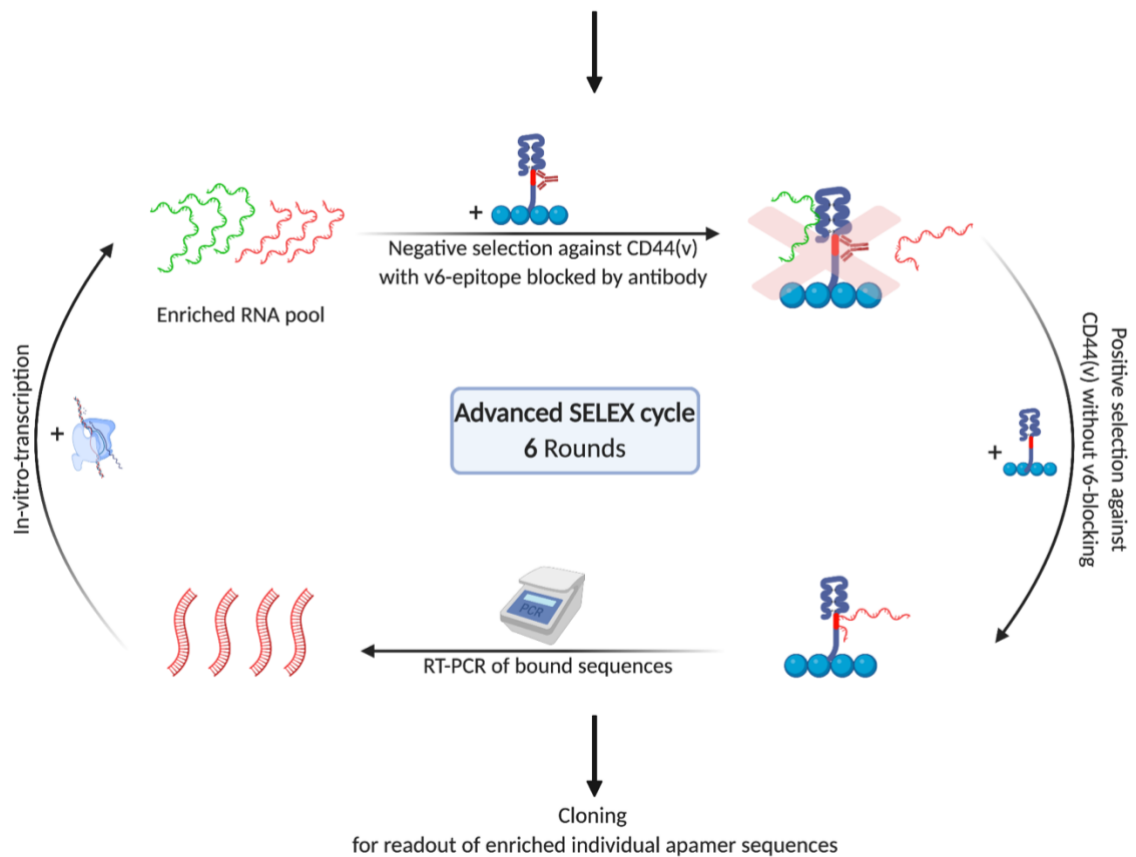


Figure 8. Schematic representation of the whole SELEX cycle: In the 6 rounds of basic selection, the RNA aptamer pool was precleared against the empty matrix and then subjected to the selection process for binding properties toward the CD44(v) protein. In the following 6 rounds of advanced selection, the preselected aptamer pool was subjected to a negative selection step against CD44 with the v6 exon region blocked by a specific antibody, prior to standard positive selection [110].

5.1.1. Enriched aptamer sequences

The whole SELEX cycle was carried out in 2 identical setups (H1 and H2). After 12 selection rounds, the enriched aptamer pool was cloned using a bacterial plasmid system. 20 single-clone colonies per setup were picked to read out individual aptamer codes by sequencing. Of the 40 sequenced clones, 36 carried aptamer information, the remaining 4 turned out to be empty vectors. There was strong redundancy among the 36 enriched aptamer sequences resulting in only 8 unique aptamer codes. The variable region of the enriched RNA aptamers is shown. Abundance indicates the number of reads in the sequencing process of 36 clones.

Label	Aptamer code	Abundance
H1_PosNeg1	<u>AUGGAAGGUAGGAGGAGAUUGUCA</u>	<u>16</u>
H1_PosNeg3	AGCGAGGGAGGAGGCCGCAUGAUGC	1
H1_PosNeg4#	AUGGAAUGUAGGAGGACAUUGUCAG	1
H1_PosNeg8	AUGGAAGGUAGGAGGAUGGUUCCA	1
H1_PosNeg16	GGAGAGGAGGAAGAUGGUUCCA	1
H2_PosNeg1	<u>UAAAUCAACAUAGGUGGAUGGUGGU</u>	<u>7</u>
H2_PosNeg2#	<u>GACAUCAGCCAGGGUGUAGGGGGAG</u>	<u>8</u>
H2_PosNeg15	UAGAUCAACAUAGGUGGAUGGUGGU	1

Table 4. Enriched aptamer sequences after 12 rounds of SELEX

5.1.2. Analysis of aptamer sequence motifs

The enriched aptamer sequences showed similarities in the RNA code. To evaluate homology and sequence alignment, the LocARNA-Alignment & Folding tool [113] was used. It provided an ontology tree, depicting the degree of relation between sequences, as well as a homology-analysis of aligned sequences.

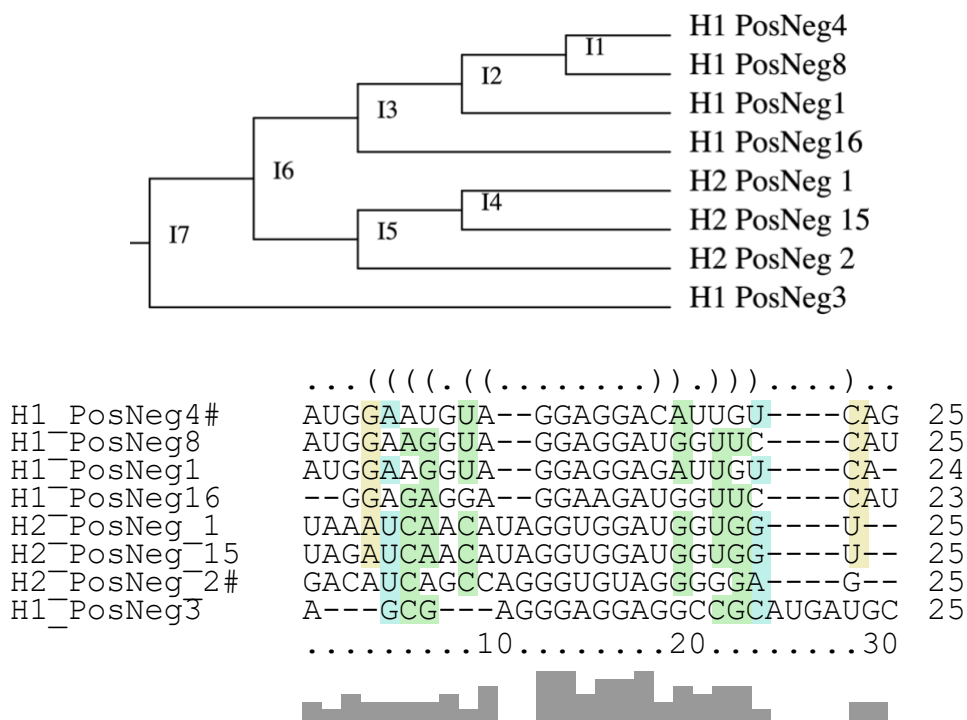
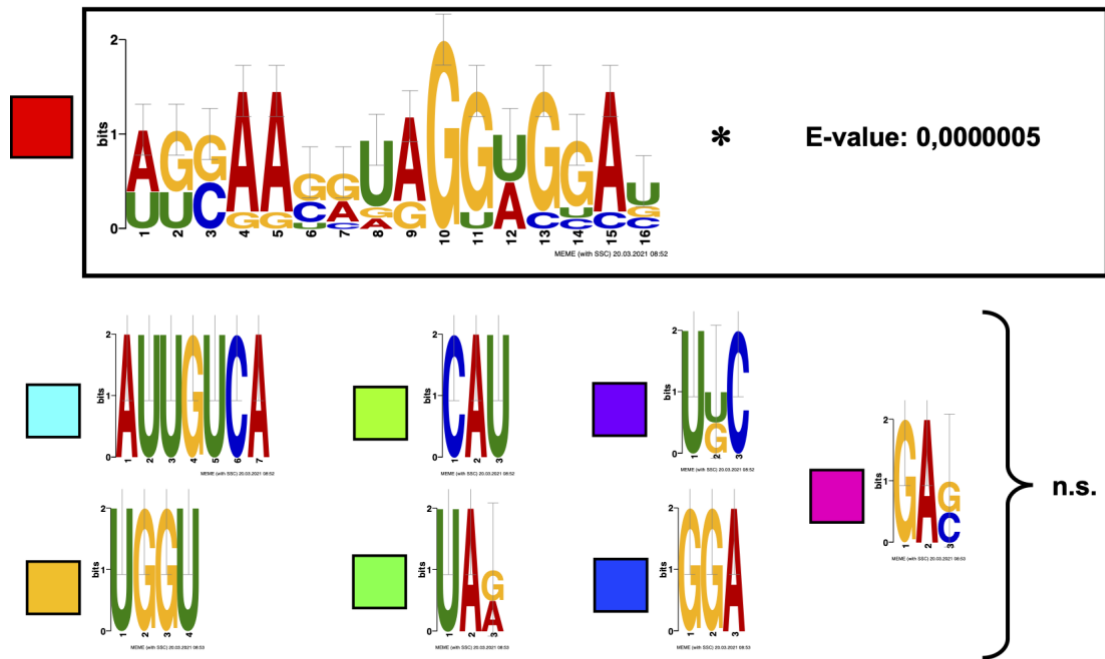


Figure 9. Analysis of aptamer sequences with the LocARNA Alignment & Folding tool [113]: The upper panel shows the degree of relation between sequence codes in an ontology tree. The closer the brackets are to the sequence names, the more similarity can be found between those sequences. The lower panel shows the degree of homology between sequences for each nucleotide position, indicated by height of the grey bar.

The ontology analysis revealed that the sequences from SELEX-setup H1 showed closer similarity to each other than to sequences from SELEX-setup H2 and vice versa. Hence, a slightly different population of aptamers was enriched in each setup. Differences in nucleotide codes were more abundant at the ends of the sequences, while the middle was dominated by a rather conserved pattern, as depicted by homology analysis. This conserved region was enriched throughout both SELEX setups (H1&H2), indicating that this pattern may be crucial for binding to the target during SELEX.

To get deeper insight about the conserved regions, the aptamer sequences were subjected to the MEME suite motif discovery algorithm (v. 5.3.3) [115]. The tool looks for structural motifs of different lengths throughout all input sequences and assigns a score to discovered motifs.



Name	Motif Locations
H1_PosNeg1	Red bar from position 1 to 16
H1_PosNeg3	Red bar from position 1 to 16, cyan bar from position 17 to 20, purple bar from position 21 to 24, green bar from position 25 to 28
H1_PosNeg4#	Red bar from position 1 to 16, cyan bar from position 17 to 20
H1_PosNeg8	Red bar from position 1 to 16, purple bar from position 21 to 24, green bar from position 25 to 28
H1_PosNeg16	Blue bar from position 1 to 4, purple bar from position 5 to 8, red bar from position 9 to 16
H2_PosNeg1	Green bar from position 1 to 4, red bar from position 5 to 16, yellow bar from position 17 to 20
H2_PosNeg2#	Purple bar from position 1 to 4, red bar from position 5 to 16, blue bar from position 17 to 20
H2_PosNeg15	Green bar from position 1 to 4, red bar from position 5 to 16, yellow bar from position 17 to 20

Figure 10. Discovery of motifs in the aptamer sequences with the MEME-suite tool: A color identifier is assigned to every discovered motif. The E-value is an estimate of the probability that a motif of similar quality can be found if all input sequence codes were to be shuffled. Hence, it describes the probability that the motif is a random sequence artifact [115]. Only the red motif shows a statistically significant E-value. The lower panel depicts motif locations on the aptamer sequences. The height of the colored bars correlates inversely with the probability that each motif would generate an equally scored match if the individual input sequence was to be shuffled.

The red motif could be found centered on every aptamer code with significant reproducibility. Minor, nonsignificant motif variations clustered towards the ends of the aptamer sequences, as proposed before. Hence, the red motif code was most likely responsible for aptamer binding toward the target of selection in the SELEX process.

To find out whether the novel advanced SELEX approach was sufficient to generate aptamers with specificity for the CD44v6 exon or if only specificity for the whole CD44 protein was achieved, the binding properties of the aptamers were assessed for using cellular systems.

The most abundantly enriched aptamers H1_1, H2_1 and H2_2# were chosen for further biological assays. Their respective molecular weights comprised 33,6kDa for H1_1, 33,9kDa for H2_1 and 34,0kDa for H2_2#. Full details on the aptamer RNA sequences are listed in section 8.1. (**Supplement 1**).

5.2. Evaluation the expression of CD44v6 and CD44s in cell line systems

As a prerequisite for biological experiments with the generated aptamers, a suitable cellular system had to be chosen. Based on prior experiments and a query of openly accessible cell line transcriptome databases, human cell lines with high and low expression of CD44v6 and CD44s were preselected. Cell lines were also chosen with regard to accessibility in our laboratory. For confirmation, selected cell lines were assessed for CD44v6 and CD44s expression by flow cytometry.

5.2.1. Assessment of CD44v6 expression of cell lines

The expression of CD44 exon variant 6 (CD44v6) was measured in two human cell lines. Nonfixated cells were subjected to staining with a labeled antibody specific for CD44v6 (VFF-18). After gating, corrected mean fluorescent intensity values were compared.

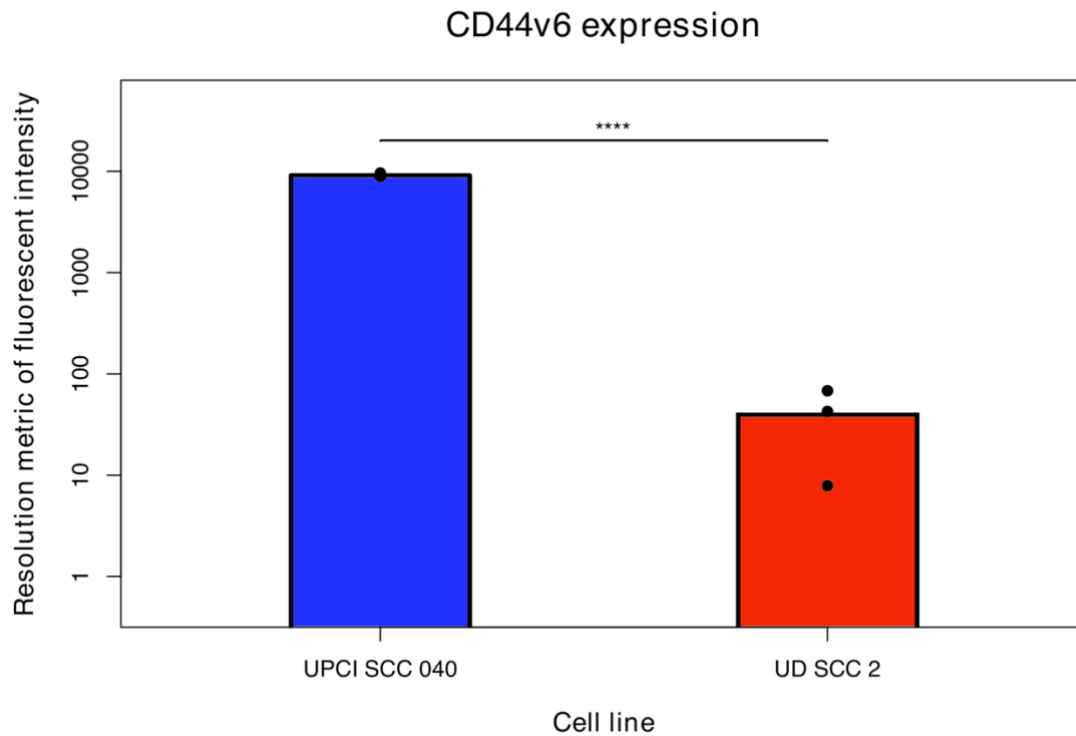


Figure 11. CD44v6 expression of cell lines: Protein expression was assessed by flow cytometry. After gating, the geometric mean of fluorescent intensity was corrected for background and dispersal, and from that the resolution metric was calculated. The scale is logarithmic.

Regarding this result, UPCI-SCC-040 and UD-SCC-2, two squamous cell carcinoma lines derived from head and neck cancers, were chosen for further experiments. Since the expression of CD44v6 was 1000-fold higher in UPCI-SCC-040 than in UD-SCC-2, the first was chosen as a positive control and the second as a negative control for future assessment of aptamer specificity toward CD44v6.

5.2.2. Assessment of CD44s expression of cell lines

Standard CD44 (CD44s) expression was measured in four human cell lines. Nonfixed cells were subjected to staining with a CD44s-specific primary antibody followed by a labeled secondary antibody. After gating, corrected mean fluorescent intensity values were compared.

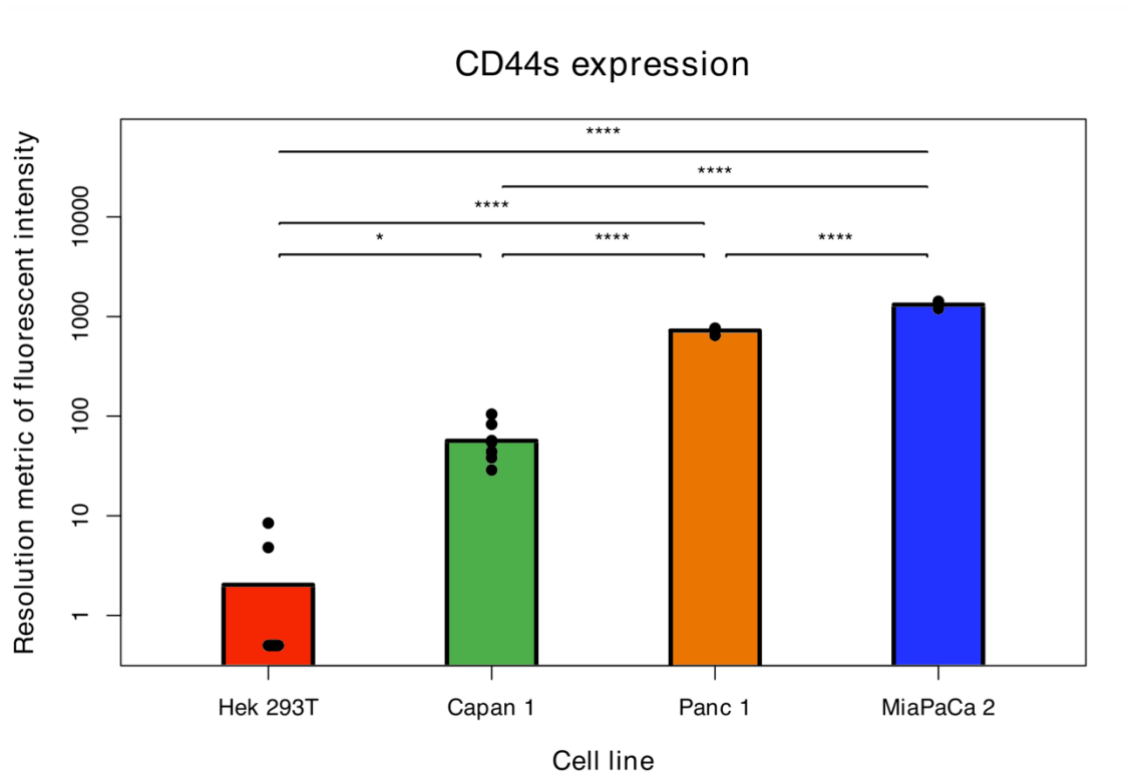


Figure 12. CD44s expression of cell lines (1): Protein expression was assessed by flow cytometry. After gating, the geometric mean of fluorescent intensity was corrected for background and dispersal, and from that the resolution metric was calculated. The scale is logarithmic.

MiaPaCa2 and Panc 1 showed high CD44s expression while Capan 1 had an intermediate/low expression profile. All three lines are immortalized cell clones of Pancreatic ductal adenocarcinoma. The human embryonic kidney cell line Hek 293T showed virtually no expression of CD44s, so it was chosen as a negative control.

Subsequently, the CD44s expression of the previously mentioned head and neck cancer cell lines UPCI-SCC-040 and UD-SCC-2 was compared. No differences in CD44s expression were found between the cell lines.

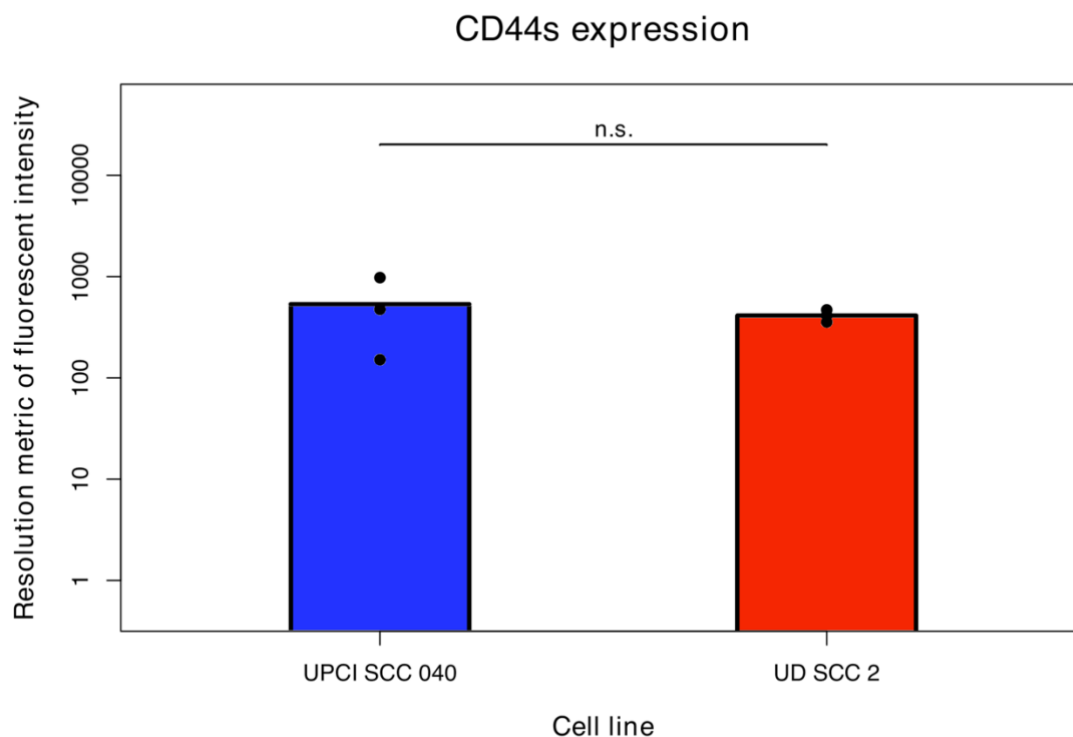


Figure 13. CD44s-expression of cell lines (2): Protein expression was assessed by flow cytometry. After gating, the geometric mean of fluorescent intensity was corrected for background and dispersal, and from that the resolution metric was calculated. The scale is logarithmic.

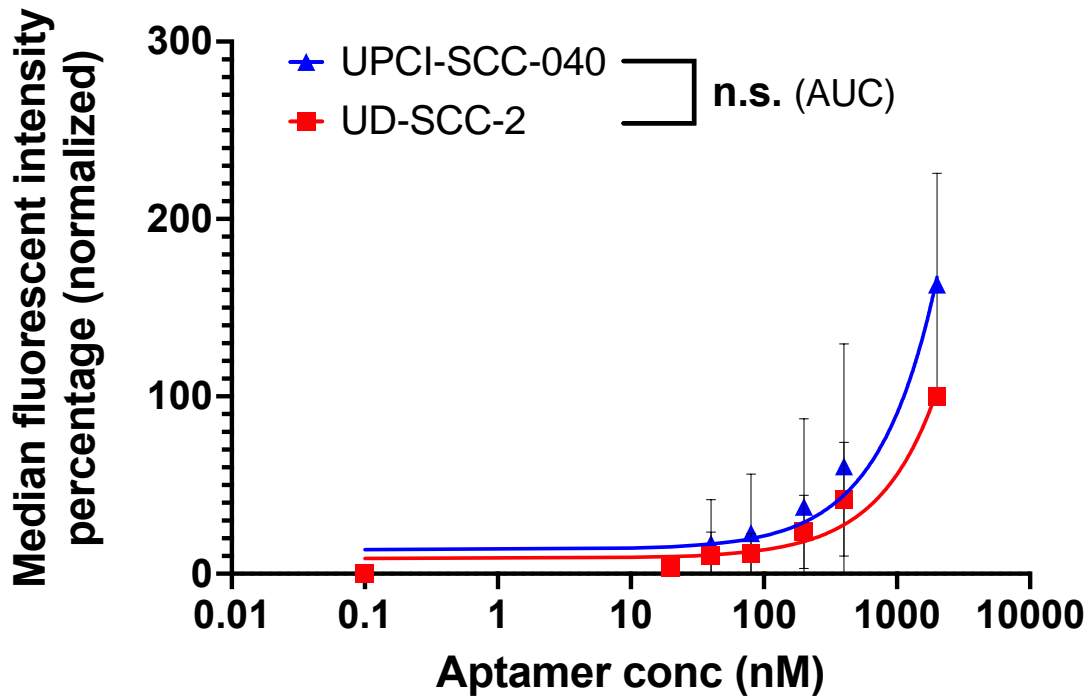
5.3. Evaluation of aptamer-to-target specificity

To assess the specificity of the generated aptamers toward their protein targets, a modified approach of flow cytometry was implemented. The aptamers H1_1, H2_1, and H2_2# were labeled with the Cy3 fluorescent dye and their binding properties were tested on the selected cell lines expressing CD44v6 or CD44s.

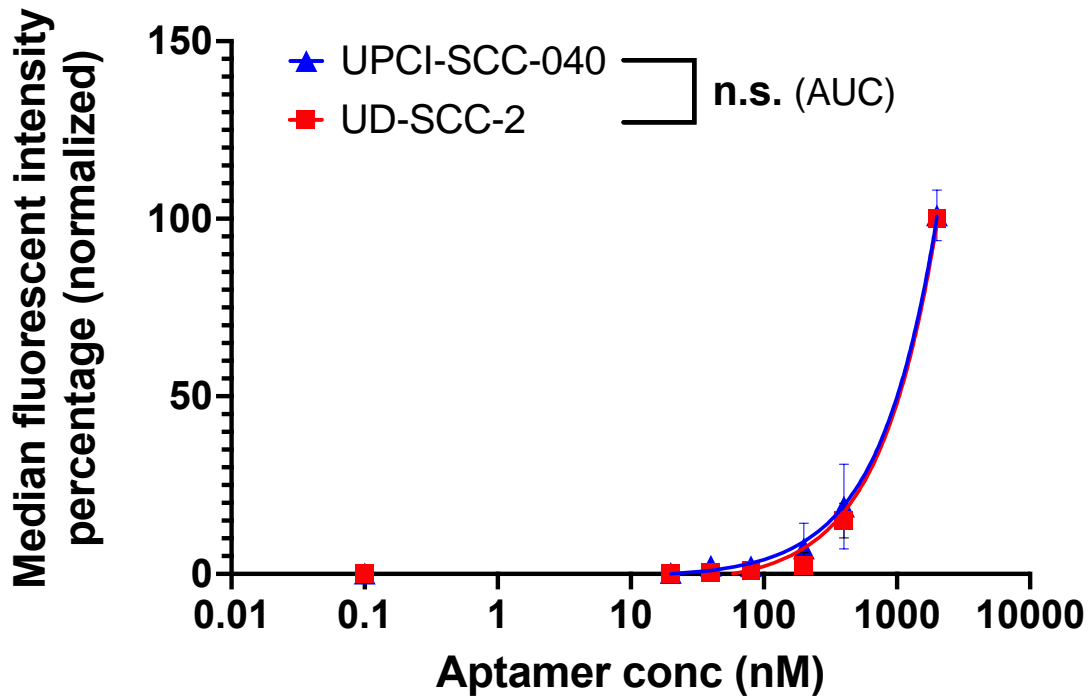
5.3.1. Assessment of aptamer binding to CD44v6 by flow cytometry

The low CD44v6-expressing cell line UD-SCC-2 and the high CD44v6-expressing cell line UPCI-SCC-040 were chosen to evaluate whether the advanced SELEX setup generated sufficient aptamer specificity toward the variant 6 region of CD44. Nonfixed cells were subjected to staining with labeled aptamers. After gating, normalized median fluorescent intensity values were assessed and the areas under the curve (AUC) were compared for both cell lines.

Aptamer H1_1



Aptamer H2_1



Aptamer H2_2#

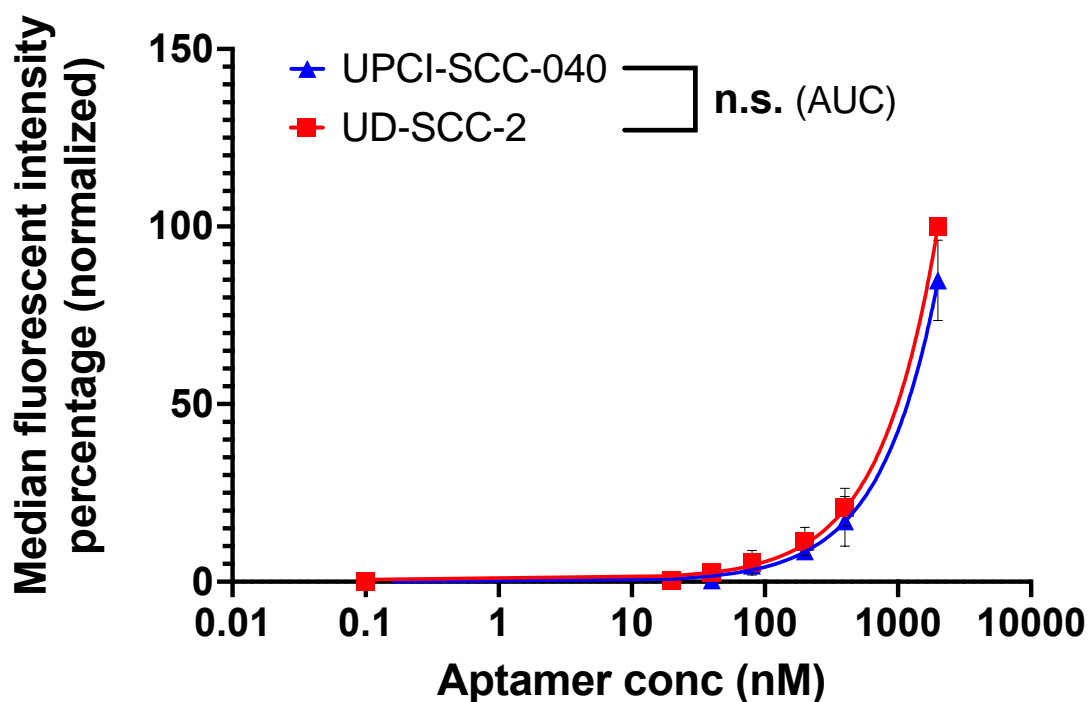


Figure 14. Evaluation of binding of the aptamers to the v6 exon region of CD44: Flow cytometry was performed with Cy3-labeled aptamers H1_1, H2_1, and H2_2# after binding to the high-expressing CD44v6 cell line UPCI-SCC-040 and the low-expressing CD44v6 cell line UD-SCC-2. The median fluorescent intensity was measured and normalized with respect to the maximum value. The area under the curve for each graph was compared using an unpaired t test.

No differences in signal intensity could be found between high and low CD44v6-expressing cell lines. Both curves are rising sharply, so it can be assumed, that the aptamers are binding to the cell surface but not specifically to the v6 region of CD44.

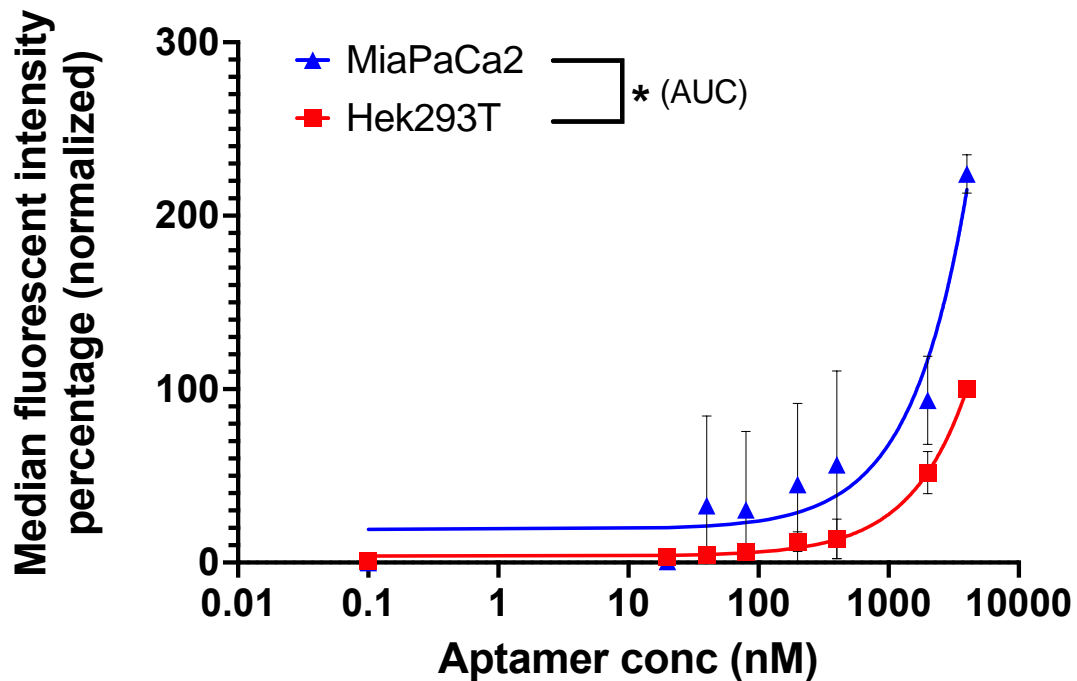
Hence, the addition of modified advanced selection cycles to the SELEX process could not generate sufficient aptamer specificity toward the v6 region of CD44.

The next logical step was to assess whether the aptamers are reliably binding to the CD44 protein itself. Since the cell lines UPCI-SCC-040 and UD-SCC-2 do not show differences in CD44s expression (see 5.2.2., Figure 10), the results shown above are in line with that hypothesis.

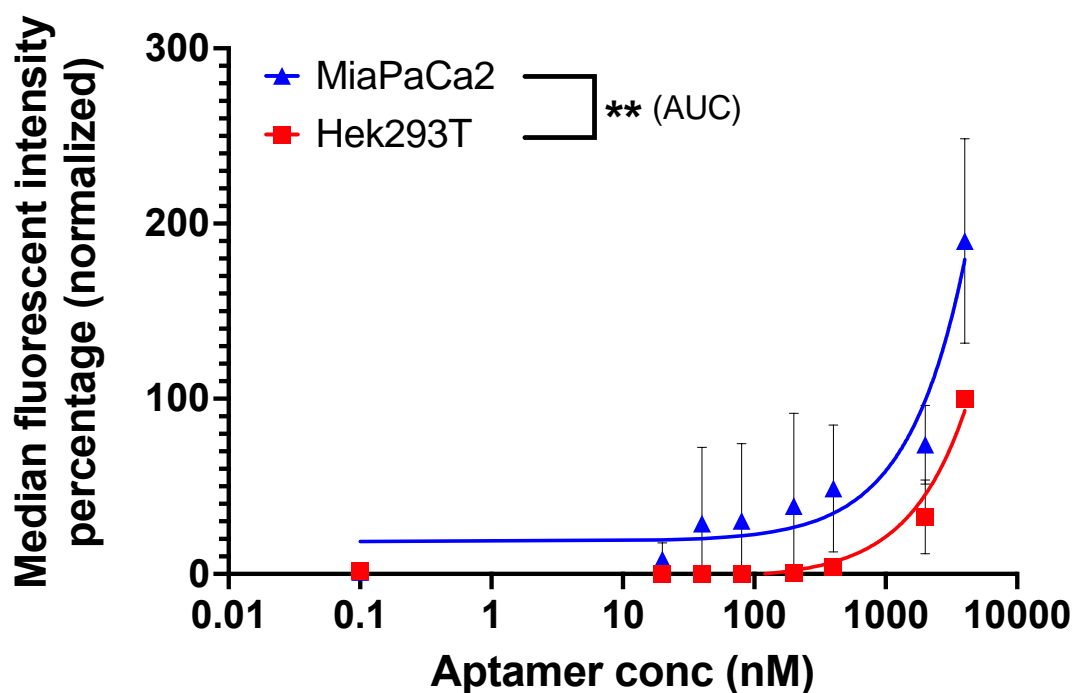
5.3.2. Assessment of aptamer binding to CD44 by flow cytometry

The same approach of modified flow cytometry was applied using the MiaPaCa2 cell line as a high-expressing CD44 model and the Hek 293T cell line as a negative control.

Aptamer H1_1



Aptamer H2_1



Aptamer H2_2#

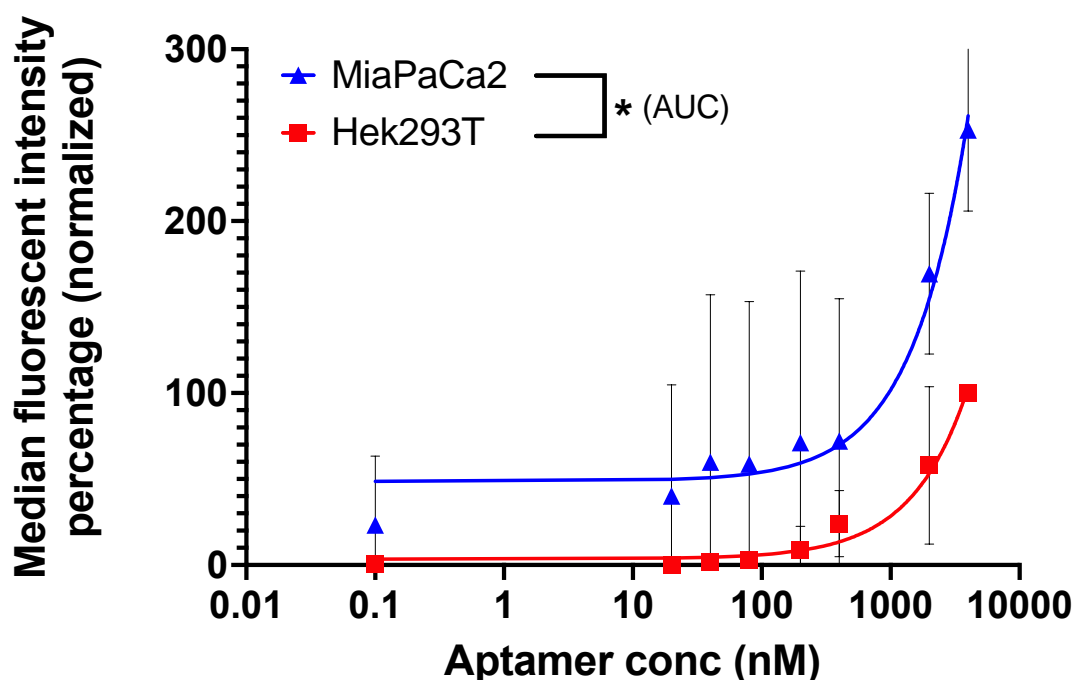


Figure 15. Evaluation of aptamer binding to CD44: Flow cytometry was performed with Cy3-labeled aptamers H1_1, H2_1, and H2_2# after binding to the high CD44s-expressing cell line MiaPaCa2 and the low CD44s-expressing cell line Hek 293T. The median fluorescent intensity was measured and normalized with respect to the maximum value. The area under the curve for each graph was compared using an unpaired t test.

A significant difference in the area under the curve for signal intensity could be found after aptamer staining when comparing the high CD44 expressing cell line MiaPaCa2 with the low CD44 expressing cell line Hek 293T. The results indicate that the aptamers specifically bind to the CD44s protein.

5.3.3. Confirmation of aptamer binding to CD44s by UV cross-linking

To fully confirm that the aptamers are binding to the CD44 protein specifically, a pragmatic experiment was performed. High CD44-expressing MiaPaCa2 cells were seeded in dishes and incubated with an extremely high amount of (H1_1/H2_1/H2_2#) aptamers and an unselected mock aptamer library as a control. After a sufficient binding

time, cell plates were irradiated with UV light to ensure cross-link formation between bound aptamer RNA and cell surface proteins, as described by Wagenmakers et al. [123]. Cells were harvested and thoroughly lysed using RIPA buffer and sonication. The lysates were loaded onto an SDS-PAGE and the gel was stained with RNA dye. A picture of the (strongly magnified) RNA signal was saved. Then, Western blotting was performed, the blotting membrane was stained for CD44s, and a picture of the protein signal was saved. The RNA-band signal and the protein-band signal were overlapped using the size ruler ladder as a reference.

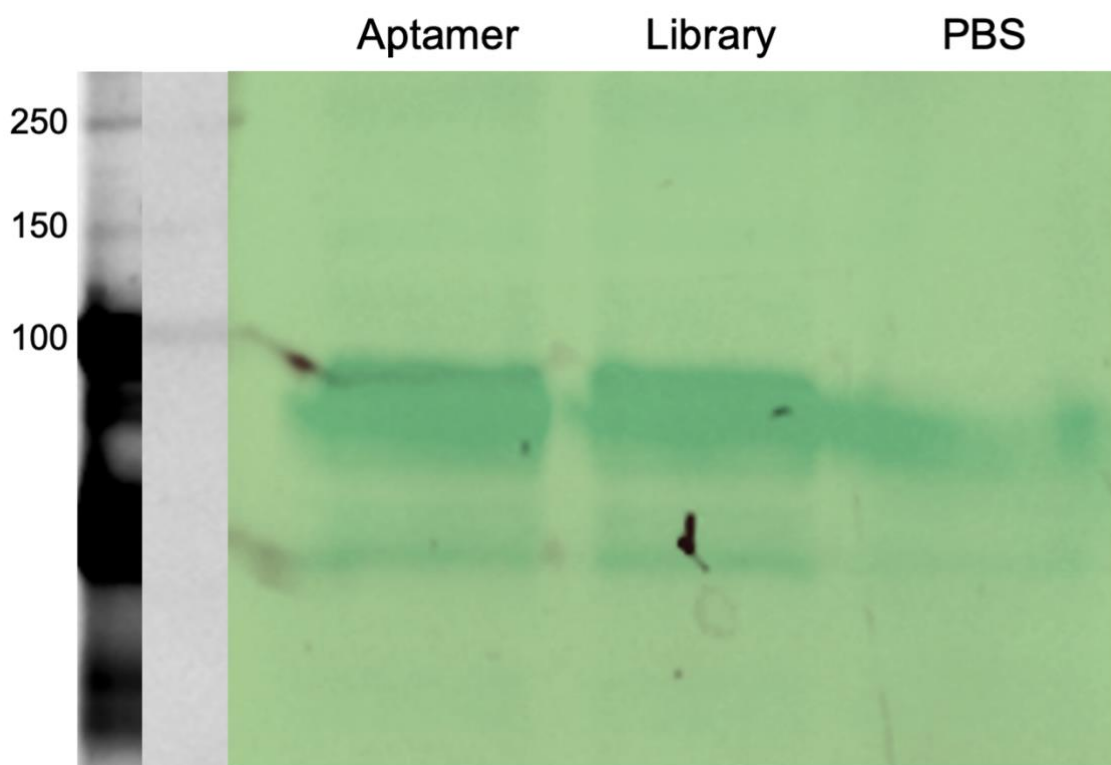
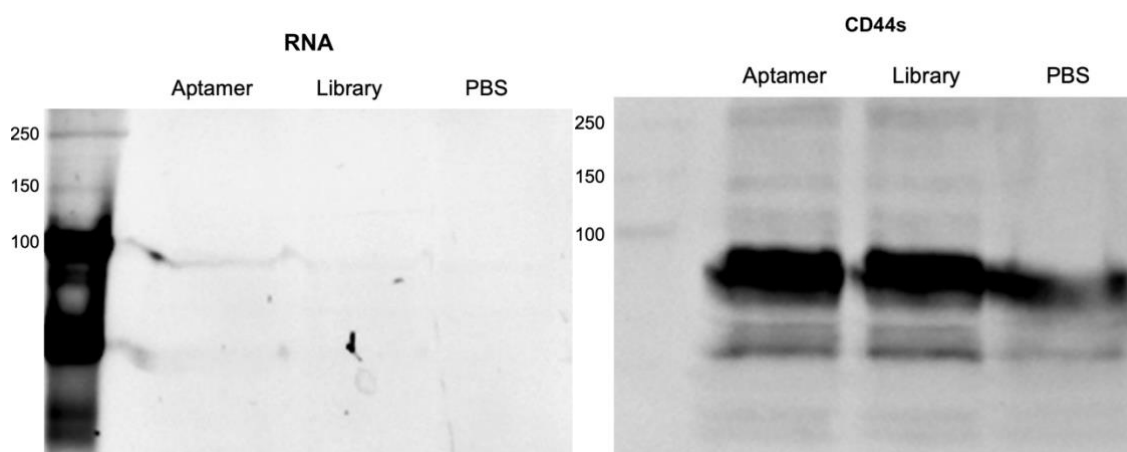


Figure 16. Aptamer cross-linking to CD44s on the cell surface: After incubation of an identical amount of aptamer RNA and control RNA with MiaPaCa2 cells and UV cross-linking, the cell membrane lysate was analyzed on SDS-PAGE. The RNA signal and the CD44 protein signal were obtained. One signal was enhanced with a green filter, the other signal with a red filter, and the images were overlapped using the ladder as a reference. Bad picture quality could not be avoided due to the need of strong signal magnification.

The strong RNA signal of all aptamer bands overlaps perfectly with the signal of the CD44 protein, indicating that the aptamers bind specifically to CD44. No RNA bands can be found in the PBS-only control. The mock aptamer library control shows several, very faint RNA-bands, indicating unspecific binding to the cell surface, as expected. This assay confirms that the SELEX cycle generated aptamers that bind specifically to the CD44 protein.

5.4. In vitro biological effects of CD44-specific aptamers enhanced with 5-Fluorouracil

To assess the biological efficacy of the generated aptamers in cancer treatment, the RNA backbones of the molecules were modified. Instead of each Uracil residue, 5-Fluorouracil (5FU) was incorporated into the aptamer RNA during synthesis. 5FU is a chemotherapeutic drug commonly used in the clinical treatment of pancreatic ductal adenocarcinoma [9].

The number of 5-Fluorouracil molecules differs between individual aptamers:

H1_1: 17 residues of 5-Fluorouracil.

H2_2: 19 residues of 5-Fluorouracil.

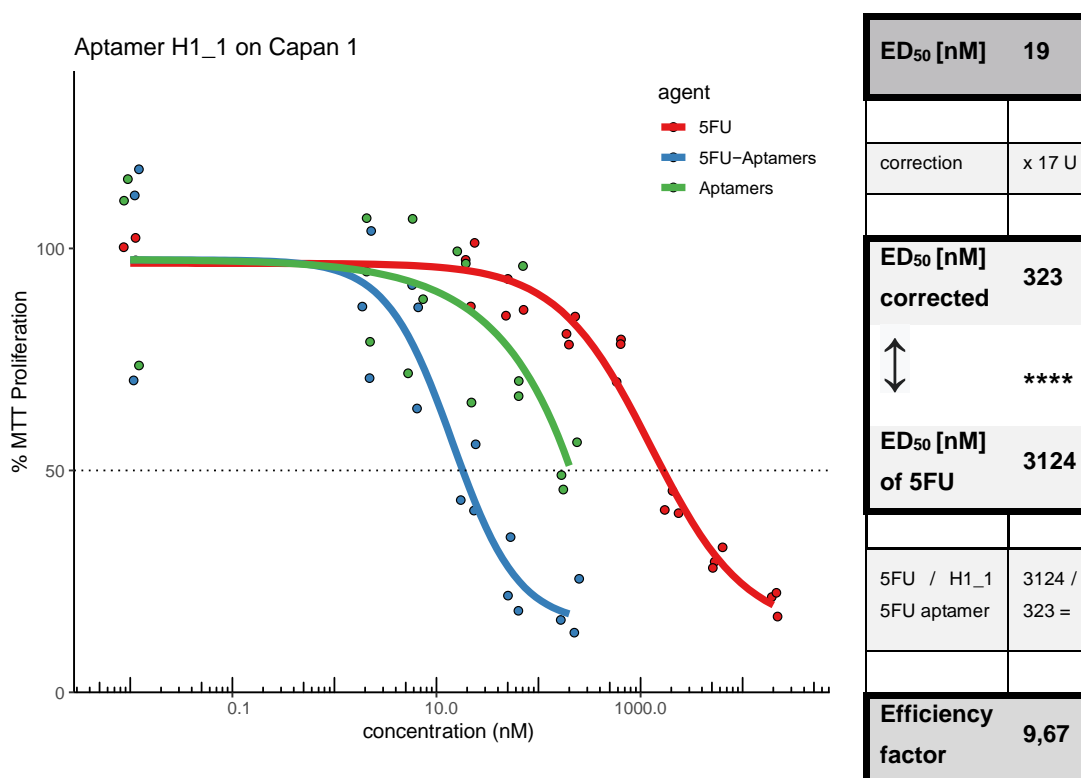
H2_2#: 15 residues of 5-Fluorouracil.

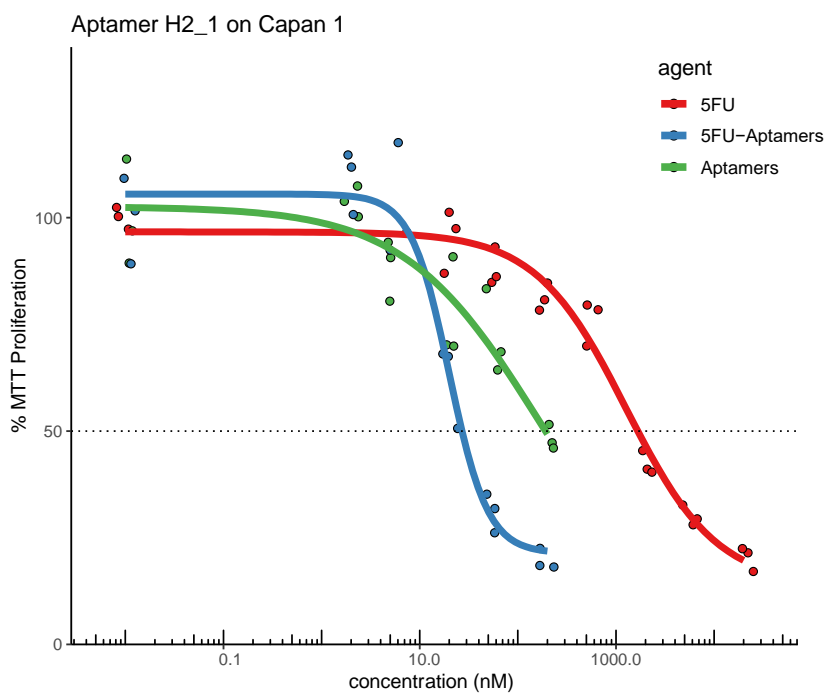
All concentration values were corrected for the individual 5-Fluorouracil content of the aptamer prior to statistical comparison.

5.4.1. The effect of aptamers on cancer cell proliferation

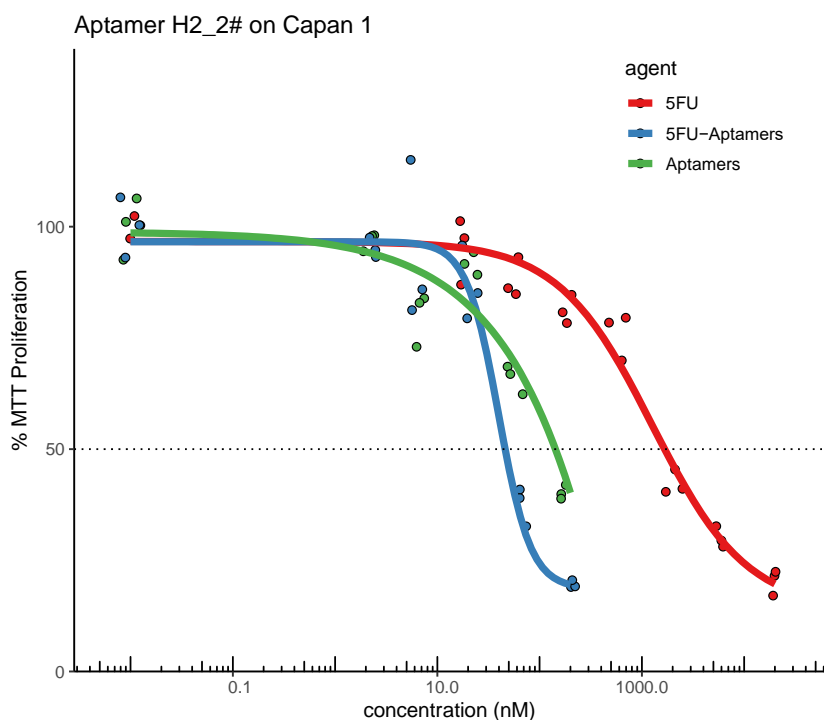
An MTT proliferation assay was performed using the cancer cell line Panc 1 as a high CD44 expressing system and the cancer cell line Capan 1 as an intermediate/low CD44 expressing system. Cells were treated with different concentrations of unmodified aptamers, pure 5FU and 5FU-modified aptamers. After 72h, the number of viable cancer cells was assessed. ED₅₀ values were calculated for each agent and corrected values for 5FU-modified aptamers were compared to the effect of pure 5FU. Additionally, an efficiency factor was calculated by dividing the ED₅₀ value of pure 5FU by the corrected ED₅₀ value of the 5FU-modified aptamer. The factor can be used to quantify the amplification of 5FU potency by combination of the drug with the CD44-directed aptamer targeting system.

The intermediate/low CD44-expressing cancer cell line Capan 1 showed the following results:





ED₅₀ [nM]	19
correction	x 19 U
ED₅₀ [nM] corrected	361
↕	****
ED₅₀ [nM] of 5FU	3124
5FU / H2_1 / 5FU aptamer	3124 / 361 =
Efficiency factor	8,65



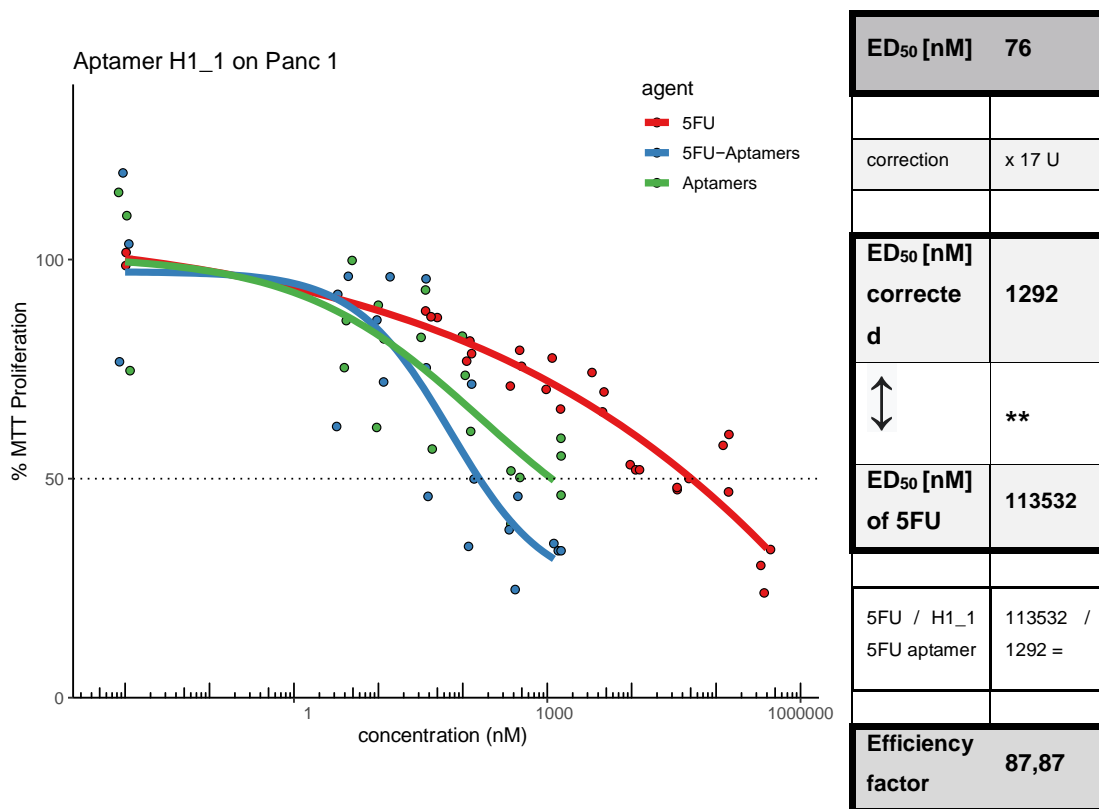
ED₅₀ [nM]	41
correction	x 15 U
ED₅₀ [nM] corrected	615
↕	****
ED₅₀ [nM] of 5FU	3124
5FU / H2_2# / 5FU aptamer	3124 / 615 =
Efficiency factor	5,08

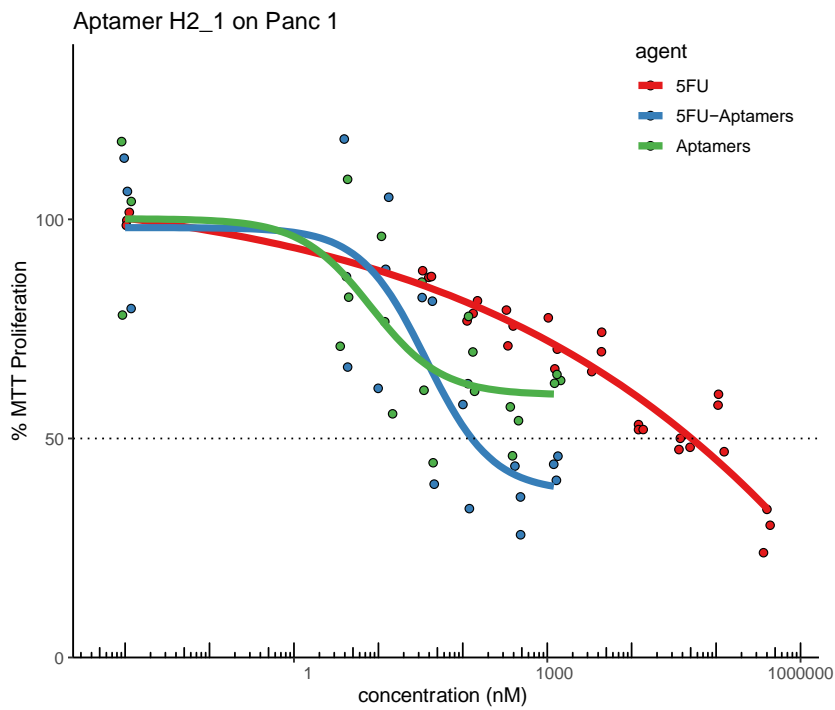
Figure 17. MTT-proliferation assay with 5FU-aptamers on Capan 1 cancer cells: A constant amount of Capan 1 cancer cells per well was seeded of a 96-well plate. Cells were treated with increasing concentrations of pure aptamer, pure 5FU and 5FU-modified aptamer for 72h. After incubation, MTT reagent was added and the number of cells in each well was quantified. The ED₅₀ values were calculated for each treatment. The values of 5FU-modified aptamers were corrected for the individual 5FU amount by multiplication of the initial ED₅₀ by the Uracil content

of the aptamer. The corrected values of the replicates were compared using an unpaired t test. Additionally, the efficiency factor was calculated by division of the ED₅₀ value of pure 5FU by the ED₅₀ value of 5FU-modified aptamer.

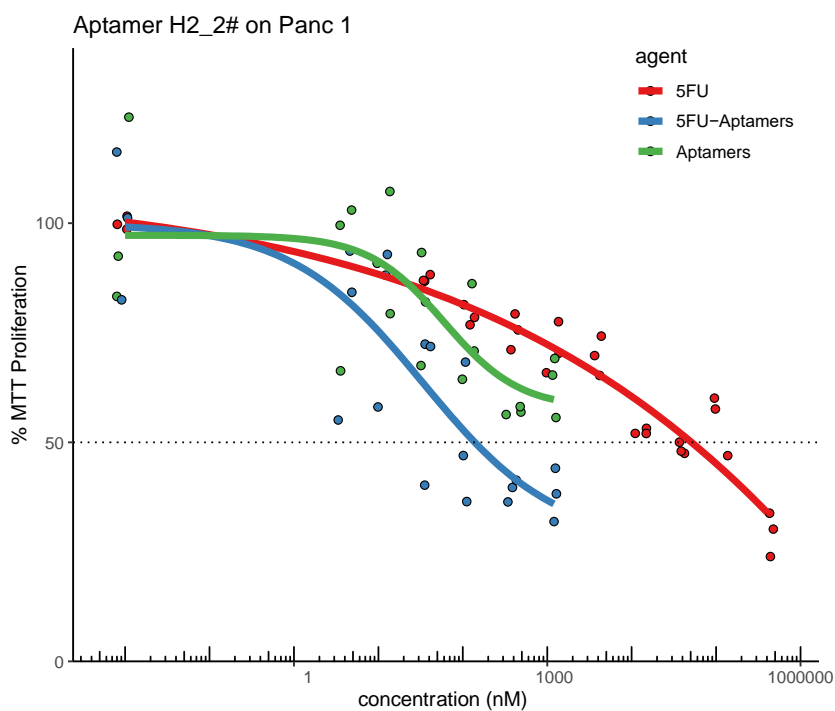
The results show that 5FU-modified aptamers are 5-10 times more efficient in inhibiting proliferation than 5FU alone in intermediate/low CD44 expressing Capan 1 cancer cells. Therefore, the specific targeting of 5FU to CD44 by the aptamer carrier system significantly enhances the cytostatic effect of 5FU.

The same assay was repeated with the high CD44-expressing cancer cell line Panc 1 showing the following results:





ED₅₀ [nM]	53
correction	x 19 U
ED₅₀ [nM] corrected	1007
↕	**
ED₅₀ [nM] of 5FU	113532
5FU / H2_1 / 5FU aptamer	113532 / 1007 =
Efficiency factor	112,74



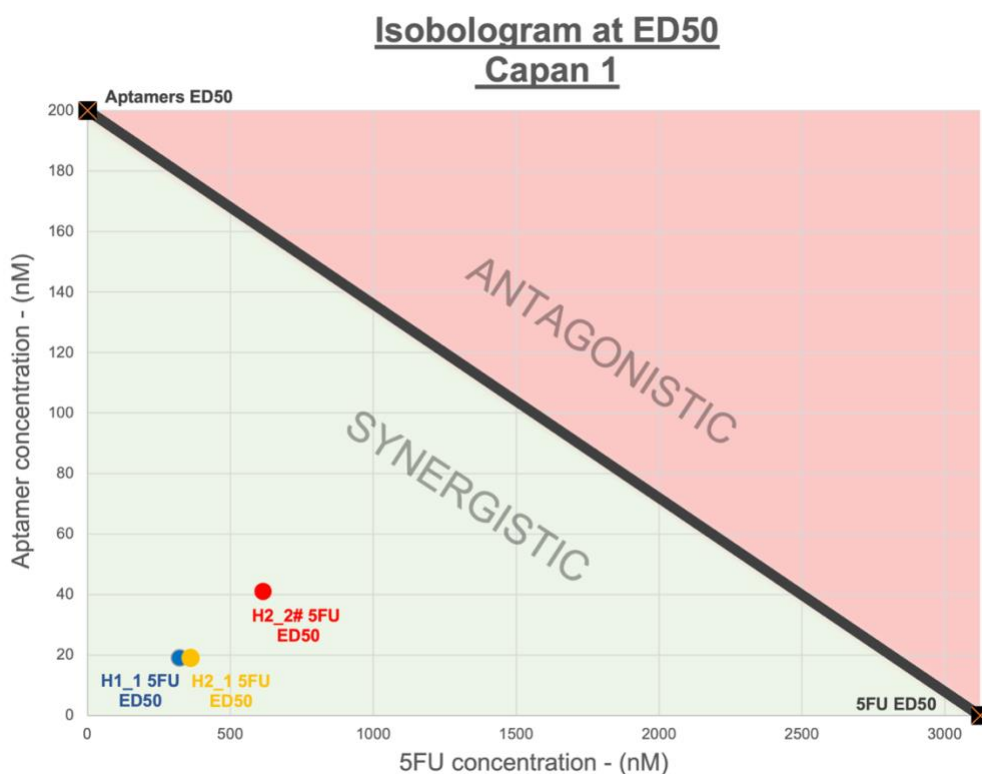
ED₅₀ [nM]	49
correction	x 15 U
ED₅₀ [nM] corrected	735
↕	**
ED₅₀ [nM] of 5FU	113532
5FU / H2_2# / 5FU aptamer	113532 / 735 =
Efficiency factor	154,47

Figure 18. MTT-proliferation assay with 5FU-aptamers on Panc 1 cancer cells: A constant amount of Panc 1 cancer cells per well was seeded of a 96-well plate. Cells were treated with increasing concentrations of pure aptamer, pure 5FU and 5FU-modified aptamer for 72h. After incubation, MTT reagent was added and the number of cells in each well was quantified. The ED₅₀ values were calculated for each treatment. The values of 5FU-modified aptamers were corrected for the individual 5FU amount by multiplication of the initial ED₅₀ by the Uracil content

of the aptamer. The corrected values of the replicates were compared using an unpaired t test. Additionally, the efficiency factor was calculated by division of the ED₅₀ value of pure 5FU by the ED₅₀ value of 5FU-modified aptamer.

Once again, it becomes evident that incorporation of 5-Fluorouracil into targeted aptamers significantly enhances the cytostatic effect of 5FU. The effect of 5FU-modified aptamers was 87-154 times stronger than that of 5FU alone in the high CD44 expressing cell line Panc 1. In the intermediate/low CD44-expressing cell line Capan 1, the efficiency factors reached only 5 to 10. Therefore, the efficiency of the 5FU-modified aptamers is strongly correlated with the amount of CD44 expression of cancer cells.

An additional observation can be deduced from the graphs: The aptamer-only controls (green lines) also show a restricting effect on cancer cell proliferation, even without the presence of 5FU. This indicates that the aptamers interfere with some biological pathways of the cancer cells that are connected to the CD44 protein. To resolve, whether the effect of 5FU-modified aptamers is merely the combination of the effects of 5FU alone and of aptamers alone (additive), or if the effect is more than additive (synergistic), or even the opposite (antagonistic), isobologram graphs were prepared. Each datapoint above the line of additivity indicates antagonistic effects, while each point below the line indicates synergistic effects of the two agents within each 5FU-enhanced aptamer.



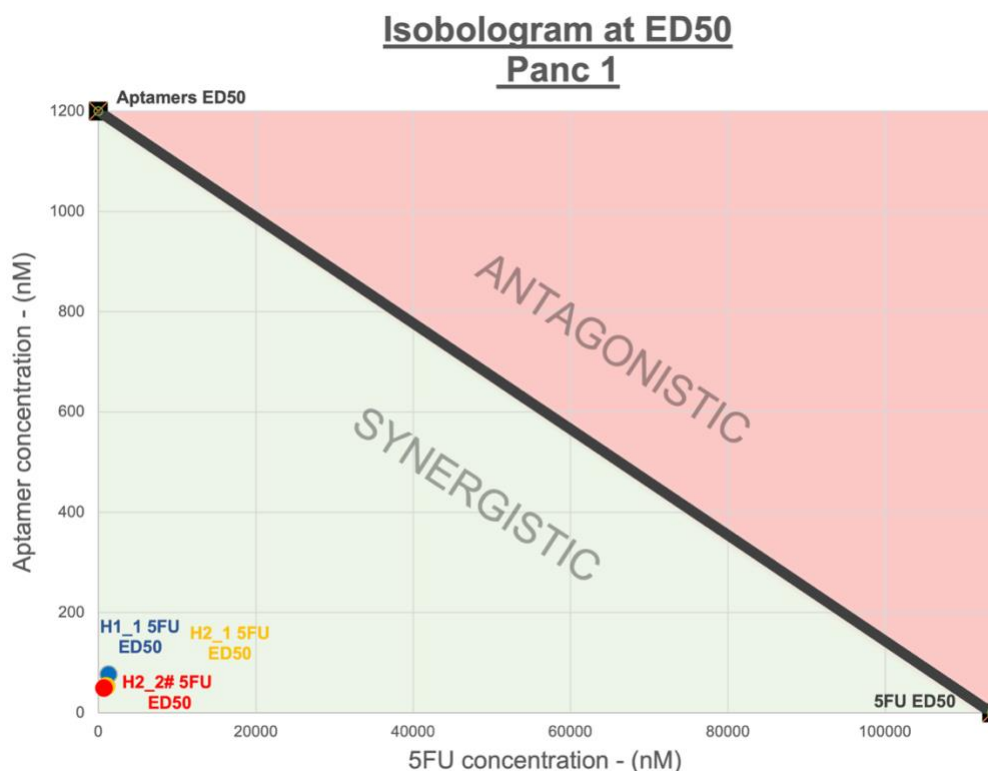


Figure 19. Isobologram graphs depicting the effects of 5FU-modified aptamers on Capan 1 and Panc 1 cancer cell lines: The x-axis depicts 5FU concentration, the y-axis depicts aptamer concentration. A line of additivity is drawn between the mean ED₅₀ value of pure 5FU and the mean ED₅₀ value of pure aptamers, marked on the respective axes. The 5FU-modified aptamers were located as data points on the graph by using the corrected concentration of 5FU at ED₅₀ as x coordinate and the (uncorrected) concentration of aptamer at ED₅₀ as y coordinate.

It is evident that the properties of pure 5-Fluorouracil and pure aptamers become highly synergistic in the 5FU-modified aptamers. The effect is stronger in the high CD44 expressing cell line Panc 1 than in the intermediate/low CD44 expressing cell line Capan 1 (the dots are closer to 0). Hence, the generated aptamers are more than mere carriers of 5FU – they strongly enhance the efficiency of the drug in a synergistic way.

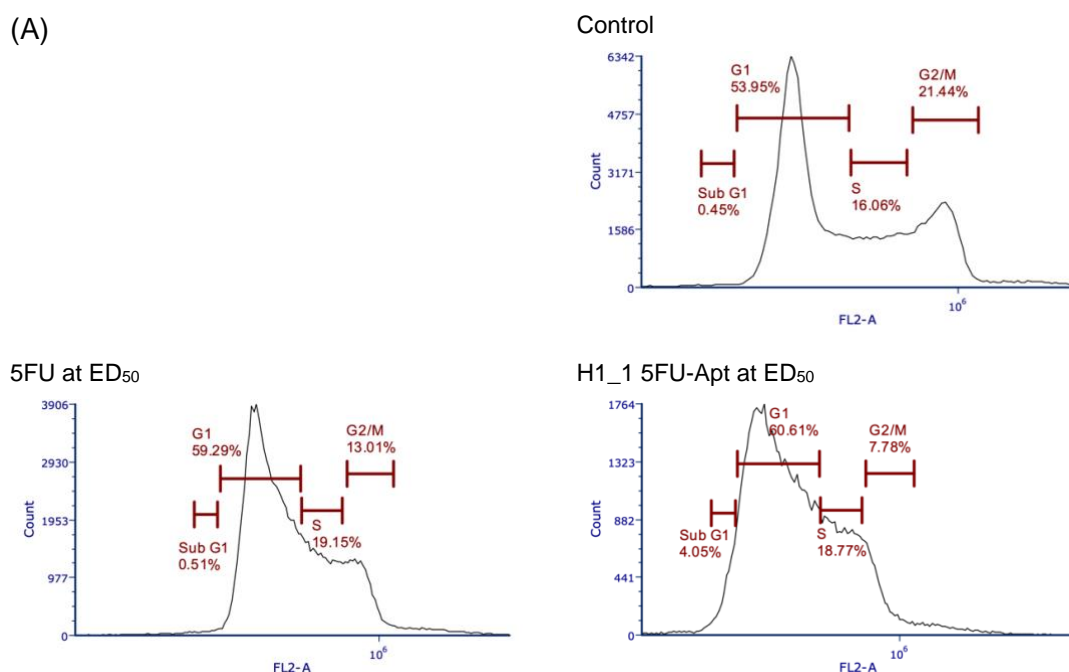
5.4.2. The effects of aptamers on the cancer cell cycle

To further elucidate the mechanistic effects of aptamer treatment on cancer cells, cell cycle analysis by propidium iodide (PI) staining was performed. Capan 1 cells were treated with different agents at the previously calculated ED₅₀ (see 5.4.1). The assay included:

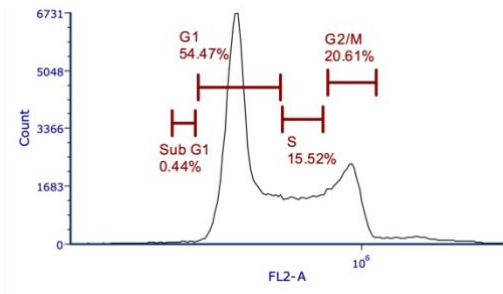
- untreated controls
- treatment with 5FU only at its ED₅₀ concentration (3124 nM)
- 5FU-modified aptamers at their individual ED₅₀ concentrations
 - o H1_1-5FU-aptamer (19 nM)
 - o H2_1-5FU-aptamer (19 nM)
 - o H2_2#-5FU-aptamer (41 nM)
- aptamers without 5FU at the same corresponding concentrations as above
 - o H1_1-aptamer (19 nM)
 - o H2_1-aptamer (19 nM)
 - o H2_2#-aptamer (41 nM)
- 5FU only with concentration corresponding to the equimolar amount inside of the 5FU-modified aptamers.
 - o 5FU equimolar to H1_1-5FU-aptamer (323 nM)
 - o 5FU equimolar to H1_1-5FU-aptamer (361 nM)
 - o 5FU equimolar to H1_1-5FU-aptamer (615 nM)

After treatment, the cells were fixated and stained with propidium iodide. Its fluorescent intensity was assessed by flow cytometry to quantify the amount of intracellular DNA. Cell fractions were attributed to cycle phases, as shown by Guo et al. [124]. The exact same marker positions were preserved for all samples and the percentages of cells per phase were compared. Figure 20 (A) shows an example of the cell cycle distribution as measured after different treatments. Figure 20 (B) summarizes all the different treatment groups with their corresponding statistical significance.

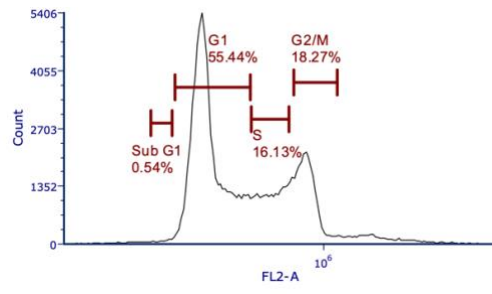
(A)



H1_1 Apt equimolar to 'H1_1 5FU-Apt at ED₅₀'



5FU equimolar to 'H1_1 5FU-Apt at ED₅₀'



(B)

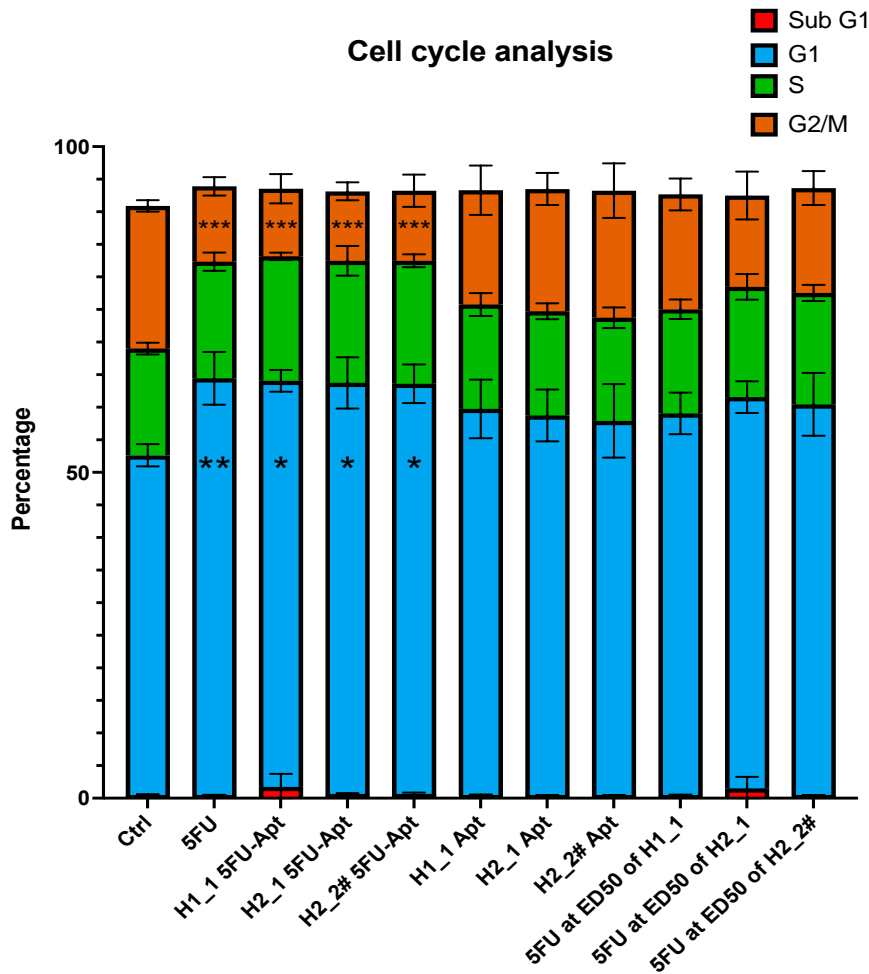


Figure 20. Cell cycle analysis of Capan 1 cells after aptamer treatment: (A) A constant amount of Capan 1 cancer cells was seeded per well in a 24-well plate. Cells were treated with pure 5FU at its ED₅₀, 5FU-enhanced aptamers at their ED₅₀, pure aptamers at the same concentration and pure 5FU at equimolar concentration as in the treatment group '5FU-modified aptamers at ED₅₀'. After 24 hours the cells were fixated and stained with PI. The fluorescent signal was measured by FC and markers were applied to quantify cell populations in each cell cycle. The markers were kept in preserved positions for each measurement. (B) The percentage of cells per cell cycle was compared to untreated controls by one-way ANOVA with Turkey post hoc correction for multiple comparisons. Since the replicates showed slight variabilities and not all cells could be included in the range of the markers, the bars do not reach 100%.

Treatment with a sufficient amount of 5FU (at its ED₅₀-concentration) and with 5FU-enhanced aptamers at their ED₅₀ significantly increased the portion of cells in the G1 phase and reduced the portion of cells in G2/M. Aptamers alone failed to induce that effect. The results indicate that, on the one hand, sufficient 5FU treatment causes G1 arrest in proliferating cancer cells. On the other hand, the cytostatic effect of 5FU is strongly amplified by the incorporation of 5FU into our CD44-targeted aptamers. The application of equimolar amounts of pure 5FU does not induce the same effect as the modified aptamers.

Since the cytostatic effect of 5FU-modified aptamers strongly exceeds the effect of equimolar 5FU in cancer cells, it seems probable that the aptamers themselves also contribute to the observed cytostatic effects, although not through G1 arrest. To elucidate, which cellular pathways could be involved in the mechanism of action of our aptamers, an in-silico approach was implemented.

5.5. In silico modeling of aptamer binding to the CD44s protein

To model the interaction between the RNA aptamers and the CD44 protein, the HADDOCK2.2 server tool was chosen [120], that could be addressed under <https://milou.science.uu.nl/services/HADDOCK2.2/haddockserver-easy.html>. The server returns a 'HADDOCK score' for each possible binding cluster between RNA and protein based on the weighted sum of various properties:

- van der Waals intermolecular energy
- electrostatic intermolecular energy
- distance restraints energy
- radius of gyration restraint energy
- direct RDC restraint energy
- intervector projection angle restraints energy
- pseudo contact shift restraint energy
- diffusion anisotropy energy
- dihedral angle restraints energy
- symmetry restraints energy
- buried surface area
- binding energy and desolvation energy [121]

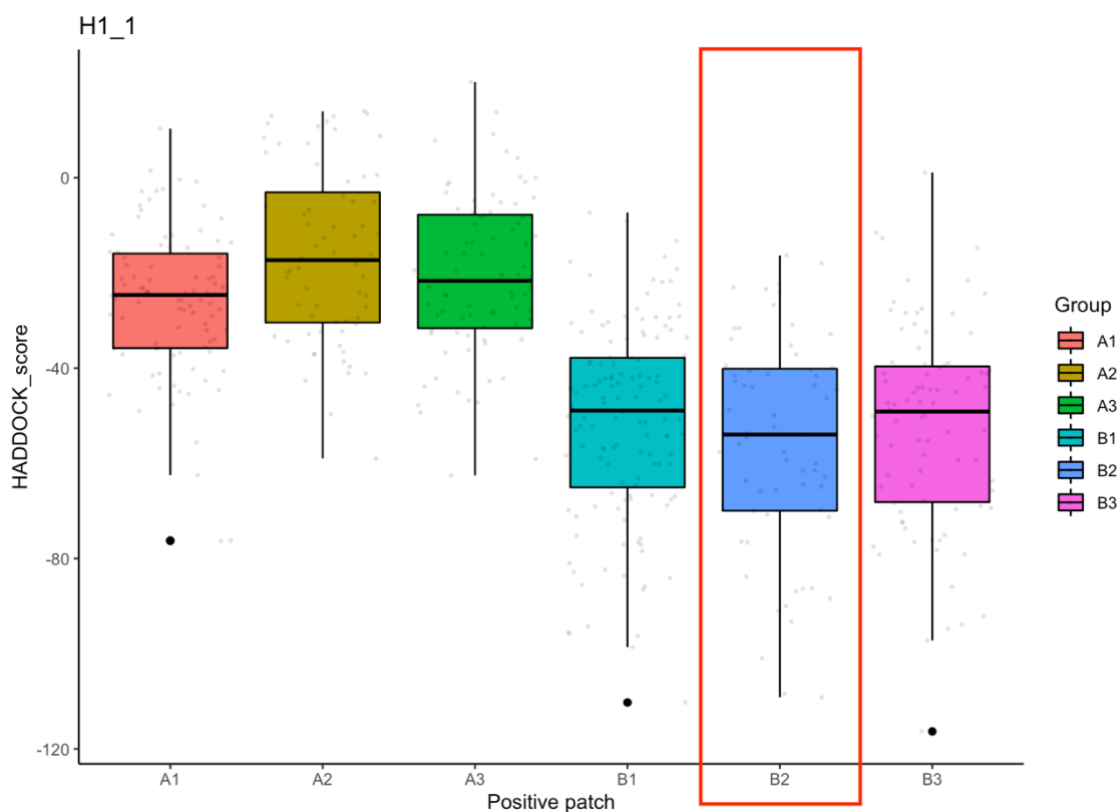
Inclusion of many parameters in an optimized score promises a valid estimation of the most realistic cluster of interactions between protein and RNA.

A high-resolution crystal structure of the human CD44s extracellular domain complex (4PZ3) was obtained from RCSB PDB as a .pdb file [117] (<https://www.rcsb.org/structure/4PZ3>). Six positively charged patches were located on the protein surface using the BindUP server tool [118] (<http://bindup.technion.ac.il>).

Tertiary RNA structures for each aptamer (H1_1, H2_1, and H2_2#) were calculated using the MC-Fold-MC-Sym-pipeline [119] (<http://www.major.irc.ca/MC-Fold/>). After refinement, the top-ranked RNA .pdb files based on minimal free energy were obtained for each aptamer.

5.5.1. Estimation of the most favorable binding patch of CD44

The coupling simulation of tertiary RNA aptamer structures to the six positive patches on the CD44s extracellular protein domain was performed on the HADDOCK2.2 server, yielding HADDOCK scores for each interaction. Lower scores indicate a more favorable binding composition.



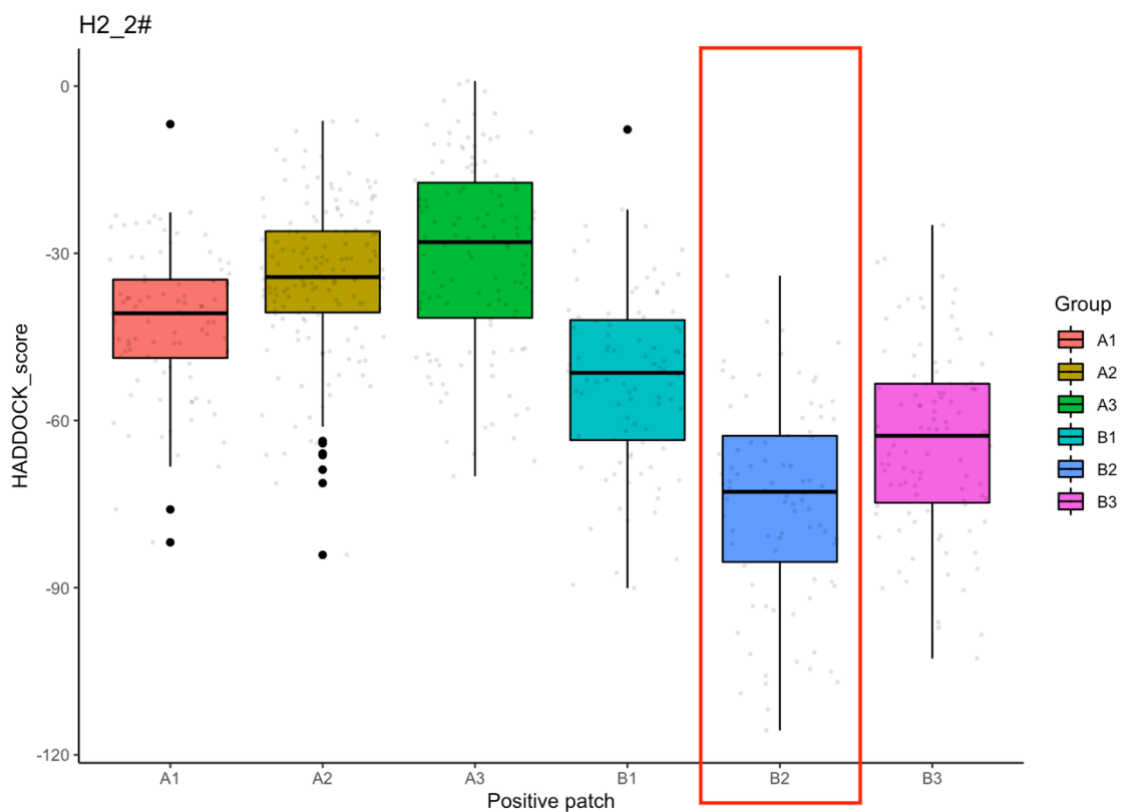
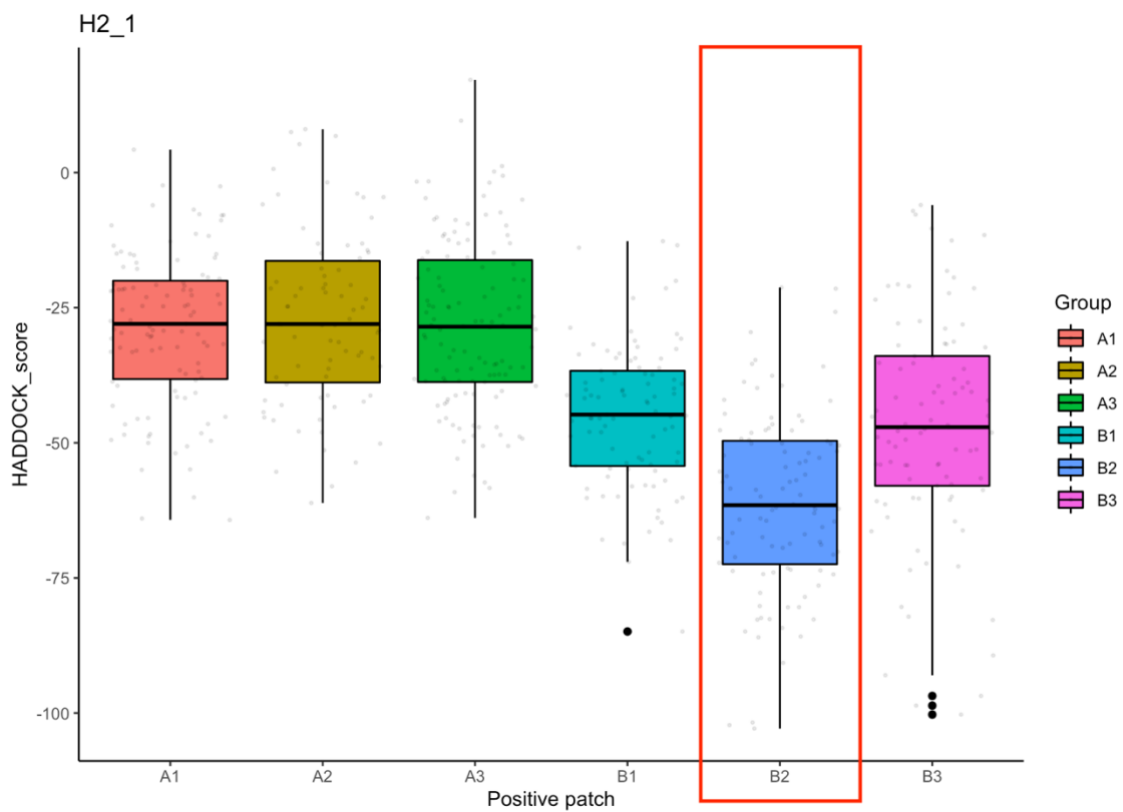
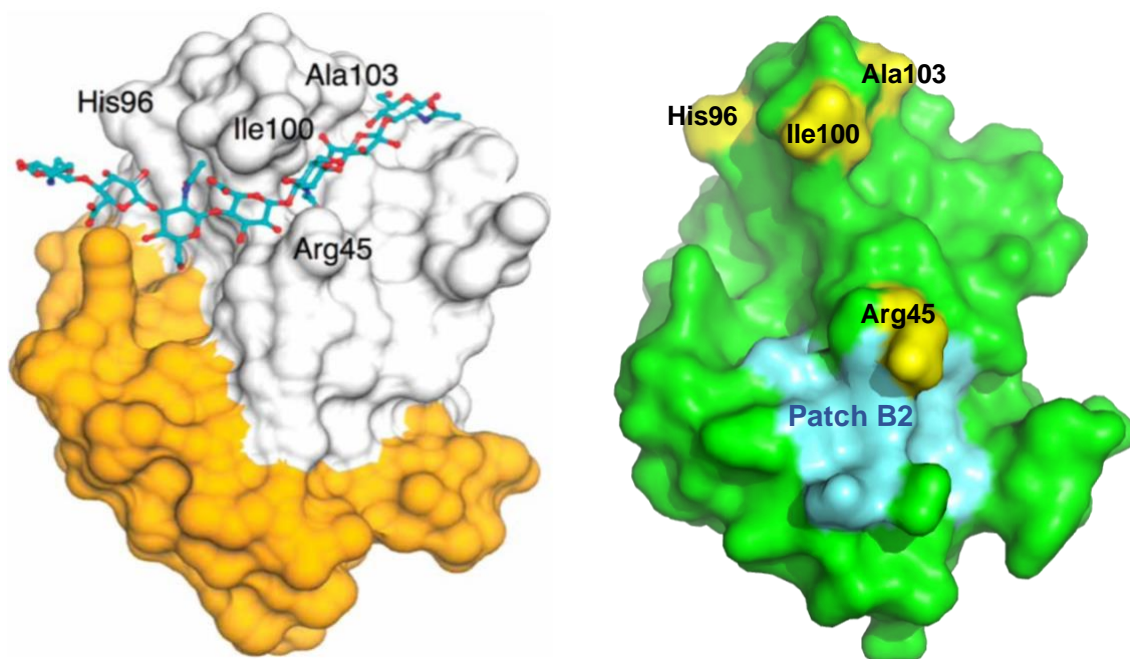


Figure 21. Comparison of HADDOCK scores of CD44-aptamer interaction clusters: The HADDOCK scores of the binding clusters were compared by median for each positive protein patch (A1-B3) and for each aptamer. Lower scores indicate more favorable binding properties. Calculation of statistical significance is not indicated since only the lowest HADDOCK scores are of interest.

It becomes evident that patch B2 shows the lowest HADDOCK score for each aptamer interaction. That domain of the extracellular region of the CD44s protein has the highest probability of being the actual target of binding of the three aptamers.

5.5.2. Visualization of aptamer binding to CD44

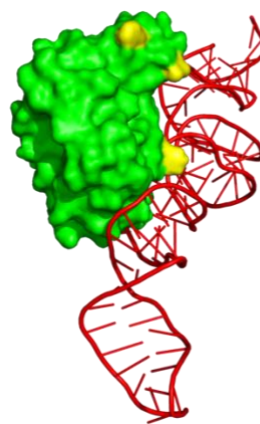
To understand the biological significance of these findings, the structures and their interactions were visualized using the PyMOL2.5 software [122] (<https://pymol.org/2/#page-top>). Figure 22 (A) shows the CD44s extracellular protein domain with its known binding site for interaction with hyaluronic acid [125] and patch B2, the proposed binding site of the aptamers. Next, the protein model that was used in the HADDOCK calculations is shown. Figure 22 (B) shows the aptamers H1_1, H2_1, and H2_2# (front and side view) in the optimal calculated binding configuration according to the HADDOCK score on the B2 patch of the CD44 protein.



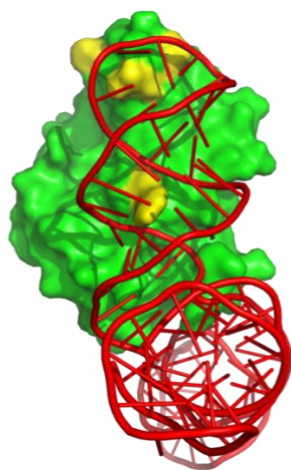
Aptamer H1_1 front



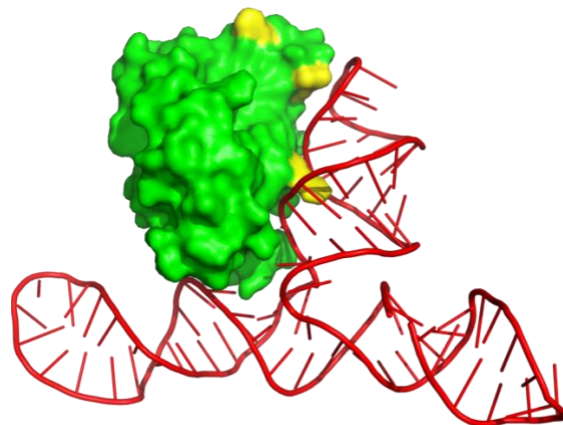
Aptamer H1_1 side



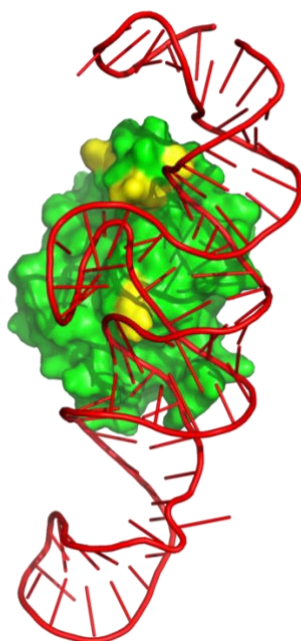
Aptamer H2_1 front



Aptamer H2_1 side



Aptamer H2_2# front



Aptamer H2_2# side

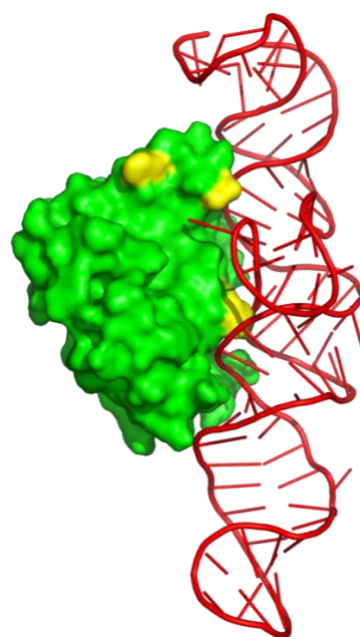


Figure 22. Visualization of aptamer binding to the CD44s protein: The upper panel shows the CD44s model with the hyaluronan binding site from Banerji et al. [125] next to the model that was obtained from RCSB PDB for HADDOCK calculations. The highlighted residues correspond to the marked amino acids in the referenced protein model. Patch B2 on the protein is marked in blue. The lower panel shows the top-ranked clusters of aptamers H1_1, H2_1, and H2_2# according to the HADDOCK score binding to the B2 patch of the CD44s extracellular protein domain. Each complex is shown from the front and from the side for better orientation.

Considering the results of the HADDOCK calculation and visualization of the molecular binding clusters, the following assumptions can be deduced: All aptamers favor the same specific patch on the surface of the extracellular domain of the CD44s protein as their binding target. When coupled to that domain in the most realistic configuration, all aptamers clearly obstruct the hyaluronan binding pocket of CD44 between Arg45 and Ile100. These observations show a possible mechanism by which the generated aptamers may be able to influence cellular pathways of cancer cells.

6. Discussion

The treatment of advanced pancreatic ductal adenocarcinoma poses a challenge in clinical routine due to its complex heterogeneity and aggressiveness [11], [12], [13], [14], [16], [17]. In this study, we generated an approach to overcome the limitations of conventional chemotherapy by implementing a targeted drug delivery system. We enriched aptamers specific for the CD44 protein, which is overexpressed in PDAC and associated with undesirable tumor traits and reduced overall survival [53], [55], [54], [56], [57], [61], [62], but it was not possible to direct aptamer specificity toward the subregion of exon variant 6 on CD44. Finally, we were able to successfully integrate the cytostatic drug 5FU into our aptamers and show significant antitumor treatment effects dependent on CD44 expression.

6.1. Evaluation of the modified SELEX protocol

To synthesize specific aptamers for CD44 and its variant 6, we developed a modified SELEX protocol. First, a recombinant CD44 protein containing all exon variants was generated in a mammalian expression model (see 4.6.). Mammalian expression was necessary to preserve post-translational modifications of the protein as expected in vivo. Then a pool of random aptamer oligonucleotides was selected for binding properties to that protein (see 4.7.4.). In the advanced SELEX setup, we tried to direct the binding specificity of the aptamers towards the region of exon 6 on the CD44 protein by incorporation of a negative selection step (see 4.7.5.).

The modified SELEX cycle yielded 3 strongly enriched aptamer sequences (H1_1, H2_2 and H2_2#) (see 5.1.1.). All of those sequences showed highly conserved motif patterns in the center (see 5.1.2.), indicating directed selection pressure during the SELEX process. The enriched aptamers were labeled with a fluorescent dye, and their binding specificity was assessed in cell line systems by flow cytometry. No specific binding to exon variant 6 of CD44 could be observed, only specificity towards standard CD44 (see 5.3.1. and 5.3.2.). CD44 could be confirmed as the cellular target of our selected aptamers by gel electrophoresis (see 5.3.3.).

In conclusion, we were able to generate aptamers specific for the standard CD44 extracellular protein domain, but the implementation of the modified SELEX protocol failed to convey binding specificity to the variant exon 6 of CD44. One possible explanation for the failure can be found during the negative selection step of the advanced SELEX setup. The antibody that was used to block the v6 exon during aptamer selection has a size of approximately 150kDa [126] while the whole CD44 protein can

show a size of 82kDa to 200kDa [47]. The region of variant exon 6 spans a range of only 42 amino acids out of the 742 amino acids of the protein [127]. Hence, it is possible that the antibody, which is almost the same size as the protein, does not cleanly cover the small region of 42 amino acids of the variant 6 exon on CD44. It is rather binding to a tertiary metastructure of CD44v6 and thus the v6 pocket might still be accessible for aptamers during negative selection. Additionally, the interaction of CD44v6 with the antibody could cause conformational changes to the protein, as described by Škerlová et al. [128]. This could release other aptamer structures that were already bound from the complex, and therefore reduce the efficiency of the negative selection step during advanced SELEX. Another possible explanation lies in the fact that the small region of exon variant 6 is rather hidden below the main bulk of the hyaluronan binding domain of CD44 and thus might not be accessible for the RNA aptamers. According to Chen et al., this region is so cramped that it cannot even be resolved by crystallography [129]. Taking into account the size of the aptamer RNA in relation to the protein (see 5.5.), it is possible that the aptamers were not able to access the exon variant 6 pocket at all.

A possible improvement for future attempts to generate aptamers specific for CD44v6 would be to use two different proteins during the SELEX-cycle: one version of CD44 containing exon v6 for positive selection and a version without v6 for negative selection. This approach would dispose of all interferences that might be caused by the implementation of an antibody. Also, the fact that the pocket of exon variant 6 might be not accessible wouldn't matter anymore. The aptamers' binding specificity would be directed towards tertiary metastructures of CD44 that are only present if exon v6 is, and not towards v6 itself.

6.2. Evaluation of cytostatic effects of CD44-specific aptamers in vitro

Despite the setback with respect to the side project, we were able to generate specific aptamers for the CD44s protein. The enriched aptamer sequences H1_1, H2_2 and H2_2# were enhanced by exchanging every Uracil residue with 5-Fluorouracil during transcription (see 4.7.3.). The modified aptamers were then evaluated for their biological effects on proliferation and cell cycle in pancreatic cancer cell line systems (see 4.12. and 4.13.).

An intermediate/low CD44 expressing pancreatic cancer cell line and a high CD44 expressing one were treated with 5FU-modified aptamers. In both cases, the reduction of proliferation that was achieved by aptamer treatment was significantly stronger compared to equimolar 5FU-only controls. The efficacy of aptamer treatment increased

markedly with higher expression of CD44 (see 5.4.1.). That effect was stronger than just an addition of the effects of pure aptamers and pure 5FU, confirming that our 5FU-modified aptamers are more than mere drug carriers (see 5.4.1., Isobolograms). Even in a cell culture system, where the accessibility of chemotherapy is the same for all cancer cells, the aptamers have shown superior anticancer activity compared to 5FU alone. These observations reveal a promising advantage that is especially important for in vivo application: Lower doses of drugs are necessary to induce cytostatic effects in cancer cells, thus reducing cytotoxicity to bystander cells [130]. By combination of these properties with CD44-specific targeting, our aptamers could be able to significantly reduce the adverse side effects associated with the cytostatic treatment of pancreatic cancer.

The analysis of cancer cell cycle distribution after treatment with 5FU-modified aptamers showed a significant accumulation of cells in the G1 phase and a reduction in the population transitioning to G2/M. The same effect was only reached by a 10-fold amount of free 5FU (see 5.4.2.). Consistent with the findings of Mahajan et al. and Gao et al. [77], [131], this alteration of the cell cycle indicates a state of G1 arrest, that is induced by 5FU treatment. Therefore, the main effect of our modified aptamers is exerted by the delivery of 5FU to the cancer cells and not by some other unspecific side interaction.

Of course, additional work needs to be done before transitioning to experimental models of higher order. A knockout of CD44 in cancer cell lines must be performed to clearly show the CD44 dependence of cytostatic aptamer effects. Furthermore, a mechanistic analysis of cellular aptamer uptake by inhibition of all possible pathways and assessment of intracellular aptamer processing is required, as described by Mahajan et al. [77].

6.3. Evaluation of the aptamer binding site on CD44 and its biological relevance

Besides the strong enhancement of 5FU-efficacy by modified aptamers, an additional observation caught our attention: Aptamers alone, without 5FU, also showed considerable inhibition of cell proliferation, almost reaching a reduction of 50% (see 5.4.1.). But interestingly, this effect was not based on cell cycle arrest, as it was observed with the 5FU-modified counterparts (see 5.4.2.). Therefore, there might be a way by which aptamers alone exhibit a biological effect on cancer cells. To elucidate possible pathways of action, we calculated the most probable binding sites of our aptamers based on the crystal structure of CD44 (see 4.14.).

The computed estimation shows that each individual aptamer consistently favors one specific binding patch of the CD44 protein (see 5.5.1.). When that specific patch is mapped on the protein surface, it becomes evident that the binding region of our aptamers lies in close proximity to the domain of interaction with hyaluronic acid [125]. Visualization of the aptamer models bound to that patch discloses that the hyaluronan binding pocket of CD44 becomes severely obstructed by our generated aptamers (see 5.5.2.). Therefore, our aptamers could exert a biological effect on cancer cells by interfering with binding of hyaluronan to its receptor molecule CD44.

The interaction of CD44 with hyaluronic acid is known to be an important driver of tumor aggression in many cancer entities [132], [133]. One of the main proposed mechanisms is the cross-linking of CD44 receptor domains through large molecules of hyaluronic acid, thus bringing lipid rafts loaded with cell surface receptors into close proximity [134]. This activates different ErbB receptor tyrosin kinases, TGF-beta1 receptors and their corresponding mediated downstream pathways [135], [136], [137]. Hyaluronan-CD44 dependent effects include PI3K/Akt activation with consecutive overexpression of MDR1 and enhanced drug resistance [138], FAK stimulation that leads to resistance to apoptosis [139], and src/MAPK activated cell proliferation [140]. Strong expression of hyaluronic acid was even shown to be associated with shorter survival in patients with PDAC [141]. Although in vivo, the stromal cancer microenvironment is usually the main source of hyaluronan [142], cultured pancreatic cancer cells also synthesize and excrete hyaluronic acid, although to a minor extent [143], [144]. Taking all of this into consideration, the hypothesis can be proposed that our aptamers exert a cytostatic effect on cancer cells by interference with hyaluronan/CD44-axis pathways. Similar approaches have already shown that the inhibition of interaction between CD44 and hyaluronic acid in tumor cells had antitumoral effects such as increased apoptosis rate [145], reduced proliferation [146] and increased drug sensitivity [138].

More work needs to be done to elucidate how exactly the interaction of our aptamers with CD44 affects the downstream pathways of the protein receptor in cancer cells. This can be achieved by evaluating the phosphorylation patterns of the signaling mediators, as it was done by Mahajan et al. [77]. Overall, there are many possible benefits to our novel aptamers that must be evaluated in experimental models of higher order. The specificity towards CD44 has the potential to overcome stromal barriers, the strong enhancement of 5FU cytotoxicity might lead to superior cancer growth impairment while reducing therapy associated side effects to bystander cells. And finally, the interaction with the hyaluronan binding domain of CD44 could lead to a variety of beneficial antitumor effects. Taking all these different findings into account, our generated aptamers comprise a very promising new approach for the treatment of pancreatic cancer.

7. References

1. Siegel, R.L., et al., *Cancer statistics, 2023*. CA Cancer J Clin, 2023. **73**(1): p. 17-48.
2. Siegel, R.L., K.D. Miller, and A. Jemal, *Cancer statistics, 2018*. CA Cancer J Clin, 2018. **68**(1): p. 7-30.
3. Rahib, L., et al., *Projecting cancer incidence and deaths to 2030: the unexpected burden of thyroid, liver, and pancreas cancers in the United States*. Cancer Res, 2014. **74**(11): p. 2913-21.
4. De La Cruz, M.S., A.P. Young, and M.T. Ruffin, *Diagnosis and management of pancreatic cancer*. Am Fam Physician, 2014. **89**(8): p. 626-32.
5. Ducreux, M., et al., *Cancer of the pancreas: ESMO Clinical Practice Guidelines for diagnosis, treatment and follow-up*. Ann Oncol, 2015. **26 Suppl 5**: p. v56-68.
6. Park, W., A. Chawla, and E.M. O'Reilly, *Pancreatic Cancer: A Review*. Jama, 2021. **326**(9): p. 851-862.
7. Peddi, P.F., et al., *Multi-institutional experience with FOLFIRINOX in pancreatic adenocarcinoma*. Jop, 2012. **13**(5): p. 497-501.
8. Neoptolemos, J.P., et al., *Comparison of adjuvant gemcitabine and capecitabine with gemcitabine monotherapy in patients with resected pancreatic cancer (ESPAC-4): a multicentre, open-label, randomised, phase 3 trial*. Lancet, 2017. **389**(10073): p. 1011-1024.
9. Conroy, T., et al., *FOLFIRINOX versus gemcitabine for metastatic pancreatic cancer*. N Engl J Med, 2011. **364**(19): p. 1817-25.
10. Chan, K.K.W., et al., *Real-world outcomes of FOLFIRINOX vs gemcitabine and nab-paclitaxel in advanced pancreatic cancer: A population-based propensity score-weighted analysis*. Cancer Med, 2020. **9**(1): p. 160-169.
11. Yamano, M., et al., *Genetic progression and divergence in pancreatic carcinoma*. Am J Pathol, 2000. **156**(6): p. 2123-33.
12. Feldmann, K., et al., *Mesenchymal Plasticity Regulated by Prrx1 Drives Aggressive Pancreatic Cancer Biology*. Gastroenterology, 2021. **160**(1): p. 346-361.e24.
13. Froeling, F.E., et al., *Retinoic acid-induced pancreatic stellate cell quiescence reduces paracrine Wnt- β -catenin signaling to slow tumor progression*. Gastroenterology, 2011. **141**(4): p. 1486-97, 1497.e1-14.
14. Provenzano, P.P., et al., *Enzymatic targeting of the stroma ablates physical barriers to treatment of pancreatic ductal adenocarcinoma*. Cancer Cell, 2012. **21**(3): p. 418-29.

15. Hosein, A.N., R.A. Brekken, and A. Maitra, *Pancreatic cancer stroma: an update on therapeutic targeting strategies*. Nat Rev Gastroenterol Hepatol, 2020. **17**(8): p. 487-505.
16. Yao, J., et al., *Cyclopamine reverts acquired chemoresistance and down-regulates cancer stem cell markers in pancreatic cancer cell lines*. Swiss Med Wkly, 2011. **141**: p. w13208.
17. Hsu, C.P., et al., *CD44 Predicts Early Recurrence in Pancreatic Cancer Patients Undergoing Radical Surgery*. In Vivo, 2018. **32**(6): p. 1533-1540.
18. Ishiwata, T., et al., *Pancreatic cancer stem cells: features and detection methods*. Pathol Oncol Res, 2018. **24**(4): p. 797-805.
19. Nimmakayala, R.K., et al., *Metabolic programming of distinct cancer stem cells promotes metastasis of pancreatic ductal adenocarcinoma*. Oncogene, 2021. **40**(1): p. 215-231.
20. Bailey, P., et al., *Genomic analyses identify molecular subtypes of pancreatic cancer*. Nature, 2016. **531**(7592): p. 47-52.
21. Danilova, L., et al., *Programmed Cell Death Ligand-1 (PD-L1) and CD8 Expression Profiling Identify an Immunologic Subtype of Pancreatic Ductal Adenocarcinomas with Favorable Survival*. Cancer Immunol Res, 2019. **7**(6): p. 886-895.
22. Chalmers, Z.R., et al., *Analysis of 100,000 human cancer genomes reveals the landscape of tumor mutational burden*. Genome Med, 2017. **9**(1): p. 34.
23. Schizas, D., et al., *Immunotherapy for pancreatic cancer: A 2020 update*. Cancer Treat Rev, 2020. **86**: p. 102016.
24. Brahmer, J.R., et al., *Safety and activity of anti-PD-L1 antibody in patients with advanced cancer*. N Engl J Med, 2012. **366**(26): p. 2455-65.
25. Corti, A., et al., *Targeted drug delivery and penetration into solid tumors*. Med Res Rev, 2012. **32**(5): p. 1078-91.
26. Moore, M.J., et al., *Erlotinib plus gemcitabine compared with gemcitabine alone in patients with advanced pancreatic cancer: a phase III trial of the National Cancer Institute of Canada Clinical Trials Group*. J Clin Oncol, 2007. **25**(15): p. 1960-6.
27. Fang, Y.T., et al., *Recent advances in targeted therapy for pancreatic adenocarcinoma*. World J Gastrointest Oncol, 2023. **15**(4): p. 571-595.
28. Löhr, M., et al., *Frequency of K-ras mutations in pancreatic intraductal neoplasias associated with pancreatic ductal adenocarcinoma and chronic pancreatitis: a meta-analysis*. Neoplasia, 2005. **7**(1): p. 17-23.
29. Zeitouni, D., et al., *KRAS Mutant Pancreatic Cancer: No Lone Path to an Effective Treatment*. Cancers (Basel), 2016. **8**(4).

30. Rinehart, J., et al., *Multicenter phase II study of the oral MEK inhibitor, CI-1040, in patients with advanced non-small-cell lung, breast, colon, and pancreatic cancer*. J Clin Oncol, 2004. **22**(22): p. 4456-62.
31. Pettazoni, P., et al., *Genetic events that limit the efficacy of MEK and RTK inhibitor therapies in a mouse model of KRAS-driven pancreatic cancer*. Cancer Res, 2015. **75**(6): p. 1091-101.
32. Kuehn, R., et al., *Angiogenesis, angiogenic growth factors, and cell adhesion molecules are upregulated in chronic pancreatic diseases: angiogenesis in chronic pancreatitis and in pancreatic cancer*. Pancreas, 1999. **18**(1): p. 96-103.
33. Seo, Y., et al., *High expression of vascular endothelial growth factor is associated with liver metastasis and a poor prognosis for patients with ductal pancreatic adenocarcinoma*. Cancer, 2000. **88**(10): p. 2239-45.
34. Pàez-Ribes, M., et al., *Antiangiogenic therapy elicits malignant progression of tumors to increased local invasion and distant metastasis*. Cancer Cell, 2009. **15**(3): p. 220-31.
35. Kindler, H.L., et al., *Gemcitabine plus bevacizumab compared with gemcitabine plus placebo in patients with advanced pancreatic cancer: phase III trial of the Cancer and Leukemia Group B (CALGB 80303)*. J Clin Oncol, 2010. **28**(22): p. 3617-22.
36. Lu, X. and Y. Kang, *Hypoxia and hypoxia-inducible factors: master regulators of metastasis*. Clin Cancer Res, 2010. **16**(24): p. 5928-35.
37. Ramanathan, R.K., et al., *Phase IB/II Randomized Study of FOLFIRINOX Plus Pegylated Recombinant Human Hyaluronidase Versus FOLFIRINOX Alone in Patients With Metastatic Pancreatic Adenocarcinoma: SWOG S1313*. J Clin Oncol, 2019. **37**(13): p. 1062-1069.
38. Moore, M.J., et al., *Comparison of gemcitabine versus the matrix metalloproteinase inhibitor BAY 12-9566 in patients with advanced or metastatic adenocarcinoma of the pancreas: a phase III trial of the National Cancer Institute of Canada Clinical Trials Group*. J Clin Oncol, 2003. **21**(17): p. 3296-302.
39. Bendell, J., et al., *Safety and Efficacy of Andecaliximab (GS-5745) Plus Gemcitabine and Nab-Paclitaxel in Patients with Advanced Pancreatic Adenocarcinoma: Results from a Phase I Study*. Oncologist, 2020. **25**(11): p. 954-962.
40. Dotan, E., et al., *Phase Ib Study of Wnt Inhibitor Ipafricept with Gemcitabine and nab-paclitaxel in Patients with Previously Untreated Stage IV Pancreatic Cancer*. Clin Cancer Res, 2020. **26**(20): p. 5348-5357.
41. Prieto-Vila, M., et al., *Drug Resistance Driven by Cancer Stem Cells and Their Niche*. Int J Mol Sci, 2017. **18**(12).
42. Lonardo, E., P.C. Hermann, and C. Heeschen, *Pancreatic cancer stem cells - update and future perspectives*. Mol Oncol, 2010. **4**(5): p. 431-42.

43. Telen, M.J., et al., *A blood group-related polymorphism of CD44 abolishes a hyaluronan-binding consensus sequence without preventing hyaluronan binding*. J Biol Chem, 1996. **271**(12): p. 7147-53.
44. Aruffo, A., et al., *CD44 is the principal cell surface receptor for hyaluronate*. Cell, 1990. **61**(7): p. 1303-13.
45. Carter, W.G. and E.A. Wayner, *Characterization of the class III collagen receptor, a phosphorylated, transmembrane glycoprotein expressed in nucleated human cells*. J Biol Chem, 1988. **263**(9): p. 4193-201.
46. Ponta, H., L. Sherman, and P.A. Herrlich, *CD44: from adhesion molecules to signalling regulators*. Nat Rev Mol Cell Biol, 2003. **4**(1): p. 33-45.
47. Yang, H. and R.M. Binns, *Isolation and characterization of the soluble and membrane-bound porcine CD44 molecules*. Immunology, 1993. **78**(4): p. 547-54.
48. Skelton, T.P., et al., *Glycosylation provides both stimulatory and inhibitory effects on cell surface and soluble CD44 binding to hyaluronan*. J Cell Biol, 1998. **140**(2): p. 431-46.
49. Günthert, U., et al., *A new variant of glycoprotein CD44 confers metastatic potential to rat carcinoma cells*. Cell, 1991. **65**(1): p. 13-24.
50. Neame, S.J., et al., *CD44 exhibits a cell type dependent interaction with triton X-100 insoluble, lipid rich, plasma membrane domains*. J Cell Sci, 1995. **108 (Pt 9)**: p. 3127-35.
51. Tsukita, S., et al., *ERM family members as molecular linkers between the cell surface glycoprotein CD44 and actin-based cytoskeletons*. J Cell Biol, 1994. **126**(2): p. 391-401.
52. Bourguignon, L.Y., et al., *CD44 interaction with c-Src kinase promotes cortactin-mediated cytoskeleton function and hyaluronic acid-dependent ovarian tumor cell migration*. J Biol Chem, 2001. **276**(10): p. 7327-36.
53. *The Human Protein Atlas*. Available from: <https://www.proteinatlas.org/ENSG00000026508-CD44/pathology/pancreatic+cancer#Location>.
54. Li, X.P., et al., *Expression of CD44 in pancreatic cancer and its significance*. Int J Clin Exp Pathol, 2015. **8**(6): p. 6724-31.
55. Liu, Y., et al., *CD44 overexpression related to lymph node metastasis and poor prognosis of pancreatic cancer*. Int J Biol Markers, 2018. **33**(3): p. 308-313.
56. Nam, K., et al., *CD44 regulates cell proliferation, migration, and invasion via modulation of c-Src transcription in human breast cancer cells*. Cell Signal, 2015. **27**(9): p. 1882-94.
57. Bjorge, J.D., et al., *Simultaneous siRNA targeting of Src and downstream signaling molecules inhibit tumor formation and metastasis of a human model breast cancer cell line*. PLoS One, 2011. **6**(4): p. e19309.

58. Liu, X., et al., *Homophilic CD44 Interactions Mediate Tumor Cell Aggregation and Polyclonal Metastasis in Patient-Derived Breast Cancer Models*. *Cancer Discov*, 2019. **9**(1): p. 96-113.
59. Todaro, M., et al., *CD44v6 is a marker of constitutive and reprogrammed cancer stem cells driving colon cancer metastasis*. *Cell Stem Cell*, 2014. **14**(3): p. 342-56.
60. Jiang, W., et al., *CD44 regulates pancreatic cancer invasion through MT1-MMP*. *Mol Cancer Res*, 2015. **13**(1): p. 9-15.
61. Al-Hajj, M., et al., *Prospective identification of tumorigenic breast cancer cells*. *Proc Natl Acad Sci U S A*, 2003. **100**(7): p. 3983-8.
62. Nallasamy, P., et al., *Pancreatic Tumor Microenvironment Factor Promotes Cancer Stemness via SPP1-CD44 Axis*. *Gastroenterology*, 2021. **161**(6): p. 1998-2013.e7.
63. Dalla Pozza, E., et al., *Pancreatic ductal adenocarcinoma cell lines display a plastic ability to bi-directionally convert into cancer stem cells*. *Int J Oncol*, 2015. **46**(3): p. 1099-108.
64. Orian-Rousseau, V., et al., *CD44 is required for two consecutive steps in HGF/c-Met signaling*. *Genes Dev*, 2002. **16**(23): p. 3074-86.
65. Matzke-Ogi, A., et al., *Inhibition of Tumor Growth and Metastasis in Pancreatic Cancer Models by Interference With CD44v6 Signaling*. *Gastroenterology*, 2016. **150**(2): p. 513-25.e10.
66. Chen, C., et al., *Gemcitabine resistance of pancreatic cancer cells is mediated by IGF1R dependent upregulation of CD44 expression and isoform switching*. *Cell Death & Disease*, 2022. **13**(8): p. 682.
67. Kuo, Y.C., et al., *Identification and Clinical Significance of Pancreatic Cancer Stem Cells and Their Chemotherapeutic Drug Resistance*. *Int J Mol Sci*, 2023. **24**(8).
68. Gu, J., et al., *CDCA8/SNAI2 Complex Activates CD44 to Promote Proliferation and Invasion of Pancreatic Ductal Adenocarcinoma*. *Cancers (Basel)*, 2022. **14**(21).
69. Al-Hassan, J.M., et al., *Fraction B From Catfish Epidermal Secretions Kills Pancreatic Cancer Cells, Inhibits CD44 Expression and Stemness, and Alters Cancer Cell Metabolism*. *Front Pharmacol*, 2021. **12**: p. 659590.
70. Askan, G., et al., *Pancreatic cancer stem cells may define tumor stroma characteristics and recurrence patterns in pancreatic ductal adenocarcinoma*. *BMC Cancer*, 2021. **21**(1): p. 385.
71. Chih-Po, H.S.U., et al., *CD44 Predicts Early Recurrence in Pancreatic Cancer Patients Undergoing Radical Surgery*. *In Vivo*, 2018. **32**(6): p. 1533.

72. Tuerk, C. and L. Gold, *Systematic evolution of ligands by exponential enrichment: RNA ligands to bacteriophage T4 DNA polymerase*. Science, 1990. **249**(4968): p. 505-10.
73. Ellington, A.D. and J.W. Szostak, *In vitro selection of RNA molecules that bind specific ligands*. Nature, 1990. **346**(6287): p. 818-22.
74. Manley, J.L., *SELEX to identify protein-binding sites on RNA*. Cold Spring Harb Protoc, 2013. **2013**(2): p. 156-63.
75. Urak, K.T., et al., *In vitro RNA SELEX for the generation of chemically-optimized therapeutic RNA drugs*. Methods, 2016. **103**: p. 167-74.
76. Osborne, S.E. and A.D. Ellington, *Nucleic Acid Selection and the Challenge of Combinatorial Chemistry*. Chem Rev, 1997. **97**(2): p. 349-370.
77. Mahajan, U.M., et al., *Tumor-Specific Delivery of 5-Fluorouracil-Incorporated Epidermal Growth Factor Receptor-Targeted Aptamers as an Efficient Treatment in Pancreatic Ductal Adenocarcinoma Models*. Gastroenterology, 2021. **161**(3): p. 996-1010.e1.
78. Rusconi, C.P., et al., *RNA aptamers as reversible antagonists of coagulation factor IXa*. Nature, 2002. **419**(6902): p. 90-94.
79. Richardson, F.C., et al., *An evaluation of the toxicities of 2'-fluorouridine and 2'-fluorocytidine-HCl in F344 rats and woodchucks (Marmota monax)*. Toxicol Pathol, 1999. **27**(6): p. 607-17.
80. Sauerborn, M., et al., *Immunological mechanism underlying the immune response to recombinant human protein therapeutics*. Trends Pharmacol Sci, 2010. **31**(2): p. 53-9.
81. Shigdar, S., et al., *Aptamers: Cutting edge of cancer therapies*. Mol Ther, 2021. **29**(8): p. 2396-2411.
82. Shukla, D., et al., *Pegaptanib sodium for ocular vascular disease*. Indian J Ophthalmol, 2007. **55**(6): p. 427-30.
83. Mullard, A., *FDA approves second RNA aptamer*. Nat Rev Drug Discov, 2023. **22**(10): p. 774.
84. Mingru, Z., et al., *The first Application of 68Ga labeled ssDNA Aptamer Sgc8 in Colorectal Patients*. Journal of Nuclear Medicine, 2018. **59**(supplement 1): p. 53.
85. *Preclinical and phase 1A clinical evaluation of an anti-VEGF pegylated aptamer (EYE001) for the treatment of exudative age-related macular degeneration*. Retina, 2002. **22**(2): p. 143-52.
86. Wu, L., et al., *Aptamer-Based Cancer Cell Analysis and Treatment*. ChemistryOpen, 2022. **11**(10): p. e202200141.
87. Razlansari, M., et al., *Development and classification of RNA aptamers for therapeutic purposes: an updated review with emphasis on cancer*. Molecular and Cellular Biochemistry, 2023. **478**(7): p. 1573-1598.

88. Amano, R., et al., *Specific inhibition of FGF5-induced cell proliferation by RNA aptamers*. Scientific Reports, 2021. **11**(1): p. 2976.
89. Zhao, J., et al., *Development of aptamer-based inhibitors for CRISPR/Cas system*. Nucleic Acids Res, 2021. **49**(3): p. 1330-1344.
90. Zhou, J. and J.J. Rossi, *Aptamer-targeted cell-specific RNA interference*. Silence, 2010. **1**(1): p. 4.
91. Dhanya, C.R., A.S. Mary, and M. Madhavan, *Aptamer-siRNA chimeras: Promising tools for targeting HER2 signaling in cancer*. Chem Biol Drug Des, 2023. **101**(5): p. 1162-1180.
92. Lv, H., et al., *Aptamer-functionalized targeted siRNA delivery system for tumor immunotherapy*. Biomed Mater, 2022. **17**(2).
93. Camorani, S., et al., *Aptamer-Functionalized Nanoparticles Mediate PD-L1 siRNA Delivery for Effective Gene Silencing in Triple-Negative Breast Cancer Cells*. Pharmaceutics, 2022. **14**(10).
94. Porciani, D., et al., *Aptamer-Mediated Codelivery of Doxorubicin and NF- κ B Decoy Enhances Chemosensitivity of Pancreatic Tumor Cells*. Mol Ther Nucleic Acids, 2015. **4**(4): p. e235.
95. Ding, C., et al., *Multivalent Aptamer Functionalized Ag₂S Nanodots/Hybrid Cell Membrane-Coated Magnetic Nanobioprobe for the Ultrasensitive Isolation and Detection of Circulating Tumor Cells*. Advanced Functional Materials, 2020. **30**(16): p. 1909781.
96. Ma, S., et al., *Clinical application and detection techniques of liquid biopsy in gastric cancer*. Mol Cancer, 2023. **22**(1): p. 7.
97. Ghasemii, K., et al., *Advances in aptamer-based drug delivery vehicles for cancer therapy*. Biomater Adv, 2022. **140**: p. 213077.
98. Earnest, K.G., et al., *Development and characterization of a DNA aptamer for MLL-AF9 expressing acute myeloid leukemia cells using whole cell-SELEX*. Sci Rep, 2021. **11**(1): p. 19174.
99. Liu, B., et al., *Recent advances in aptamer-based therapeutic strategies for targeting cancer stem cells*. Mater Today Bio, 2023. **19**: p. 100605.
100. Cruz-Hernández, C.D., et al., *Aptamers as Theragnostic Tools in Prostate Cancer*. Biomolecules, 2022. **12**(8).
101. Bottari, F., et al., *Do Aptamers Always Bind? The Need for a Multifaceted Analytical Approach When Demonstrating Binding Affinity between Aptamer and Low Molecular Weight Compounds*. Journal of the American Chemical Society, 2020. **142**(46): p. 19622-19630.
102. Biesecker, G., et al., *Derivation of RNA aptamer inhibitors of human complement C5*. Immunopharmacology, 1999. **42**(1-3): p. 219-30.
103. Odeh, F., et al., *Aptamers Chemistry: Chemical Modifications and Conjugation Strategies*. Molecules, 2019. **25**(1).

104. Milla, P., F. Dosio, and L. Cattel, *PEGylation of proteins and liposomes: a powerful and flexible strategy to improve the drug delivery*. *Curr Drug Metab*, 2012. **13**(1): p. 105-19.
105. Park, J.Y., et al., *Enhancement of in vivo targeting properties of ErbB2 aptamer by chemical modification*. *PLoS One*, 2023. **18**(9): p. e0291624.
106. Lakhin, A.V., V.Z. Tarantul, and L.V. Gening, *Aptamers: problems, solutions and prospects*. *Acta Naturae*, 2013. **5**(4): p. 34-43.
107. Chetan, C. and N. Muniasamy, *Aptamers for Targeted Delivery: Current Challenges and Future Opportunities*, in *Role of Novel Drug Delivery Vehicles in Nanobiomedicine*, K.T. Rajeev, et al., Editors. 2019, IntechOpen: Rijeka. p. Ch. 1.
108. Zhou, J. and J. Rossi, *Aptamers as targeted therapeutics: current potential and challenges*. *Nat Rev Drug Discov*, 2017. **16**(3): p. 181-202.
109. Tim Bushnell, P.D. *Modern Flow Cytometry*. Available from: <https://www.amrepflow.org.au/public/documents/MFCeBook4.pdf>.
110. *Created with BioRender.com*.
111. Kuchta, R.D., P. Benkovic, and S.J. Benkovic, *Kinetic mechanism whereby DNA polymerase I (Klenow) replicates DNA with high fidelity*. *Biochemistry*, 1988. **27**(18): p. 6716-25.
112. AbouHaidar, M.G. and I.G. Ivanov, *Non-enzymatic RNA hydrolysis promoted by the combined catalytic activity of buffers and magnesium ions*. *Z Naturforsch C J Biosci*, 1999. **54**(7-8): p. 542-8.
113. Raden, M., et al., *Freiburg RNA tools: a central online resource for RNA-focused research and teaching*. *Nucleic Acids Res*, 2018. **46**(W1): p. W25-w29.
114. Bailey, T.L. and C. Elkan, *Fitting a mixture model by expectation maximization to discover motifs in biopolymers*. *Proc Int Conf Intell Syst Mol Biol*, 1994. **2**: p. 28-36.
115. *Multiple Em for Motif Elicitation*. Explanation of the E-value]. Available from: https://meme-suite.org/meme/doc/examples/meme_example_output_files/meme.html.
116. Kodzius, R., et al., *CAGE: cap analysis of gene expression*. *Nat Methods*, 2006. **3**(3): p. 211-22.
117. Berman, H., K. Henrick, and H. Nakamura, *Announcing the worldwide Protein Data Bank*. *Nature Structural & Molecular Biology*, 2003. **10**(12): p. 980-980.
118. Paz, I., et al., *BindUP: a web server for non-homology-based prediction of DNA and RNA binding proteins*. *Nucleic Acids Res*, 2016. **44**(W1): p. W568-74.
119. Parisien, M. and F. Major, *The MC-Fold and MC-Sym pipeline infers RNA structure from sequence data*. *Nature*, 2008. **452**(7183): p. 51-5.

120. van Zundert, G.C.P., et al., *The HADDOCK2.2 Web Server: User-Friendly Integrative Modeling of Biomolecular Complexes*. J Mol Biol, 2016. **428**(4): p. 720-725.
121. *HADDOCK2.2 scoring function*. Available from: <https://www.bonvinlab.org/software/haddock2.2/scoring/>.
122. Schrödinger, L., *The PyMOL Molecular Graphics System. Version 2.0*.
123. Wagenmakers, A.J., R.J. Reinders, and W.J. van Venrooij, *Cross-linking of mRNA to proteins by irradiation of intact cells with ultraviolet light*. Eur J Biochem, 1980. **112**(2): p. 323-30.
124. Guo, X., et al., *Cell cycle perturbation and acquired 5-fluorouracil chemoresistance*. Anticancer Res, 2008. **28**(1a): p. 9-14.
125. Banerji, S., et al., *Structures of the Cd44-hyaluronan complex provide insight into a fundamental carbohydrate-protein interaction*. Nat Struct Mol Biol, 2007. **14**(3): p. 234-9.
126. Janeway CA Jr, T.P., Walport M, et al. , *The structure of a typical antibody molecule*, in *Immunobiology: The Immune System in Health and Disease*. 2001: New York: Garland Science.
127. Sreaton, G.R., et al., *Genomic structure of DNA encoding the lymphocyte homing receptor CD44 reveals at least 12 alternatively spliced exons*. Proc Natl Acad Sci U S A, 1992. **89**(24): p. 12160-4.
128. Škerlová, J., et al., *Molecular mechanism for the action of the anti-CD44 monoclonal antibody MEM-85*. J Struct Biol, 2015. **191**(2): p. 214-23.
129. Chen, K.L., et al., *Structural Characterization of the CD44 Stem Region for Standard and Cancer-Associated Isoforms*. Int J Mol Sci, 2020. **21**(1).
130. Zhu, G., et al., *Self-assembled, aptamer-tethered DNA nanotrains for targeted transport of molecular drugs in cancer theranostics*. Proc Natl Acad Sci U S A, 2013. **110**(20): p. 7998-8003.
131. Gao, L., et al., *Colon cancer cells treated with 5-fluorouracil exhibit changes in poly-lactosamine-type N-glycans*. Mol Med Rep, 2014. **9**(5): p. 1697-702.
132. Chen, L. and L.Y.W. Bourguignon, *Hyaluronan-CD44 interaction promotes c-Jun signaling and miRNA21 expression leading to Bcl-2 expression and chemoresistance in breast cancer cells*. Molecular Cancer, 2014. **13**(1): p. 52.
133. Torre, C., et al., *Reduction of Hyaluronan-CD44-Mediated Growth, Migration, and Cisplatin Resistance in Head and Neck Cancer Due to Inhibition of Rho Kinase and PI-3 Kinase Signaling*. Archives of Otolaryngology-Head & Neck Surgery, 2010. **136**(5): p. 493-501.
134. Ilangumaran, S., B. Borisch, and D.C. Hoessli, *Signal transduction via CD44: role of plasma membrane microdomains*. Leuk Lymphoma, 1999. **35**(5-6): p. 455-69.

135. Midgley, A.C., et al., *Transforming growth factor- β 1 (TGF- β 1)-stimulated fibroblast to myofibroblast differentiation is mediated by hyaluronan (HA)-facilitated epidermal growth factor receptor (EGFR) and CD44 co-localization in lipid rafts.* J Biol Chem, 2013. **288**(21): p. 14824-38.
136. Bao, W., et al., *HER2 interacts with CD44 to up-regulate CXCR4 via epigenetic silencing of microRNA-139 in gastric cancer cells.* Gastroenterology, 2011. **141**(6): p. 2076-2087.e6.
137. Ito, T., et al., *Hyaluronan regulates transforming growth factor-beta1 receptor compartmentalization.* J Biol Chem, 2004. **279**(24): p. 25326-32.
138. Misra, S., S. Ghatak, and B.P. Toole, *Regulation of MDR1 Expression and Drug Resistance by a Positive Feedback Loop Involving Hyaluronan, Phosphoinositide 3-Kinase, and ErbB2*. Journal of Biological Chemistry, 2005. **280**(21): p. 20310-20315.
139. Fujita, Y., et al., *CD44 signaling through focal adhesion kinase and its anti-apoptotic effect.* FEBS Lett, 2002. **528**(1-3): p. 101-8.
140. Hatano, H., et al., *RHAMM/ERK interaction induces proliferative activities of cementifying fibroma cells through a mechanism based on the CD44-EGFR.* Laboratory Investigation, 2011. **91**(3): p. 379-391.
141. Cheng, X.B., et al., *Prognostic impact of hyaluronan and its regulators in pancreatic ductal adenocarcinoma.* PLoS One, 2013. **8**(11): p. e80765.
142. Itano, N., L. Zhuo, and K. Kimata, *Impact of the hyaluronan-rich tumor microenvironment on cancer initiation and progression.* Cancer Sci, 2008. **99**(9): p. 1720-5.
143. Kultti, A., et al., *Accumulation of Extracellular Hyaluronan by Hyaluronan Synthase 3 Promotes Tumor Growth and Modulates the Pancreatic Cancer Microenvironment.* BioMed Research International, 2014. **2014**: p. 817613.
144. Jiang, B.W., QR; Wan, YP; Wu, TT; Liu, WJ; He, LM; Pan, QW; Tang, ZH, *PROBABLE MOLECULAR MECHANISM OF PANCREATIC CANCER CELLS MIGRATION PROMOTED BY HIGH MOLECULAR WEIGHT HYALURONIC ACID.* ACTA MEDICA MEDITERRANEA, 2019. **35** (4): **2099**.
145. Lokeshwar, V.B., et al., *Antitumor Activity of Hyaluronic Acid Synthesis Inhibitor 4-Methylumbelliferone in Prostate Cancer Cells.* Cancer Research, 2010. **70**(7): p. 2613-2623.
146. Ghatak, S., S. Misra, and B.P. Toole, *Hyaluronan oligosaccharides inhibit anchorage-independent growth of tumor cells by suppressing the phosphoinositide 3-kinase/Akt cell survival pathway.* J Biol Chem, 2002. **277**(41): p. 38013-20.

8. Supplement

8.1. Supplement 1: Sequence information

8.1.1. SELEX library primers

Library Primer 18_25	5'	CGGGGATCCATGGGCACTATTTATATCAACN25AATGTCGTTGGTGGCCC	3'
Forward Primer 17_24	5'	CGCGAATTCTAATACGACTCACTATAGGGGCCACCAACGACATT	3'
Reverse Primer (17_25)	5'	CCCGACACCGCGGGATCCATGGGCACTATTTATATCAA	3'

8.1.2. Aptamer oligonucleotide primers

Aptamer Forward Primer	5'	CGCGAATTCTAATACGACTCACT	3'
Aptamer Reverse Primer	5'	GACACCGCGGGATCCAT	3'
Aptamer H1_1 Oligo	5'	CGCGAATTCTAATACGACTCACTATAGGGGCCACCAACGACATTATGGAAGG TAGGAGGAGATTGTCA GTTGATATAAATAGTGCCCATGGATCCCGCGGTGTC	3'
Aptamer H2_1 Oligo	5'	CGCGAATTCTAATACGACTCACTATAGGGGCCACCAACGACATTTAAATCAAC ATAGGTGGATGGTGGT GTTGATATAAATAGTGCCCATGGATCCCGCGGTGTC	3'
Aptamer H2_2# Oligo	5'	CGCGAATTCTAATACGACTCACTATAGGGGCCACCAACGACATTGACATCAG CCAGGGTGTAGGGGGAG GTTGATATAAATAGTGCCCATGGATCCCGCGGTG TC	3'

8.1.3. Aptamer RNA sequence details

Aptamer H1_1 RNA	5'	CGCGAAUUCUAAUACGACUCACUAUAGGGGCCACCAACGACAUUA UGGAAGGUAGGAGGAGAUUGUCA GUUGAUUAUUAAUAGUGCCCAUGGAUCCCGCGGUGUC	3'	33,6 kDa
Aptamer H2_1 RNA	5'	CGCGAAUUCUAAUACGACUCACUAUAGGGGCCACCAACGACAUUU AAAUCAACAUAGGUGGAUGGUGGU GUUGAUUAUUAAUAGUGCCCAUGGAUCCCGCGGUGUC	3'	33,9 kDa
Aptamer H2_2# RNA	5'	CGCGAAUUCUAAUACGACUCACUAUAGGGGCCACCAACGACAUUG ACAUCAGCCAGGGUGUAGGGGGAG GUUGAUUAUUAAUAGUGCCCAUGGAUCCCGCGGUGUC	3'	34,0 kDa

8.2. Supplement 2: MTT proliferation assay readout R-script

```
library(svglite) library(RColorBrewer) library(ggplot2) library(gsignif)
library(readxl) library(drc) library(magrittr) library(dplyr) library(ggpubr)
library(ggthemes) library(cowplot) library(scales) library(pBrackets)

mtt.dat.anova <- read_xlsx("Datasheet")

### replace zero to 0.001 for concentration

mtt.dat.anova <- mtt.dat.anova[] mtt.dat.anova$concentration[mtt.dat.anova$concentration
== 0] <-0.01 mtt.dat.anova <- mtt.dat.anova[!is.na(mtt.dat.anova$cell_count),]

### mean and sd

mtt.dat <- mtt.dat.anova %>% group_by(cell_line, agent, concentration) %>%
summarize(mean = mean(cell_count),

sd = sd(cell_count)) cell_lines <- unique(mtt.dat$cell_line)

p <- ggplot(mtt.dat, aes( x = concentration,
y = mean,
color = agent

)) + geom_errorbar(

aes(ymax = mean + sd, ymin = mean - sd), lwd = 1,
alpha = 0.5

)+
scale_color_manual(values = brewer.pal(length(
unique(mtt.dat$agent) ), "Set1")) + geom_jitter(
```

```

data = mtt.dat.anova,
aes(x = concentration, y = cell_count, fill = agent), size = 2,
width = 0.1,
shape = 21,
color = "black"

)+
scale_fill_manual(values = brewer.pal(length(
unique(mtt.dat$agent)
), "Set1")) +
xlab("concentration (nM) ") +
ylab("% MTT Proliferation") + scale_x_continuous(breaks = log_breaks(n = 5),

trans = log10_trans(), labels = function(n) {

format(n, scientific = FALSE) }

)+
scale_y_continuous(expand = c(0, 0), limits = c(0, 140)) + stat_smooth(

method = "drm",
method.args = list(fct = L.4(

names = c("b", "lower", "upper", "ed50") )),

se = FALSE,
aes(y = mean, color = agent), size = 2

)+
geom_hline(yintercept = 50, lty = "dotted") +

annotation_logticks(sides = "b") + ggtitle("Aptamer H2_2# on Panc 1") +
theme(legend.position = c(0.1, 0.2)) + theme_classic2()

print(p)

ED50 <-
drm(cell_count ~ concentration,

agent,
data = mtt.dat.anova,
fct = LL.4(names = c("b", "lower", "upper", "ed50")))

summary(ED50)
ed.summary <- ED(ED50, c(50), interval = "delta")

```

9. Appendix

9.1. Acknowledgements

I would like to thank Prof. Dr. med. Julia Mayerle, Prof. Dr. Kirsten Lauber and PD Dr. Ujjwal Mukund Mahajan for facilitation of this project, their constant supervision and helpful feedback. I am especially grateful for the kind and patient support by Dr. Mahajan who helped me grow and evolve in the scientific field from my very beginning, who was always available for questions and advice and who taught me so much about science on multiple levels.

I would also like to thank all my colleagues of the laboratory and the clinical team. You created a very supportive and pleasant environment, I really enjoyed working with all of you. Special thanks go to Dr. Ivonne Regel for very insightful feedback and the organizational support.

Lastly, I would like to thank my parents, my brother, my girlfriend, and my cat for all the emotional support, insights from other points of view and helpful discussions. You kept my back free during hard times and I could not have completed this project without you.

9.2. Curriculum vitae

Work experience

- 04.2023 – 09.2023 **Assistant Doctor of Internal Medicine at Großhadern Clinic (LMU)**
Clinical patient care with a focus on gastroenterology
- 03.2018 – 06.2023 **Experimental doctoral thesis under Prof. Dr. med. Julia Mayerle**
- Development of a new therapeutic approach for treatment of pancreatic carcinoma via a 'targeted drug delivery' RNA system
 - FöFoLe-scholarship from LMU, abstract prize at DPC (Göttingen 2019)
 - Several co-publications within the scope of the doctoral thesis
- 01.2023 – 04.2023 **Working student at "Elektroniksystem- und Logistik- GmbH" (ESG)**
Cross-disciplinary role in medical consulting, software development, graphic design, and product design in the field of system simulation
- 10.2022 – 01.2023 **Consulting project for ambulatory surgeries in Großhadern Clinic**
Elaboration of an optimization concept with the MeCuM-SiGma team
- 08.2020 – 08.2021 **Working student in a surgical outpatient clinic (MVZ Neuhausen)**
Assistance with with endoscopic interventions and small surgeries
- 04.2017 – 03.2018 **Tutor in the dissection course of Anatomical Medicine (LMU)**
Supervision and teaching of 30 students on human anatomy

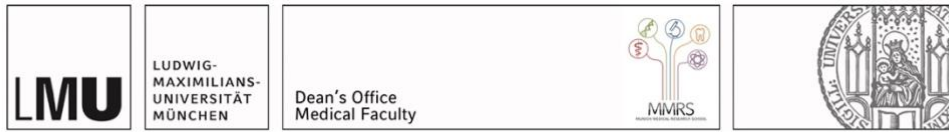
Course of study

- 10.2023 – currently **Study of Digital Engineering (University of applied sciences, MUC)**
- 10.2015 – 12.2022 **Study of Medicine (LMU Munich)**
Overall grade of state examination: 1.33
Scholarship of „Max Weber-Programm“ and „Studienstiftung“
- 09.2007 - 06.2015 **High School Gymnasium Miesbach**
Abitur grade (A-levels): 1.0

Skillset

- Clinical patient care | experimental scientific benchwork | clinical studies | scientific writing | software design and engineering | consulting | advanced presentation skills
- Software: Good knowledge of Python, JavaScript, R, GraphPad Prism, Blender, Microsoft Office, Photo-, Sound- and Videoediting
- Languages: German (mother tongue), Russian (second mother tongue), Englisch (fluent), Italian (basic)

9.3. Affidavit



Affidavit

Julian Peterhansl

Surname, first name

Street

Zip code, town

Country

I hereby declare, that the submitted thesis entitled

„Generation of CD44-specific aptamers for targeted approaches in the treatment of pancreatic cancer“

is my own work. I have only used the sources indicated and have not made unauthorised use of services of a third party. Where the work of others has been quoted or reproduced, the source is always given.

I further declare that the dissertation presented here has not been submitted in the same or similar form to any other institution for the purpose of obtaining an academic degree.

München, den 12.12.2023

Place, date

Julian Peterhansl

Signature doctoral candidate

Affidavit

January 2023